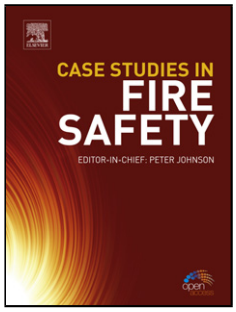

Title: Oxidation of magnesium alloys at elevated temperatures in air: A review

Author: Qiyang Tan Andrej Atrens Ning Mo Ming-Xing Zhang

PII: S0010-938X(16)30290-6
DOI: http://dx.doi.org/doi:10.1016/j.corsci.2016.06.018
Reference: CS 6826

To appear in:

Received date: 20-1-2016
Revised date: 15-6-2016
Accepted date: 15-6-2016

Please cite this article as: Qiyang Tan, Andrej Atrens, Ning Mo, Ming-Xing Zhang, Oxidation of magnesium alloys at elevated temperatures in air: A review, Corrosion Science http://dx.doi.org/10.1016/j.corsci.2016.06.018

Oxidation of magnesium alloys at elevated temperatures in air: A review

Qiyang Tan[1], Andrej Atrens[1], Ning Mo[1], and Ming-Xing Zhang[1,*]

[1] School of Mechanical and Mining Engineering, The University of Queensland, St. Lucia, QLD 4072, Australia

Corresponding author: mingixng.zhang@uq.edu.au, +61733468709

Highlights

- The oxidation behaviours of Mg alloys from low to high temperatures are reviewed.
- Characteristics of MgO during oxidation is discussed.
- Mechanisms of Mg oxidation is presented.
- Effect of various alloying elements is analysed.

Abstract

This paper reviews (i) the oxidation of Mg alloys at elevated temperatures in air; (ii) the influence of alloying elements on the oxidation of Mg alloys; and (iii) the progress in the development of oxidation-resistant Mg alloys. Low oxidation rates have been shown by Mg alloys containing the alloying elements, Ca, Be and rare earth elements. However, these alloying elements may also decrease mechanical properties, such as ductility.

Keywords: A. Magnesium; A. Alloy; C. Oxidation

1. Introduction

Mg alloys have been used since Sir Humphry Davy firstly produced pure Mg in 1808 [1]. Mg is the eighth most common element in the earth, and the third most abundant element dissolved in seawater, after sodium and chlorine [2]. Applications and production of Mg alloys are increasing. In 2013, the global production of Mg reached 1.82 million tonnes [3].

The major advantage of Mg alloys is their low density. Mg is the lightest structural engineering metal [4]. Mg alloys have good castability, good weldability, high damping capacity, relatively high thermal and electrical conductivity, and are recyclable [5-8]. However, the wider use of Mg alloys is restricted because Mg alloys have poor cold workability, low creep resistance, low wear resistance and low corrosion resistance [8-17]. The low corrosion resistance is caused in part by the fact that Mg is a chemically active element, and the surface films are not particularly protective. Mg also has a high affinity to

oxygen [18] so that Mg alloys have typically a low oxidation resistance in air at high temperatures. Furthermore, Mg alloys can cause fires during manufacturing processes, such as machining, casting and heat treatment, and their surface can easily become degraded. This poor oxidation resistance significantly restricts their wider engineering applications [19-22]. For example, to date, Mg alloys are restricted in aircraft interiors because Mg alloys can ignite at high temperatures [23-25]. Hence, the development of Mg alloys with increased oxidation resistance would widen the applications of Mg alloys, particularly at elevated temperatures.

The present paper reviews the research on the oxidation of Mg alloys, and on the development of oxidation resistant Mg alloys.

2. Characteristics

2.1 Magnesium oxide

Mg alloys exposed in an oxygen-containing gas form magnesia (MgO) on the surface through the following chemical reaction [26]:

$$2\mathrm{Mg} + \mathrm{O}_2 = 2\mathrm{MgO} \quad (1)$$

MgO has a face centred cubic (fcc) lattice structure with a lattice parameter of 4.21 Å. Mg ions occupy all octahedral sites [27]. MgO has a high melting point of 2942 ± 50 °C [28] and calcined or fused magnesia is widely used as a (high-temperature) insulator [26].

However, MgO is not chemically stable in aqueous solutions. MgO reacts with water to form $Mg(OH)_2$, which provides limited corrosion protection in aqueous solutions having pH values less than pH = 12 [8, 11, 29, 30]. MgO also provides little protection to Mg alloys against oxidation in air at high temperatures [27].

2.2 Solid and semi-solid alloys

Fig. 1 presents typical oxidation behaviour, as exemplified by the weight gain of the AZ91 in air versus time, from the thermogravimetric analysis (TGA) study of Czerwinski [31, 32]. For clarity, the figure has been replotted with a logarithmic scale for the Y-axis scale. There were

typically two oxidation stages: (i) an initial parabolic stage, and (ii) an acceleration stage. The initial parabolic stage has been considered to be an incubation period [26]. At 197 °C, there was only the initial parabolic stage during which there was essentially zero weight gain at times greater than 10 min. The overall weight gain was low, indicating slow oxidation. The low weight gain can be attributed to the formation of a protective layer of MgO. In contrast, the oxidation rates accelerated after a parabolic stage at temperatures above 400 °C. This indicated that a protective oxide layer formed on the surface and provided protection for some time. Subsequently, the oxide layer could no longer protect the substrate from oxidation. With increasing temperature from 437°C to 487°C, the incubation period decreased from 25 to 13 minutes. The same behaviour occurred for the solid Mg alloy after partial melting, as at 472 °C and 487 °C.

Fig. 2 exhibits the corresponding macroscopic surface morphologies of the AZ91 after oxidation in air [32]. Fig. 2a shows that at 387 °C (i.e. below 400 °C) the surface was flat after 10 hour oxidation. Fig. 2b shows that at 497 °C, the substrate was fully covered by dark oxide nodules after 1 hour. Fig. 2c shows that at the higher temperature of 547 °C, there resulted the typical cauliflower morphology as the product of the burning of the Mg alloy.

2.2.1 Temperatures less than 400 °C

Czerwinski [26] considered that amorphous MgO forms on Mg alloys at room or at low temperatures. However, it seems more likely that the MgO formed at these low temperatures is crystalline. This is based on the possible similarity to the passive film formed on stainless steel, where more recent research has shown that the film is crystalline [33, 34] even though the earlier researchers assumed that the surface film was amorphous [35]. Fournier et al. [29] measured the oxide thickness formed on pure Mg in an O_2 atmosphere at different temperatures using XPS. The oxide thickness was 1.5 nm after 15 min at room temperature, 2.6 nm after 15 min at 300 ℃, and 4.3 nm after 60 h at 300 ℃, which was similar to the thickness as the Al_2O_3 oxide layer formed on pure Al [36, 37]. However, once the oxidation temperature exceeded 400 ℃, the oxide grew rapidly to 4.3 nm in 15 min. Low oxidization rates below 400 ℃ were also reported by Medved et al. [38] on Mg alloys including AM50, AM60 and AE42. The oxidation weight gains at 200 ℃ and 400 ℃ were negligible up to 10 hour.

These results indicated that 400 °C is a critical temperature for the oxidation of Mg alloys. Below 400 °C, the MgO layer formed on Mg alloys is compact and provides protection of the substrate from further oxidation [32]. Above 400 °C, the oxidation becomes faster after a parabolic growth period and the protective capacity of the MgO disappears.

Jeurgens et al. [39] used real-time in-situ spectroscopic ellipsometry (RISE) to study the oxidation kinetics of a Mg-2.63 at.% Al alloy at 31 °C and various low oxygen pressures. Fig. 3 shows that the variation of oxide film thickness followed parabolic kinetics. The present authors considered that this indicates (i) the separation of the two reactants by the MgO oxide layer formed, and (ii) the control of the oxidation by transport of species within the MgO oxide layer.

Hence, at low temperatures, the MgO layer is considered a compact film that provides protection to the substrate from oxidation

2.2.2 Temperatures above 400 °C

At temperatures above 400 °C, non-protective oxidation occurred in both pure Mg and Mg alloys [29, 38]. Fig. 1 indicates initial parabolic growth kinetics followed by significant weight gain at temperatures above 400 °C. Czerwinski and co-workers [26] considered the parabolic growth stage as an incubation period, in which a compact protective thin oxide films formed and separated the two reactants. However, after the incubation period, the oxide layer was broken and nodular oxide growth began [26, 31, 32]. Once the oxide layer was broken, non-protective oxidation occurred and the oxidation kinetics were rapid, indicating that the oxidation rate was significantly accelerated. Growth of oxide nodules replaced the uniform layer formed at the initial stage. With increasing oxidation time, the nodules coalesced into a continuous layer that covered the entire alloy surface as illustrated in Fig. 2b. Fig. 1 allows estimation of the time to the onset of accelerated oxidation for AZ91. The incubation period was ~25 minutes at 437 °C, and was decreased to ~13 minutes at 487 °C, indicating a decrease in oxidation resistance.

Similar results were reported for AM, AE, ZC, ZE series of Mg alloys in the temperature range from 400 to 500 °C [38, 40, 41]. At temperatures below 400 °C, the weight gains of AM60 and AE42 for 12 hour followed a parabolic law. At 450 °C, linear growth started after

~2 hour, and this period was shortened to 1.5 hour at 500 °C [38]. Lee and co-workers [40] found that, for a SiC reinforced ZC63 Mg alloy based composite, there was a negligible weight gain after 5 hour in air at 410 °C; but, the incubation period only lasted for 1 hour at 450 °C, and 0.4 hour at 470 °C, followed by linear oxidation kinetics. Lopez and co-workers [41] reported a similar phenomenon in ZE41, which is a high-temperature Mg alloy. The critical temperature was 450 °C. TGA test showed that the oxidation followed parabolic kinetics for about 5 hour below 450 °C. In contrast, at 500 °C linear kinetics started after a 1.5 hour incubation period. Leontis and Rhines [42] reported similar results for the oxidation of pure Mg over a temperature range from 500 °C to 575 °C.

In summary, there is a critical temperature, which ranges from 400 to 450 °C depending on the composition of the Mg alloy. Below this critical temperature, the growth of the MgO film is slow, and the oxide protects the substrate from oxidation. Above this critical temperature, oxidation consists of two stages. In the initial stage, which is also the incubation period, the oxidation follows parabolic kinetics. Then, there is linear growth kinetics, which represents the accelerated oxidation stage. Higher temperatures are associated with a shorter incubation period.

2.3 Ignition and burning

Oxidation at high temperatures may cause ignition and burning of a Mg alloy. A feature of Mg burning is the emissions of significant heat and bright visible light [43]. There is a significant Mg vapour pressure [26, 31, 43, 44] when the alloy becomes semi-solid or molten at high temperatures. The Mg vapour saturates the porous oxide and provides a large surface area between vaporised Mg and oxygen, and creates conditions that favour ignition and burning [43]. Fig. 2c shows the intensive surface oxide sponges and cauliflower morphology, which is regarded the result burning of the Mg alloy [26, 31].

The ignition temperature was conceived as a means to characterise the susceptibility of initiating burning of Mg alloys. Because of the exothermic nature of Mg burning, the ignition temperature has been measured as the temperature associated with a sharp increase of the alloy temperature [26, 27, 43] when the Mg alloy was subjected to a temperature ramp in air in a furnace. The ignition temperature of pure Mg ranged from 620 °C to 650 °C [45-47], which is close to or equal to the melting temperature of pure Mg of 650 °C. For Mg alloys,

ignition may occur at lower temperatures, either below or slightly above the solidus, because localized melting of the alloy significantly accelerates the Mg evaporation rate. For example, the ignition temperature of AZ91 was measured to be 600 °C in one test [48] and 520 °C in air in another test in which the holding time was 20 min [49]. This indicates that there can be a wide variation in the measured ignition temperature, which clearly depends on the method of measurement.

The oxidation products of burning Mg alloys are more complicated than the products of oxidation without burning. Temperature between 3000 °C to 5000 °C have been reported in a Mg flame due to the large amounts of heat generated in the burning of Mg [50, 51]. At these high temperatures, nitrogen, which does not appreciably react with Mg at lower temperatures, becomes a reactant by the following reaction [43, 52]:

$$3\mathrm{Mg} + \mathrm{N}_2 = \mathrm{Mg}_3\mathrm{N}_2 \quad (2)$$

Thus, the products of burning of pure Mg include MgO and the greenish yellow magnesium nitride, Mg_3N_2. In Mg-Al alloys, aluminium nitride AlN and Mg-Al spinel $MgAl_2O_4$ have also been detected after burning [43, 53].

2.4 Molten alloys

Mg is typically melted in mild steel crucibles at temperatures above 650 °C, which is the melting temperature of pure Mg [54]. The oxidation of molten Mg is more rapid than oxidation at lower temperatures, and there is typically the tendency for ignition and burning of molten Mg [55]. Balart et al. [56] found that the oxidation of molten AZ91 in air involved (i) the formation of an oxidation layer, (ii) nodular growth, and (iii) ignition and burning. The surface had two distinct characteristic regions: (i) the layer growth region and (ii) the nodular growth region. There were also yellow nitrides on the surface, as a result of burning. These characteristics are schematically shown in Fig. 4. The macroscopic uniform oxide layer is considered a product formed during the initial oxidation stage. After the initial oxidation period, there is oxidation associated with an oxidation product in the form of oxide nodules, and subsequently the alloy ignites and burns. Some of the burning products remain on the Mg alloy surface. The high vapour pressure of Mg at these temperatures means that oxidation

associated with the uniform layer growth has been quickly replaced by oxidation with nodular growth, and burning with the associated cauliflower morphology.

Liu and co-workers [57] using TGA measurements found that pure Mg and AZ91 exposed at 760 °C in air containing 0.001 vol.% HFC-134a exhibited linear oxidation kinetics without an incubation period. This implied that the rapid oxidation occurred directly on the surface of the melt. The oxidation products on the surface of the pure Mg were MgO and Mg_3N_2, whereas the surface of the AZ91 melt contained MgO with small amounts of Mg_3N_2, AlN, $MgAl_2O_4$ [57]. AlN and Mg_3N_2 were considered as burning products as a result of the chemical reaction of nitrogen with Al and Mg vapour during burning [56]. When the temperature was above 850 °C, a freshly exposed surface spontaneously burst into flame [54].

2.5 Flammability

Mg alloys are prone to burn when in contact with an open flame or other heat source, and Mg flames are difficult to extinguish [23, 24, 43]. The term flammability was used by Czerwinski [23] to describe the tendency to continued burning of the Mg alloy despite flame removal.

Liu et al. [24] found that the burning of AZ31, WE43 and ZE10, studied using a cone calorimeter at a radiation power of 65 kW/m^2, showed the following common characteristics. The side and upper faces of the specimens developed protuberances. The number of protuberances increased, these protuberances began to ignite and became more prominent. The initial small saffron flames changed to a strong dazzling white flame, and the specimens burned steadily. However, the burning characteristic after heat source removal was not analysed in this study.

Prasad et al. [58, 59] found that there was no burning before melting in their study of the flammability of a range of Mg-X binary alloys (X = Al, Ca, Si, Sn, Sr, La, Mn, Zn, Zr, Ce, Gd, and Nd), AZ61 and AZ91, using a flame test as illustrated in Fig. 5 as a top view. One end of the horizontal Mg alloy sample (typically 20 mm in diameter and 200 mm in length) was subjected to a liquefied petroleum gas (LPG) flame with a temperature of ~1100 °C. Thermo-couples allowed estimation of the flame temperature, and the temperature at the ends of the Mg alloy sample.

In all tests there was no burning until the specimen tip melted. Melting occurred at the melting temperature for pure Mg. For Mg alloys, burning typically commenced at lower temperatures because Mg alloys start to melt at temperatures lower than that of pure Mg.

Fig. 6 shows a typical test for AZ61. The tip of the AZ61 specimen was subjected to the LPG flame. Localized ignition occurred after the specimen tip melted (Fig 6a) followed by burning of the specimen tip (Fig. 6b). The fact that burning required alloy melting indicates that Mg vapour is the burning species [58]. This indicates that the mechanism of burning for Mg alloys involves the alloy melting, vaporization of Mg, and the burning of Mg vapour. After the specimen end had been subjected to the LPG flame for some time, the specimen tip melted and often a blob of molten Mg alloy separated from the specimen tip and fell to the foundry floor.

Fig. 6c illustrates what typically happened when the LPG flame was removed from the end of the Mg specimen. The burning blob of molten Mg alloy continued to burn until all the Mg was consumed. The burning end of the Mg specimen extinguished. This was attributed to the heat conduction away from the hot end of the horizontal specimen by conduction along the specimen. When the LPG flame was applied to the end of the horizontal specimen, there was sufficient heat input to maintain molten Mg at the end of the specimen, and the molten Mg provided sufficient Mg vapour to maintain burning. When the LPG flame was removed, the heat generated by the burning Mg was less than the heat conducted away from the hot end of the horizontal specimen by conduction along the specimen. As a result, the end of the horizontal Mg specimen cooled, the molten Mg solidified. At this stage, the Mg vapour was insufficient to maintain the flame, and the flame extinguished. In contrast, the molten blob of Mg on the sand of the foundry floor continued to be molten because, in that case, there was little conduction of heat away from the molten blob, and the flame of the burning Mg alloy provided sufficient heat and Mg vapour to maintain the Mg flame [58].

Marker [60], from the Federal Aviation Administration (FAA), studied the flammability of AZ31, WE43 and EV31A through both the laboratory and a full-scale aircraft fire tests. Mg alloys ignited and burned with an intense flame after melting. This again indicates that Mg vapour is the burning species because the burning required alloy melting. AZ31 burned steadily despite the removal of the heat source in these experiments. In contrast, burning ceased on heat removal for the Mg alloys containing the rare earth (RE) elements (WE43 and EV31A). Unfortunately, the mechanism of the RE elements in the flammability resistance

was not analysed. The present authors consider that the RE elements promoted formation of dense oxide layer on the surface of molten Mg alloys, which prevented the further vaporisation of Mg, and therefore suppressed the burning. Subsequently, Marker [61] showed, using full scale flammability tests, that the use of WE43 in the construction of seat frames did not cause a significant change to the survivability to a survivable aircraft accident compared with the use of standard aluminium alloys.

Burning of Mg is accompanied by the vaporisation of Mg. The Mg vapour significantly expands the contact area with oxygen, and leads to the burning with a flame. In addition, the burning of Mg is a vigorous exothermic process that releases a large amount of heat [23, 58]. The heat generated contributes the steady flame, and makes the flame difficult to extinguish. Thus, Mg alloys were historically prohibited from use in the aircraft cabin. To widen the applications of Mg alloys in the aerospace industry, development of ignition-resistant and non-flammable Mg alloys is desirable.

3. Mechanisms

3.1 P-B ratio

MgO-magnesia is the major oxidation product of Mg alloys. However, MgO provides marginal oxidation protection, unlike Al_2O_3 and Cr_2O_3, which effectively protect Al alloys and stainless steels from oxidation [27]. As previously mentioned, there is a critical temperature above which the oxidation rate of Mg alloys becomes significant.

In an early study in 1923, Pilling and Bedworth [62] suggested that the protective ability of an oxide formed on a metal can be indicated by the Pilling–Bedworth ratio (P-B ratio). The P-B ratio, R_{PB}, is given by:

$$R_{\mathrm{PB}} = \frac{M_{\mathrm{oxide}}\rho_{\mathrm{metal}}}{nM_{\mathrm{metal}}\rho_{\mathrm{oxide}}} \tag{3}$$

where the numerator relates to the volume of the elementary cell of the metal oxide; the denominator relates to the volume of the elementary cell of the corresponding metal, from which the oxide is created; M is the atomic or molecular mass, n is the number of metal atoms in one molecule of the oxide, ρ denotes density, and the subscripts are self-explanatory.

The oxide layer is expected to be not protective if the R_{PB} value is less than 1.0. A protective layer may be associated with R_{PB} values between 1.0 and 2.0. If R_{PB} the value is greater than 2.0, the oxide layer is expected to be thick, tend to chip off, and provide little protection.

The R_{PB} value of MgO on Mg is 0.81. Thus, the oxide layer is not compact, and may not be able to provide protection to the substrate from oxidation, particularly at elevated temperatures [44, 62], even though MgO is easily formed due to the high affinity of Mg to oxygen.

3.2 Diffusion of Mg^{2+} ions

The understanding of the oxidation of Mg can be helped by a consideration of the transport of species through the oxide that forms on the Mg surface during oxidation. The following paragraphs briefly reviews the mechanism of diffusion-controlled growth of the MgO layer based on Czerwinski [27].

In MgO, the typical point defects are Schottky defects. These point defects form in a lattice containing oppositely charged ions when ions leave lattice sites and create vacancies that allow the diffusion of Mg^{2+} [63]. The formation of a cation vacancies can be described by the following reaction [64]:

$$\frac{1}{2}O_2 = O_o + 2h^{\cdot} + V''_{Mg} \quad (4)$$

where O_o, $h^{\cdot}$, V''_{Mg} represent an O ion, an electron hole in the valence band, and a magnesium vacancy site with double ionisation, respectively [65].

Wagner's oxidation theory [66] indicates that Mg oxidation involves the outward diffusion of Mg-cations through the MgO surface layer, from the metal-oxide interface to the oxide-air interface. Thus, the growth of the MgO layer is primarily governed by the outward diffusion of Mg-ions.

The MgO film is thin and assumed crack-free at the beginning of the oxidation. Thickening of the oxide layer is accompanied by the outward diffusion of Mg-ions, which leads to the inward vacancy flux, which may create voids at the metal-oxide interface [26]. Accumulation

and segregation of such defects eventually introduces internal stress in the oxide film. At the critical thickness, the internal stress is sufficiently high to cause cracking [67]. Such cracks can act as transport channels for Mg vapour [31], and therefore promote oxidation.

Assuming a crack-free continuous surface oxide layer, the thickness of the oxide layer is related to the diffusion of Mg^{2+} cations. The thickening rate, $\frac{\mathrm{d}X}{\mathrm{d}t}$, can be expressed by Fick's first law [27]:

$$\frac{\mathrm{d}X}{\mathrm{d}t} = \Omega \Delta c \frac{D}{X} \tag{5}$$

where, X is the oxide thickness, t is time, Ω is the volume of the oxide per reactant ion, Δc represents the concentration difference across the oxide film, and D is the diffusion coefficient of the Mg^{2+} ions inside the oxide.

Early studies showed that both lattice and grain boundary diffusion contributed to the oxidization [68]. Hence, the diffusion coefficient D can be expressed as [69]:

$$D = D_{\mathrm{L}}(1 - f) + D_{\mathrm{B}} f \tag{6}$$

where D_{L} and D_{B} are the lattice and grain boundary diffusion coefficients, respectively, and f denotes the fraction of the diffusion along grain boundaries. Assuming a cubic shaped grain, the fraction f can be calculated from [68]:

$$f = \frac{2\delta}{E_{\mathrm{t}}} \tag{7}$$

where δ is the grain boundary width and E_{t} is the oxide grain size at oxidation time t, which can be experimentally measured. Perrow and co-workers [70] found a parabolic growth in the grain size of NiO oxide with oxidation time t. Because MgO growth has the same mechanism as NiO, which involves outward migration of cations [64], it is reasonable to assume parabolic growth in MgO in the early stage of oxidation. This can be expressed using the following equation (8):

$$E_t^2 - E_0^2 = Gt \quad (8)$$

where E_0 represents the initial grain size and G is the grain growth parameter. Substituting the equations (6)-(8) into (5), the growth rate of the MgO oxide layer is formulated as follows [71]:

$$\frac{dX}{dt} = \frac{\Omega \Delta c}{X}\left[D_L + \frac{2\delta(D_B - D_L)}{(E_0^2 + Gt)^{0.5}}\right] \quad (9)$$

This analysis of Mg diffusion and oxide growth has been used to provide a qualitative interpretation of the low oxidation rates of Mg at low temperatures below 400 °C. The growth rate of the MgO surface layer is expected to increase with temperature because both the lattice and grain boundary diffusion increase with increasing temperature [72]. It has been considered that, at low temperatures, lattice diffusion by a vacancy mechanism is the only channel for Mg ions diffusion [27], because MgO has been considered to be amorphous or monocrystalline with no grain boundaries at room temperature or at slightly higher temperatures [26, 27]. The diffusion coefficient D_L can be expressed by the Arrhenius equation [72]:

$$D_L = 1.0 \times 10^{-6} \exp\left(-\frac{150000}{RT}\right) \ \mathrm{m^2/s} \quad (10)$$

where R is the gas constant and T is the temperature (in K). Even at 400°C (673 K), the lattice Mg ion diffusion coefficient is 2.24×10^{-18} m^2/s, which is small. Hence, as there is no grain boundary diffusion, lattice diffusion is too slow to allow a substantial oxidation rate. However, there has not been an attempt to relate the actual oxide thickness and actual oxidation rate to the actual Mg ion diffusion coefficient. Thus, this model is qualitative.

Furthermore, as discussed above, there is no reason to assume that MgO formed at low temperature oxidation is amorphous. Early studies by Finch and Quarrell [73, 74] found an abnormal crystal structure of a thin MgO film, while such a structure was not observed in a

thicker MgO layer. It seemed that the abnormal crystal structure of the thin MgO film was pseudomorphic. Because the P-B ratio of MgO is 0.81, the internal stress could lead to strain in a thin MgO film and caused such a pseudomorphism. Therefore, the thin MgO film formed at low temperatures should be crystalline. At room or slightly higher temperatures, MgO could be monocrystalline without grain boundaries. Thickening the film at higher temperatures can be accompanied with transforming the monocrystalline MgO layer to a polycrystalline MgO layer. In addition, previous studies showed that the defect density in a thin MgO film was lower than that in a thick film [32].

At temperatures higher than 400 °C, diffusion is accelerated. The higher temperature accelerates the lattice diffusion of Mg^{2+} cations, and grain boundary fast diffusion (D_B) becomes possible because the MgO is polycrystalline at higher temperatures [73]. Czerwinski and Lea [27, 72] indicated that grain boundary diffusion is two orders of magnitude faster than lattice diffusion. Thus, at high temperature, the outward diffusion of Mg^{2+} cations in the polycrystalline oxide layer is significantly faster. In addition to the film thickening, the faster outward diffusion of Mg^{2+} cations is associated with faster inward vacancy flux, creating voids at the interface between the oxide layer and the metal substrate [26]. These voids cause local stress, contributing to film cracking. As a result, the interface experiences a morphological change, and cracks form within the oxide layer. The cracks can accelerate the oxidation rate by providing a path for the diffusion of Mg vapour as discussed in the next section.

3.3 Evaporation

Fig. 7 illustrates the typical morphologies that form on the Mg surface during oxidation at high temperatures. The non-protective nature of the thick oxide layers at high temperatures has been recognized for a few decades [75]. Fig. 7a illustrates the ridge morphology on AZ91 after air-oxidation at 487 °C for 1 min, from Czerwinski [32]. An oxide ridge was generated by the reaction of oxygen with Mg at oxide cracks. Fig. 7b illustrates the nodular morphology produced by an increase in the oxidation temperature or oxidation time, which is dominated by Mg evaporation [26, 32].

Mg vaporization is a typical feature of Mg oxidation at high temperatures. The vapour pressure of Mg and Al in equilibrium with solid Mg and solid Al is given, for the temperature range 298 K to 923 K, by [76]:

$$\log P_{\mathrm{Mg}} = 13.495 - \frac{7813}{T} - 0.8253 \log T \quad (11)$$

$$\log P_{\mathrm{Al}} = 14.465 - \frac{17342}{T} - 0.7927 \log T \quad (12)$$

where P is the vapour pressure (in Pa) and T is the temperature (in K). At 400 °C (673 K), the vapour pressures of Mg and Al are 0.36 Pa and 2.9×10^{-14} Pa, respectively. The vapour pressure of Mg at 400 °C is thirteen orders of magnitude greater than that of Al. The high vapour pressure of Mg at elevated temperatures contributes to the high temperature oxidation of Mg alloys. Gulbransen [44] found that the contribution of evaporation to the oxidation increased with increasing temperature for pure Mg. The vaporisation of Mg was thought to be responsible for the porous oxide film above 450 °C as the evaporation rate was 2.2×10^{-6} g cm^{-2} min^{-1}, which is two orders of magnitude higher than that at 400 °C [44]. Smeltzer [69] also found that rapid oxidation occurred in an Al-3 wt.% Mg alloy due to Mg evaporation at temperatures above 400 °C.

The high evaporation rate of Mg can lead to micro-cracks inside the MgO layer and a ridge morphology on the surface in the early stage of oxidation as shown in Fig. 7a. The Mg vapour can rapidly reach the oxide-air interface through the micro-cracks and the voids formed in the surface oxide. Reaction of the Mg vapour and oxygen forms oxide nodules [32]. Fig. 7b presents a typical oxide nodule. The surface oxide is non-protective and oxidation follows linear kinetics [27]. The linear kinetics implies that the oxidation rate does not depend on the thickness of the surface oxide layer, because oxygen and Mg vapour can easily penetrate through the open cracks and voids to the metal-oxide and oxide-air interfaces. As oxidation continues, the oxide nodules grow, coalesce and form a loose structure.

Fig. 8 provides a schematic of the Mg oxidation mechanism at high temperatures [26]. Fig. 8a proposes that, in the initial stage, a protective compact continuous oxide layer forms, through which Mg ions diffuse outwards. At this stage, the oxide growth follows parabolic kinetics. Fig. 8b shows that voids and cracks form. Voids at the Mg metal surface allow Mg

vaporization. The cracks allow penetration of oxygen and outward vapour phase diffusion of Mg vapour. The reaction of oxygen with the metal at the crack walls leads to an outward growth of ridges [26, 31]. At high temperatures, these two stages are short. Fig. 8c illustrates that further oxidation is accompanied by the growth of nodules through Mg evaporation. Mg vapour diffuses by vapour phase diffusion through the cracks, reaction with oxygen, and the deposition of the Mg oxide leads to the formation of Mg oxide nodules. Czerwinski [31, 32] claimed that an onset of accelerated oxidation is associated with the growth of oxide nodules. At this stage, there is a non-protective oxide layer, and the oxidation has linear kinetics. Fig. 8d illustrates that further oxidation leads to the coalescence of the nodules leading to the formation of a loose surface layer with high porosity. Such a morphology is also called a sponge [38]. Continuing oxidation and/or increasing temperatures can cause a violent reaction and burning, producing a cauliflower morphology [31, 32, 77].

3.4 Intermetallic phases

High temperature oxidation of a Mg alloy in air is typically associated with a change of the microstructure and melting of second phases. The eutectic temperature of the Mg-Al system is 437 °C. Above this temperature in Al-rich Mg alloys, the eutectic micro-constituent spheroidizes and melts [38, 78]. Similarly, CuMgZn intermetallic in ZC63 decomposed into α-Mg during oxidation at temperatures above 450 °C [40]. Because of the localized melting at high temperatures, liquid islands form in the alloy, which accelerate the evaporation Mg [31]. Consequently, growth of the oxide nodules is accelerated.

Fig. 9 provides a schematic of the late stage oxidation of a Mg alloy. Melting of the intermetallic compounds produces high local pressures of Mg vapour. If such a region is associated with cracks in the oxide, Mg vapour diffuses through the cracks and is oxidized at the oxide surface, contributing to the growth of the oxide nodule. The oxidation resistance in this temperature range can be improved, as shown by Pan et al. [79] by a two-step annealing method to eliminate the eutectic micro structures in Mg alloys. Pan and co-workers' work may provide an innovative approach to increase the oxidation resistance of Mg alloys.

Arrabal et al. [80] analysed the oxide morphology and elemental distribution for AZ91 after oxidation in air at 410 °C for 4 hour. After oxidation, the pore size on the surface was similar to that of the β-phase particles. EDS showed the Zn content in the β-phase reduced sharply

after oxidation while the α-Mg at the surface did not have significant changes in Zn content. Thus, Arrabal et al. [80] suggested that, in addition to the Mg vapour, the vaporisation of Zn during dissolution of the β-phase ($Mg_{17}Al_{12}$) also contributed to the film cracking and led to the superficial pores.

Intermetallic phases, particularly those in a eutectic microstructure along the grain boundaries, are also responsible for selective oxidation owing to their low melting temperature [26]. Selective oxidation causes a serrated interface between the oxide layer and the metal, which increases the surface area available for Mg evaporation and oxygen penetration.

Fig. 10 presents the model proposed by Arrabal et al. [80] describing the oxidation of AZ91. During long time exposure at high temperatures, the dissolution of the β-phase is accompanied by the formation of pores at the surface by Zn sublimation, leading to the partial break-up of the initial oxide film at the pores, and where grain boundaries intersect the surface. Thus, at the pit regions, Mg cations and Mg vapour can directly react with oxygen, resulting in the formation of loose oxide nodules. Further oxidation leads to expansion of the oxidized pit region. An Al-rich region is formed below the loose oxide because of the consumption of Mg during oxidation, leading to the local increase in Al concentration at the oxide/metal interface. Finally, the surface is replaced by a loose MgO sponge under which is an Al-rich layer [80]. This model could explain the oxidation mechanism around the eutectic temperature but it did not involve local melting or the formation of liquid islands that could accelerate the oxidation rate [26, 27, 38]. Hence, although the selective oxidation takes the intermetallic compounds into account in the oxidation of Mg alloys, the model needs further refinement.

4. Evaluation of the Mg oxidation mechanism

Due to the high affinity to oxygen, Mg alloys are easily oxidized and form MgO on the surface even at low temperatures. Because the P-B ratio of MgO is low, MgO is expected to have an incompact structure. Nevertheless, at room or relatively low temperatures, a thin MgO film covers the surface of the Mg alloy. Because the diffusion rate of Mg^{2+} in the MgO film is slow, and the defect density in a thin MgO film is low at low temperatures, the thin MgO is considered to be compact and can provide protection of the substrate from oxidation. Thus, at low temperature, the oxidation rate of Mg alloys is slow.

Above the critical temperature, which ranges from 400 to 450 °C depending on the composition of the Mg alloy, oxidation consists of two stages. In the initial stage, which is also the incubation period, the oxidation follows parabolic kinetics. Then, there is linear growth kinetics, which represents the accelerated oxidation stage. Higher temperatures are associated with a shorter incubation period.

There are a number of factors that promote oxidation. High temperature leads to faster diffusion of Mg^{2+} cations, which thickens the compact film formed at the initial stage. Thickening of the film results in a loss of protection because of the voids formed as a result of segregation of vacancies at the metal oxide interface. At higher temperatures there is, in addition, melting of the eutectic microstructure, and Mg vaporisation. All these contribute to the film cracking. The cracks within the oxide allow easy outward vapour phase diffusion of Mg vapour to the surface, and inward penetration of oxygen. As a result, the morphology of the surface oxide changes from a compact structure to a ridges morphology. Further oxidation leads to nodular growth by significant diffusion of Mg vapour through the cracks, and reaction with oxygen at the oxide-air interface. Finally, a loose structure (sponge) forms after coalescence of the nodules.

For molten Mg alloys, the oxidation is governed by the vigorous evaporation of Mg. The incompact MgO layer rapidly changes to a highly porous morphology because of the Mg vaporisation. Direct reaction of the Mg vapour with oxygen causes ignition. The large amount of heat generated by this exothermic process enables a steady flame. In addition, the molten Mg provides sufficient Mg vapour to maintain burning.

Burning of one end of a horizontal solid Mg rod occurs when there is sufficient heat to cause melting. Burning of a Mg rod continues as long as there is a heat source applied to one end. The burning stops when the heat source is removed because the heat conduction away from the hot end decreases the temperature of the Mg rod below the melting temperature, resulting in insufficient Mg vapour to maintain flame. In contrast, an isolated molten blob of Mg continues to burn until consumed.

Although the characteristics and mechanisms of the oxidation of Mg alloys at elevated temperatures have been extensively studied, there are still gaps in knowledge. In an early study, the ignition temperature of a thin magnesium ribbon was found to be 507 °C [81]. In another study, however, fine Mg powder with a particle size of 6 μm already ignited at 437 °C [82]. By comparison, the bulk forms of Mg alloys ignite only after melting as discussed in

Section 2.5. Thus, shape is a significant factor in the oxidation of Mg alloys, but, there is not a quantitative model to describe such features. However, it is clear that the ignition temperature depends on the experimental condition. Lower ignition temperature are measured for the test with slower heating rate and for samples with greater specific surface area. The important factor is the accumulation of a critical concentration of Mg vapour.

5. Common alloying elements

Chemical composition, which determines the microstructure of the Mg alloy, is another important factor influencing oxidation. Al, Zn, Cu and Mn are the four most common alloying elements in Mg alloys. The influence of these four alloying elements on oxidation of Mg alloys is reviewed in the following sections.

5.1 Al

Mg-Al based alloys are the most commonly used cast Mg alloys because of their good castability, acceptable strength and low price [54, 83]. Alloying with sufficient Al leads to (i) the formation of the β-phase ($Mg_{17}Al_{12}$) as isolated beta phase particles, or in the form of the eutectic micro-constituent, or precipitates, and (ii) refinement of the as-cast grains [84]. Thus, Mg-Al alloys have mechanical properties better than pure Mg. For example, AZ91 has a tensile strength of 130 MPa as-cast and 200 MPa in the T6 heat-treated condition [54]. In addition, a continuous $Mg_{17}Al_{12}$–phase at the surface may also provide some corrosion protection [8, 11, 85, 86].

However, at high temperatures, the oxidation resistance of Mg-Al alloys is not as good as that of pure Mg [32, 38] despite the hope that Al would lead to the formation of a protective γ-Al_2O_3 [87] film, and therefore a low oxidation rate. Leontis and Rhines [42] found that over 1.1 wt.% Al accelerated Mg oxidation. Similarly, Barrena et al. [88] reported that the weight gain of Mg-9 wt.% Al was always higher than that of Mg-6 wt.% Al within the temperature range from 500 °C to 700 °C in cyclic oxidation tests. Fast oxidation occurred when the Al content was over 10 wt.% at 400 °C [42]. This indicated that Al additions accelerated the oxidation of Mg alloys.

$MgAl_2O_4$ spinel was reported to from at room temperature for alloys containing 3.1 wt.% to 6.2 wt.% Al [89]. Shih et al. [90] considered that the $MgAl_2O_4$ spinels at the Mg-MgO interface could act as a diffusion barrier for Mg^{2+} cation. However the contribution to oxidation resistance was not significant.

The negative effect of Al on oxidation resistance of Mg alloys was attributed to the low melting temperature of the β-phase, and the eutectic microstructure, which causes selective oxidation and evaporation of Mg. Because Mg-Al based alloys are the most widely used, increasing their oxidation resistance would have technological significance.

5.2 Zn

Alloying with Zn improves the fluidity, creep resistance and strength of Mg alloys [91, 92]. Zn-containing Mg alloys show a high age-hardening response due to the formation of a rod-like β_1' phase that has a coherent or a semi-coherent interface with the matrix [93]. In addition, Zinc improves the corrosion resistance of Mg alloys by reducing the effect of impurities [8].

However, Zn decreases the oxidation resistance at elevated temperatures [42]. The low melting temperature of Mg-Zn intermetallic phases (341 °C) can cause significant evaporation of Mg and selective oxidation at high temperatures [94]. In addition, Zn tends to sublime [80], which leads to the formation of pores within both the matrix and the oxide scale, accelerating cracking of the oxide scale [42]. Hence, Zn is normally used as a ternary element, such as in the AZ series of Mg alloys, to improve the strength because the low Zn content has less influence on oxidation [32].

Although binary Mg-Zn alloys are rarely used due to their instability at elevated temperatures, Mg-Zn based alloys have gained attentions because of their good mechanical properties. For example, as-cast ZC63 has a tensile strength of 145 MPa, and 245 MPa can be achieved in the T6 heat-treated condition [54]. Improving the oxidation resistance of Mg-Zn alloys would be a good strategy to widen their range of applications.

5.3 Cu

In the Mg-Al system, Cu was reported to suppress discontinuous precipitation and increase the density of continuous precipitates [95]. Pan and co-workers [96] reported an optimal ageing response that enhanced both mechanical properties and electrical conductivity by alloying a Mg-6Zn alloy with 1 wt.% Cu. However, Cu reduces the corrosion resistance via galvanic corrosion, in which Cu-rich precipitates act as cathodes to accelerate the corrosion of the Mg matrix [8, 11, 18].

Leontis and Rhines [42] reported a sharp increase in the oxidation rate at 475 °C for pure Mg containing less than 1 wt.% Cu. Similarly, Fassel et al. [47] found a significant decrease in the ignition temperature for pure Mg containing 20 wt.% Cu. However, there have been no studies correlating this effect to Mg alloys. As Cu can increase the eutectic temperature of Mg-Zn [97], it is reasonable to expect that alloying with Cu may improve the oxidation resistance of this type of alloy through inhibiting the evaporation of Mg. Hence, the effect of Cu on oxidation resistance in Mg alloys needs further study.

5.4 Mn

Manganese is added as a ternary element to many commercial magnesium alloys, the AZ series alloys in particular, to improve the corrosion resistance [8, 30, 98]. Previous studies [99-102] showed that small addition of manganese (0.2 wt.%) can increase the tolerance limit for the impurities, Fe, Cu and Ni. Nearly 70 years ago, Leontis and Rhines [42] found that Mn has no influence on the oxidation rate of pure Mg as the solid solubility of Mn in Mg is low (2.2 wt.%) [43]. Fassel et al. [47] reported an increase of the ignition temperature of Mg alloys alloyed with Mn. However, this was contradicted by Bobryshev et al. [45] found a slight reduction in the ignition temperature of pure Mg alloyed with 2 wt.% Mn. To clarify these contradictory results, further investigations would be useful.

6. Other alloying elements

Surface engineering, such as surface coating, including PVD and CVD, has been used for decades to improve oxidation resistance [38, 101]**.** For example, Pérez et al. [103] found that a PVD-processed Mg-10.6Zr alloy could be protected from oxidation below 375 °C. However, the difference in thermal expansion coefficient between the coating and the

substrate may lead to the coating peeling off at elevated temperatures. Hence, developing oxidation-resistant alloys has been regarded as a better approach.

The selection of a possible element can be based on the P-B ratio of the oxide, and the Gibbs free energy of formation of the oxide by the following equation (13) [104, 105]:

$$a\mathrm{MgO} + b\mathrm{X} \rightarrow \mathrm{X}_b\mathrm{O}_a + a\mathrm{Mg} \quad (13)$$

where a, b present the stoichiometric numbers and X is the alloying element. For an alloying element X, if the change of Gibbs free energy associated with equation (13) is negative, the $\mathrm{X}_b\mathrm{O}_a$ oxide can form prior to MgO on the surface and protect the matrix from oxidation. For the common alloying elements, Al and Zn, the changes of their Gibbs free energy are highly positive at 700 °C (118 722 J and 24 5397 J, respectively) [105], indicating that the formation of Al_2O_3 (P-B ratio = 1.29) and ZnO (P-B ratio = 1.59) is not favoured. Thus, adding those elements cannot provide protection to Mg against oxidation.

Most alloying elements lower the solidus temperature, and therefore decrease the oxidation resistance and the ignition temperature [47] because of the tendency of localized melting. However, some alloying elements, such as Ca, Be and some RE elements have been reported to increase the oxidation resistance and the ignition temperature [47, 55] as discussed below.

6.1 Ca

Some Ca-containing Mg alloys have been characterized by adequate mechanical properties [106], which are achieved through refinement of precipitates and grain size [83, 107-109], whereas some Mg-Ca alloys are brittle [83, 108]. Li et al. [108] reported that the yield strength of AZ91D was improved 20% by alloying with 1 wt.% Ca due to the grain refinement and thinning of the β-phase. This effect was also achieved in a Ca-containing AS41, in which the coarse Mg_2Si phase was modified by alloying with 0.11 wt.% Ca [83]. However, over 1 wt.% Ca can cause brittleness in Mg-Al alloys [108].

Ca containing Mg alloys have been found to have a lower oxidation rate at high temperatures in both the solid and semi-solid state [110, 111]. You et al. [110] studied the oxidation of Ca-containing Mg alloys at temperature ranging from 440 °C to 500 °C using TGA. At 440 °C, a

1.5 wt.% and 3.0 wt.% Ca addition led to an oxidation rate somewhat lower than that of pure Mg. At 480 °C and 500 °C, the oxidations rates of the Mg-0.5 wt.% Ca, Mg-1.5 wt.% Ca and Mg-3.0 wt.% Ca binary alloys were also lower than that of pure Mg. But the oxidation rates of the Mg-3.0 wt.% Ca alloy were higher than that of the Mg-0.5 wt.% Ca alloy at all temperatures. This was attributed to the formation of the low melting temperature Mg-Mg_2Ca eutectic when the Ca content was over 0.5 wt.%. This eutectic structure melted and formed liquid islands at the higher temperatures. These liquid islands promoted Mg evaporation. The weight gain data of You et al. [110] were not normalized by the surface area, nevertheless, as a qualitative analysis, some indication is provided of how Ca affects the oxidation of Mg alloys.

You et al. [110] also investigated the surface concentration profiles of the Mg-3Ca alloy using Auger Electron Spectroscopy (AES). Fig. 11 presents their results. A Mg oxide layer with uniform Mg and O contents formed on pure Mg after oxidation at both 440 and 500 °C. In contrast, there was Ca in the surface oxide on Mg-3Ca alloy after heating at both 440 and 500 °C. At 440 °C, the surface layer was composed of an outmost layer of Mg oxide and a subsurface oxide layer containing Ca. At 500 °C, the outmost surface oxide was calcium oxide, followed by mixed oxide layers containing Mg and calcium oxides [110].

Improved oxidation resistance in Mg alloys by alloying with Ca was also reported by other researchers. Cheng et al. [111] reported AZ91 containing 1.5 wt.% Ca had negligible oxidation after exposure for 7 hour at 400 °C. XRD analysis detected both MgO and CaO on the surface of the alloy. It was considered that the CaO film was preferentially formed because Ca has a higher affinity with oxygen [112]. Lee [113] reported a low oxidation rate at 500 °C in air for AZ31 containing 0.3 wt.% Ca. In addition to the formation of CaO, the high oxidation resistance was also attributed to the formation of Al_2Ca on the grain boundaries of the α-Mg. In addition, Min et al. [114] found a 20 °C increase of the melting point of the β-phase ($Mg_{17}Al_{12}$) in AZ91 containing 0.3 wt.% Ca. According to the empirical electron theory (EET), this is attributed to the enhanced bond strengths of the β-phase by the Ca that dissolved in it. Hence, the thermal stability of β-phase was increased. The stable β-phase may contribute to oxidation resistance along the grain boundaries. Fan et al. [115] proposed a third element model for the Mg-3.5Y-0.8Ca alloy. The Ca was considered to increase the surface activity of Y in Mg-Y alloys, and to promote the formation of Y_2O_3. However, this hypothesis has not yet been experimentally confirmed.

Sakamoto et al. [116] reported a 250 °C increase in the ignition temperature of pure Mg by alloying 5 wt.% Ca. A thin dense oxide film formed on the surface of the Mg alloy melt, and was considered as a protective layer. This oxide film was considered as a Mg and Ca combined oxide because it could not be detected in both the pure Mg and pure calcium melt [112]. Similarly, this type of thin oxide film was also found on a molten AZ91 containing 2 wt.% Ca, which did not ignite up to 900 °C [117]. Unfortunately, it is not clear why such a combined oxide could provide effective protection of the molten alloy. More recently, Li et al. [118] developed a non-flammable AZ91 alloyed with Ca via liquid forging and extrusion. The ignition temperature was increased from 545 °C to 870 °C by alloying with 6 wt.% Ca, being attributed to the formation of CaO and the thermally stable Al_2Ca phase along the grain boundaries. Unfortunately, the alloy was associated with a significant reduction in elongation.

The mechanism by which Ca improves the oxidation resistance of Mg alloys is still not fully understood. The P-B ratio of CaO is 0.65, which is even lower than that of MgO (0.81) [62, 119]. Hence, the CaO film should not be sufficiently compact to provide protection. The improved oxidation resistance may be attributed to three possibilities: (i) a composite oxide layer consisting of CaO and MgO, which has a high density, forms during oxidation; (ii) Ca partially replaces Mg in the MgO, resulting in the increase in density of the MgO; and (iii) the formation of thermally stable intermetallic compounds. Alloying pure Mg with Ca leads to the formation of Mg_2Ca along the grain boundaries in the form of a eutectic micro-structure [83, 112]. As long as the oxidation temperature is below the melting temperature of the Mg-Mg_2Ca eutectic structure, they effectively block the diffusion of Mg^{2+} ions along the grain boundaries that act as fast diffusion channels, and therefore the oxidation is inhibited. In Mg-Al based alloys, the Ca addition enables the formation of Al_2Ca [108, 109], which acts as fast diffusion barriers on the grain boundaries. Furthermore, Ca could also supress the formation of the low melting temperature $Mg_{17}Al_{12}$-Mg eutectic structure and enhance the thermal stability of the β-phase, preventing selective oxidation along grain boundaries.

Although Ca can increase the oxidation resistance of Mg alloys, Ca causes brittleness which restricts the application of Ca in Mg-Al alloys [108].

6.2 RE elements

In last decade, Mg has been alloyed with various RE elements to develop new Mg alloys with better mechanical properties, formability and creep resistance at high temperatures [6, 120-125]. The oxidation resistance of Mg alloys may also be enhanced by alloying with RE elements [126-128]. This section reviews the effects of RE elements on the oxidation of Mg alloys.

6.2.1 Y

Fan et al. [129, 130] observed an improvement of oxidation resistance of Mg after alloying with more than 8 wt.% yttrium (Y). The Mg-10Y binary alloy did not burn even at temperatures up to 900 °C, when they were molten [130]. Unfortunately, over 8 wt.% Y led to significant embrittlement [83]. Thus, Mg-Y binary alloys cannot be directly used. Wang et al. [126] surface alloyed pure Mg with Y through ion implantation (Y ions of 90 keV with a dose of $5\times10^{17}cm^{-2}$ for 1h). There was a lower oxidation weight gain at both 400 °C and 500 °C compared with non-implanted pure Mg. Surface morphological examination revealed a dense, crack-free surface on the samples with Y-implantation compared with the loose oxide scale containing lots of cavities on the surface of pure Mg. Fig. 12 shows the surface morphology of both the implanted and non-implanted pure Mg surfaces. Fig. 12a shows cracks and cavities on the loose oxide scale of the non-implanted sample while the oxide scale of the implanted (Y ions of 90 keV with a dose of $5\times10^{17}cm^{-2}$ for 1 h) sample appeared dense with neither cracks nor cavities, particularly in the regions marked by number 1 in Fig. 12b. Wang and co-workers [126] considered that a combined MgO and Y_2O_3 oxide layer with a high density was responsible for the improvement of oxidation resistance because of the high P-B ratio of Y_2O_3 (1.39) [119]. In addition, nodules on the surface of the implanted sample (such as point "2" in Fig. 12b) were attributed to an outward diffusion of Y along the grain boundaries of the oxide. This is termed the segregation effect of the reactive element reported previously [131]. The outward diffusion of the reactive elements (REs) along the oxide grain boundaries inhibited the outward transport of the Mg cations and therefore inhibited oxidation [131].

Y has also been alloyed into ternary and quaternary Mg alloys at lower concentrations. A Mg-Zn-Zr alloy with 5.1 wt.% Y had constant oxidation weight gain after the parabolic growth of oxide for over 270 hour at 400 °C [132]. There was a compact and dense Y_2O_3 layer on the sample surface after oxidation [132]. Bak et al. [133] added 1 wt.% Y and 3 wt.%

Y_2O_3 into AZ91, and found that the effectiveness of Y_2O_3 was lower than that of Y in terms of reduction in oxidation rate at temperatures ranging from 400 to 500 °C. A possible explanation is the existence of some short-diffusion paths such as phase boundaries in the alloy with scattered Y_2O_3. These paths could favour the dissolution and transport of oxygen beyond the oxide scale [133]. Recently, Yu et al. [134] studied the effect of the state of Y on the oxidation resistance of Mg alloys by alloying pure Mg with both Y and Al. The weight gain of Mg-2.5Y was lower than that of Mg-2.5Y-2.5Al, indicating a better oxidation resistance. The dissolved Y in the matrix was responsible for the improvement because of the formation of protective Y_2O_3 layer on the surface. However, the added Al reacted with Y in the matrix, forming Al_2Y intermetallic compound, suppressing the formation of Y_2O_3. Thus, the oxidation resistance was deteriorated.

For molten Mg alloys, WE43 (containing 4 wt.% Y) had ignition-resistance up to 750 °C [55]. At 650 °C, when the oxide film of the molten WE43 alloy cracked, a new oxide film was re-generated rapidly and the cracks were repaired. This repair was attributed to the formation of Y_2O_3 [55].

Recently, You et al. [135] added both Ca and Y into AZ31, AZ61 and AZ91. The combination of Ca and Y led to higher ignition temperatures than the alloys containing only Ca. A similar result was found by Cheng and co-workers [111] that 0.5 wt.% Y resulted in a 25 °C increase of the ignition temperature of an AZ91-Ca alloy. In addition, Jiang et al. [136] alloyed pure Mg with both 1-3 wt.% Y and 1.5 wt.% Sn. The combination effect of Y and Sn resulted in a higher oxidation resistance than that of single addition of Y. These results indicated synergistic effects of Ca and Y, and Sn and Y so that an alloy containing both alloying elements has a higher oxidation resistance than the alloys with only Ca, Sn or Y. This could be attributed to either a dense oxide layer with a mixture of CaO or SnO_2 and Y_2O_3 or the third element effect, in which the Ca or Sn increased the surface activity of Y in Mg-Y alloys and promoted the formation of Y_2O_3.

Prasad et al. [59] studied the flammability of a series of Mg-Y binary alloys through flame test as illustrated in Fig. 5. Fig. 13 illustrates the ignition behaviour of a Mg-5Y specimen. After initial melting, only minor ignition occurred at the specimen end even after ~90 s exposure to the LPG flame (Fig. 13a), which was extinguished readily even in the presence of the LPG flame (Fig. 13b). Furthermore, the blob of the liquid alloy dropped on the foundry floor and remained unignited. There was a thin oxide on the subsequently solidified blob as

indicated by the interference colours. The resistance to oxidation and burning of the Mg-5Y alloy was attributed to the formation of a Y-containing oxide on the alloy surface, which protected the surface from further oxidation and evaporation [58].

However, large amount of Y addition could result in a decrease in mechanical properties of Mg-Al alloys [137, 138] due to the formation of massive Al_2Y phase. Normally, the Y addition in the Mg-Al system is limited to 0.25 wt.% [111]. Hence, it seems not practical to improve the oxidation resistance of Mg-Al alloys by alloying with Y.

6.2.2 Ce

Cerium has attracted increasing interest in the development of oxidation resistant Mg alloys over the past 60 years [42, 139-141]. AZ31 was surface alloyed with Ce by Wang et al. [142] through ion implantation. There was a lower oxidation weight gain of the implanted AZ31 (Ce ions of 45 keV with a dose of $1\times10^{17}cm^{-2}$) at 500 °C compared with the non-implanted AZ31. However, the oxidation kinetics followed a linear law in both implanted and non-implanted alloys, indicating the oxidation resistance improved by Ce implantation was not significant. It was considered that the pre-formed Ce_2O_3 and CeO_2 layers during implantation were responsible for the improvement of the oxidation resistance.

Recently, Lin et al. [143] found a 50 °C increase in the ignition temperatures of both AZ91 and AM50 alloyed with 0.25 wt.% Ce due to the formation of a compact Ce_2O_3 layer that has the P-B ratio of 1.16. When mixed with MgO, the combined oxide film was regarded as dense with few defects [143]. However, unlike Mg-Y alloys, there was an increased oxidation rate when the Ce content exceeded 0.25 wt.% because of the limits of the solid solubility of Ce in both alloys [143]. Fig. 14 shows the surface morphologies of the oxide films formed on AM50 at 500 °C for 60 min. Without the Ce alloying, the oxide film was loose and porous. After alloying with 0.25 wt.% Ce, as shown in Fig. 14b, the film was almost free of holes or defects and was adherent. Holes and defects emerged on the surface after alloying with 0.45 wt.% Ce due to a decrease in oxide adherence, as shown in Fig. 14c. Similar results were achieved in Lin's study for AZ91D.

The decreased oxidation resistance for Ce contents exceeding 0.25 wt.% was attributed to the formation of a thermally stable $Al_{11}Ce_3$ intermetallic compound, which consumed Ce. The formation of $Al_{11}Ce_3$ resulted in the depletion of Ce around the $Al_{11}Ce_3$ intermetallic

compound [143]. These Ce depleted localized regions became weak points for oxidation as the combined oxide layers on the surface of these regions could no longer provide oxidation protection. A similar result was reported by Li et al. [144] for AZ91. They found that the decreased oxidation resistance could be suppressed by rapid solidification even when the Ce content was as high as 0.98 wt.% in AZ91. Rapid solidification prevented the formation of the $Al_{11}Ce_3$ intermetallic phase.

In addition to the formation of a Ce oxide that could act as a protective film on the surface of the Mg alloy, segregation of cerium as CeO_2 along the MgO oxide grain boundaries could also inhibit the outward diffusion of Mg cations in the solid alloy [131], and therefore retard oxidation. This reactive element effect (REE) of Ce is schematically shown in Fig. 15. When a Mg^{2+} cation meets a Ce oxide particle on a grain boundary, Ce^{4+} cations saturate MgO through the following reaction [26]:

$$\mathrm{CeO_2} + 2\mathrm{Mg_L^{2+}} = \mathrm{Ce_L^{4+}} + 2\mathrm{MgO} + \mathrm{V''_{Mg}} \quad (14)$$

where $Mg_L{}^{2+}$, $Ce_L{}^{4+}$ are Mg and Ce cations in the lattice, respectively, and V''_{Mg} is the Mg vacancy site with double ionisation [65]. The $Ce_L{}^{4+}$ ions along the MgO grain boundaries effectively impede the grain boundary diffusion of Mg^{2+} cations, delaying oxidation. As the diffusion of Mg^{2+} cations becomes slow, the oxidation is mainly controlled by the mobility of O^{2-} anions, which is s slow process. Hence, the growth of MgO decreases, typically by orders of magnitude [27].

Prasad et al. [59] found no beneficial influence of Ce on the burning of Mg-Ce alloys in a liquefied petroleum gas (LPG) flame test as illustrated in Fig. 5. The specimen tips of both Mg-0.5 wt.% Ce and Mg-3 wt.% Ce alloys started to burn after melting.

Small alloying additions of Ce have provided some improvement to the oxidation resistance of Mg alloys. The formation of a compact Ce oxide layer on the surface could protect the substrate from further oxidation. In addition, the reactive element effect of Ce in Mg alloys, which is based on the analogy with Ni-Ce system, may also contribute to the oxidation resistance. However, it is not clear which mechanism dominates. Further investigation is required. Furthermore, contrary to Y, the presence of Ce in Mg alloys has no detrimental

effect on the mechanical properties, particularly in Mg-Al based alloys. Thus, from technological point view, Ce-containing Mg alloys are worth studying further.

6.2.3 Nd

Alloying with neodymium (Nd) to improve the oxidation resistance of Mg alloys has been an active research topic in the last decade. Wang et al. [145] found that Mg-2.87 wt.% Nd and Mg-4.5wt.% Nd were oxidation-resistant up to 500 °C for 90 min. However, there was rapid oxidation weight gains with linear kinetics for Mg-Nd with 11.2 wt.% and 25 wt.% Nd. Aydin and co-workers [46, 146] measured somewhat similar behaviour in their studies of the ignition temperature. There was a sharp 100 °C increase in the ignition temperature for Mg-0.5wt.% Nd, whereafter the ignition temperature remained constant at 770 °C for Nd content up to 6 wt.% [46].

Thermodynamic calculations indicated that the MgO should form prior to Nd_2O_3 during the initial stage of oxidation. As schematically illustrated in Fig. 16, the initially formed MgO decreased the Mg composition on the surface of α-Mg. As a result, the activity of Nd was increased, and Nd_2O_3 formed. The high oxidation resistance was attributed to the formation of a Nd_2O_3/MgO duplex layer. Nd_2O_3 has a P-B ratio of 1.13 [62] and may be a compact layer that can protect the substrate. This model would be valid for a molten alloy only if there was no convection.

However, when the Nd content is over 2.5 wt.%, $Mg_{12}Nd$ intermetallic particles form along the grain boundaries. Oxidation preferentially occurs on the $Mg_{12}Nd$ phases because of the larger change of Gibbs free energy from the reaction of the intermetallic phases with oxygen [146]. In addition, the lower melting temperature of the eutectic microstructure also contributes to the oxidation. Furthermore, in the molten state, as the Nd content increases, the formation of Nd_2O_3 causes local depletion of Nd in the liquid subsurface, leading to Mg vaporisation and ignition [147]. Thus, constant or even reversed oxidation resistance was observed at higher Nd content (above 2.5 wt.%) in both the solid and the molten state.

The effect of Nd on the oxidation of ternary Mg alloys is complex. Arrabal et al. [80] studied the solid-state oxidation resistance and microstructure of AZ91D containing 1.4 wt.% Nd. The oxidation rate at 410 °C of Nd-containing AD91D was 72% of that of the AZ91D alloy [80]. This was attributed to the reduction in selective oxidation of the $Mg_{17}Al_{12}$ β-phase

because Al was consumed through the formation of the stable Al-Nd intermetallic. Hence, the oxidation was delayed due to the smaller volume fraction of the β-phase. In a semi-solid condition, Zhao et al. [148] reported a 20 °C decrease in the ignition temperature of AZ91D containing 0.5 wt.% Nd. This decrease was attributed to the decrease in the liquidus temperature and the low eutectic temperature [148]. However, the ignition temperature was increased by 40 °C in AZ91D containing 5 wt.% Nd. The Nd_2O_3 oxide film was able to re-generate and self-heal cracks or pores on the surface of the molten alloy [148].

Compared with other RE elements, small addition of Nd is able to protect Mg alloys from oxidation. The improvement is attributed to the formation of Nd_2O_3 and the modified intermetallic phases.

6.2.4 Gd

Gadolinium (Gd) can also increase the oxidation resistance of Mg alloys [42]. Arrabal et al. [80] found that alloying AZ91 with 0.7 wt.% Gd suppressed the formation of the unstable $Mg_{17}Al_{12}$ phase, leading to the increase in oxidation resistance in the solid state. Because Mg-Y-Gd based alloys showed a high specific strength at both room and elevated temperatures [149], the study of Gd on oxidation was focused on Y-containing alloys. Liu et al. [150] studied the solid-state oxidation behaviour of an Mg-Gd-Y-Zr alloy within the temperature range from 230 to 300 °C in both O_2 and O_2 + H_2O atmospheres. Gd and Y-containing Mg alloys showed low oxidation rates and negligible oxidation weight gains after 10 hour exposure in both atmospheres. The low oxidation rates were attributed to a multi-oxide layer consisting of MgO, Y_2O_3 and Gd_2O_3 on the surface, which protected the alloy from further oxidation. Wang et al. [151] studied the oxidation kinetics of a Mg-10Gd-3Y alloy in both the solid and semi-solid states. The oxide growth kinetics obeyed the parabolic law within the temperature range from 450°C to 600 °C, as shown in Fig. 17. Because of the protective effect by both Y and Gd, neither linear growth nor catastrophically exponential kinetics occurred even at 600 °C for up to 90 min. This indicates that the protection also applied to the semi-molten alloys.

Kim et al. [105] studied the ignition of binary Mg-0.48 at.% Gd (Mg-3Gd). The ignition temperature was 707 °C. This temperature is significantly above the melting temperature of the alloy, and higher than that of Mg-3Ce and Mg-3La, for which the ignition temperatures

were 630 °C and 524 °C, respectively. Because of the P-B ratio of 1.29, Gd_2O_3 is a compact oxide that could protect the substrate from further oxidation, even when the alloy was molten. Kim and co-workers [105] claimed the higher solubility of Gd in Mg (23.5 wt.%) was responsible for the better protection. The solute concentration in the matrix increased due to the dissolution of the intermetallic phases with increased temperature. A higher solubility enabled the solute to fully homogenize in matrix during oxidation, promoting the formation of the dense layer during oxidation. Recently, Wu et al. [152] reported a high-strength, ignition-proof Mg-15.3Gd-1.9Ag-0.3Zr (GQ152K) Mg alloy that had a high ignition temperature of 935 °C. Furthermore, this alloy was able to withstand a flame at 930 °C for over 6 min. The good resistance to oxidation and good resistance to burning was attributed to the dense Gd_2O_3 and Ag_2O films on the surface.

These experimental results indicate that addition of Gd in Mg alloys appears to be an effective approach to develop new Mg alloys with improved oxidation and ignition resistance for applications at elevated temperatures.

6.2.5 La

Alloying with La and La oxide has been used to improve the mechanical properties of aluminium alloys [153, 154] but there have been limited studies on alloying with La or La oxide in Mg alloys. In 1946, Leontis and Rhines indicated that alloying with La or La oxide delayed oxidation of Mg alloys [42]. Recently, Zhao et al. [155] added La and La_2O_3 into AZ31 and found that the oxidation weight gain at 450 °C was slightly decreased compared with AZ31 without such alloying additions, as shown in Fig. 18. In Fig. 18, as La_2O_3 decomposed into La and O_2 in the Mg melts, the La_2O_3 additions were converted into La. For AZ31 alloyed with La, the lowest oxidation rates was at 0.75 wt.% La, as shown in Fig. 18a. For AZ31 with addition of La_2O_3, AZ31-0.74 wt.% La exhibited the lowest oxidation rate, as shown in Fig. 18b. The oxidation weight gains of both alloys were similar, and higher La content led to higher oxidation rates in both conditions [155].

The small protective effect of alloying with La was attributed to the formation of a duplex oxide film consisting of La_2O_3 and Al_2O_3 on the surface of the Mg-Al base alloys [156]. The P-B ratio of La_2O_3 is 1.11 [105], indicating the possibility of a compact layer. Fan et al. [157] also considered La_2O_3 as an effective inhibiter to oxygen diffusion even at high temperatures.

The increase in oxidation rate at the higher La content was attributed as a result of a reduced amount of β-$Mg_{17}Al_{12}$ in the AZ31 [155]. The "necklace" β-$Mg_{17}Al_{12}$was assumed to be an oxidation barrier [155]. A higher content La reacted with Al, forming $Al_{11}La_3$, which consumed Al in the matrix. Thus, the "necklace" β-phase was broken into discrete particles that could not delay the diffusion of ions. However, this hypothesis was not convincing because it neglected the fact that the α-Mg and β-phase eutectic structure with low melting temperature could accelerate the oxidation as discussed before [80]. The current authors consider that it is more likely that the higher La contents caused a decrease in the incipient melting of the alloy.

The weight gain kinetics in Fig. 18 indicates that the oxidation incubation period (the period of parabolic kinetics) of the AZ31-La alloys was short for all La contents. Then there was linear oxidation kinetics for all samples regardless of the content of La, which indicated that the onset of accelerated oxidation was not delayed by La. This was attributed to the low solid solubility of La in Mg, which restricted the formation of a La_2O_3 film [105].

Recently, Zhang and co-workers [158] conducted first-principle calculation and predicted a preferential segregation of La atoms on a Mg (0001) surface, and exothermic O adsorption. The released heat on the La-alloyed Mg (0001) surface was less than that on the pure Mg (0001) surface, which was assumed to be beneficial for increasing the ignition temperature of the Mg-La alloy. In addition, Zhang [158] also found that ionic bonding predominates in MgO, but that the bonds of La_2O_3 were more covalent, inferring that La_2O_3 is more compact. However, the low solid solubility of La in Mg limits the formation of the oxide. Hence, La is not a practical solute in improving the oxidation resistance of Mg alloys in the solid or semi-solid state. This could also be the main reason for the lack of interest in studying the oxidation behaviour of Mg alloys containing La.

6.3 Be

Beryllium (Be) has long been known to be beneficial to Al and Mg alloys. Small amounts of Be reduce tarnishing and the corrosion of Al at room and elevated temperatures [159]. In addition, Be can help purify Mg melts through reducing the level of inclusions, such as iron and other impurities [160]. Furthermore, small amounts of Be alloying into both Al or Mg alloys can decrease the oxidation rate [159, 161, 162] . Be is one of a few elements that has a higher affinity to oxygen than that of magnesium [160]. Thus, the assumption has been that

the decrease in oxidation rate is attributable to the formation of BeO [26, 163]. Most studies of Be containing Mg alloys and Be containing Al alloys were based on the molten state. For example, Houska [161] reported an increase in the ignition temperature of pure Mg by 200 °C through alloying with 10 ppm (wt) Be. Wikle claimed a dense BeO oxide film formed during casting Be containing Al alloys [164]. Because of the high P-B ratio of BeO (1.70) [62], the BeO film was considered a barrier to prevent oxygen penetration. Huang et al. [165] reported an increase of 200 °C in the ignition temperature of a Mg-2Ca alloy after alloying with 300 ppm (wt) Be. Zeng et al. [166, 167] reported that 0.3 wt.% Be-containing AZB910 could be melted without burning, even without a shielding gas. Fig. 19 shows macrographs of the melts of both the AZ91 and the AZB910 at 650 °C. The AZ91 melt was covered by lots of oxides (Fig. 19a) while the surface on the AZB910 was smooth and clear, indicating a higher oxidation resistance (Fig. 19b).

Through XRD and AES analysis, Zeng [166] detected an enriched Be and O layer near the surface of the AZB910. Fig. 20 presents the AES results that show the concentration profiles of the major alloying elements as a function of depth for the AZ91 and AZB910. The outmost layers (sputtering time = 0) of both alloys were enriched by Mg and O. Furthermore, the amount of Mg was slightly higher than O, suggesting Mg was in excess of that required for MgO. This is attributed to the outward diffusion of Mg^{2+} cations, which control the oxidation [26]. Below the outmost layer of both alloys, there were variations of Mg content accompanied with continuous decreases of O concentration. The V-like variation of Mg content in both alloys was attributed to the overlap of the decreasing Mg^{2+} cation concentration in the oxide and the increasing metallic Mg concentration [166]. For the AZB910, as shown in Fig. 20b, the decreasing Mg^{2+} was accompanied by an increase of Be content, indicating a mixed inner layer of BeO and MgO. This has been regarded as experimental evidence supporting the hypothesis that the high oxidation resistance of Be-containing Mg alloys is attributed to the formation of BeO [166].

Zeng et al. [167] also compared the oxidation resistance AZ91 containing 0.3 wt.% Be with AZ91 containing 5 ppm (wt) Be, and found that AZ91-5 ppm (wt) Be showed rapid oxidation at 650 °C. This implies effective protection of the Mg alloy requires a considerable amount of Be. This result was inconsistent with previous conclusion that low oxidation rates could be achieved with 5-10 ppm (wt) Be [161].

It would be expected that a stable protective BeO film requires Be to be oxidized in preference to the oxidation of Mg. The reaction of Be with MgO is as follows [167]:

$$\mathrm{Be(l) + MgO(s)} = \mathrm{BeO(s)} + \mathrm{Mg(l)} \quad (15)$$

The change of free energy in this reaction is [167]:

$$\Delta G = \Delta G^0 + \mathrm{R}T\ln\frac{\alpha_{\mathrm{Beo}}\alpha_{\mathrm{Mg}}}{\alpha_{\mathrm{MgO}}\alpha_{\mathrm{Be}}} = \Delta G^0 + \mathrm{R}T\ln\frac{\alpha_{\mathrm{Mg}}}{\alpha_{\mathrm{Be}}} \quad (16)$$

where ΔG^0 is the change of Gibbs free energy in the standard state (25 °C, 1 atm), T is the reaction temperature (in K), R is the gas constant and α represents the activity. MgO and BeO are regarded as pure solids, so both α_{BeO} and α_{MgO} are equal to 1. Applying equation (16) to the work of Zeng et al. [166] indicates that the equilibrium Be concentration is 0.88 wt.% at 650 °C. BeO could form in preference to MgO only if the concentration of Be was higher than the equilibrium concentration. Due to the segregation effect, 0.3 wt.% Be in AZ91 could possibly satisfy this thermodynamic requirement. However, when the Be concentration was as low as 5-10 ppm (wt), it would be difficult to accumulate Be up to 0.88 wt.% through segregation. Thus, experimental evidence is required to verify this hypothesis in Mg alloys containing trace of Be.

There are few studies on the oxidation of solid-state Mg alloys that contain Be. Czerwinski [168] studied the early stage of semi-solid oxidation of Be-bearing AZ91. The onset of accelerated oxidation at 487 °C was delayed by 10 ppm (wt) Be. For comparison, Czerwinski [168] reported that the alloy containing 5 ppm (wt) Be suffered rapid oxidation at the same temperature, whereas the surface of the alloy with 10 ppm (wt) Be was smooth and apparently free of oxide. Furthermore, Czerwinski [168] also investigated the weight variations of these two alloys at 487 °C in an argon atmosphere. The results are shown in Fig. 21. At the beginning, both alloys gained some weight, possibly from the reaction of Mg with the residual oxygen in the argon. Subsequently, there was weight loss, attributed to Mg evaporation. This weight loss for the 10 ppm (wt) Be-containing alloy was somewhat lower than that of the 5 ppm (wt) Be-containing alloy. This implies an evaporation suppression by

the higher amount of Be [168]. Unfortunately, the actual mechanism about how the Be supressed the Mg evaporation was not discussed.

More recently, Tan et al. [169] studied the oxidation resistance in the solid state of AZ91 micro-alloyed with Be. The oxidation weight gain at 400 °C was reduced with increasing Be content from 10 ppm (wt) to 60 ppm (wt), indicating an increase in oxidation resistance. The increased oxidation resistance was achieved by effectively extending the incubation period. In addition, Tan [169] claimed that a continuous BeO layer did not exist based on the thermodynamic calculation and EDS results. Unfortunately, there was no mechanism studies.

Based on the reactive element effect (REE) observed in NiO [170, 171], where segregation of Ce-ions along NiO grain boundaries effectively impedes the diffusion of Ni^{2+} cations, Czerwinski [168] attributed the decrease in the oxidation rate of Be-containing Mg alloys to the REE of Be. The Be^{2+} cations might segregate along the MgO grain boundaries to inhibit the outward diffusion of Mg^{2+} cations along the grain boundaries. As a result, the oxidation would be governed by the inward diffusion of oxygen ions. Since diffusion of oxygen ions is a sluggish process, the oxidation rate is considered to be reduced by orders of magnitude [172]. However, experimental evidence is required to verify this hypothesis.

Because Be has high toxicity [111] and causes grain coarsening of Mg alloys [173], the maximum acceptable content of Be in Mg alloy casting was claimed to be 0.01 wt.% (100 ppm (wt)) [166, 167, 173, 174]. Trace addition of Be can significantly increase the oxidation resistance of Mg alloys, particularly for Mg-Al based alloys in both the solid and molten state. However, the actual mechanism is not clear. Thus, further study on the oxidation resistance of Be containing Mg alloys is needed in developing new oxidation-resistant non-flammable Mg alloys.

6.4 Sr

The surface activity of an alloying element may also influence the oxidation rate. In Mg, the elements Sr, Ca, Ce, Nd, Sn, Se, Te and Li, have been regarded as surface active [175]. Previous studies found that alloying with strontium (Sr) decreased the oxidation rate of Al alloys [176, 177]. Aydin and co-workers [178] studied the oxidation behaviour of Mg-2.5 wt.% Sr and Mg-6 wt.% Sr alloys in the solid state at 500 °C. Fig. 22 shows that the oxidation had two stages: (i) the initial parabolic-oxidation stage which is also considered the incubation

period; and (ii) the stage with accelerated oxidation with linear kinetics. Alloying with Sr addition delayed the onset of linear oxidation kinetics [178].

Pekguleryuz et al. [179] reported that the effect of 75 ppm (wt) Sr addition on the oxidation rate of molten AZ91 at 680 °C for 5 hour was similar to alloying with 9 ppm (wt) Be. This result indicated that the usage of toxic Be could be replaced by Sr in molten Mg alloys. Aydin et al. [180] found that the ignition temperature of Mg-6 wt.% Sr was 200 °C higher than that of pure Mg. Fig. 23 shows that the ignition temperatures of Mg-Sr binary alloys increased with Sr content. The ignition temperature of Mg-6Sr (J6) was 854 °C, which was higher than that of the WE43 [48]. There were duplex MgO and SrO oxide layers on the Sr-containing alloys in both the solid and molten states after oxidation [178, 180]. Unlike Ce, Nd and La [46, 143, 146, 155], higher Sr contents led to higher ignition temperatures due to the high surface activity of Sr in liquid Mg [181]. Based on thermodynamic calculations [180], at 700 °C, SrO formed prior to MgO once the Sr content on the surface exceeds 75 wt.%. In addition to the formation of SrO, the oxide grain size was decreased with increasing Sr content [178]. Although finer grain size offers more grain boundaries for ion diffusion [27], Aydin claimed that the stress in the oxide could be released by the grain boundaries, resulting in a lower tendency to cracking.

Alloying with Sr does not significantly increase the oxidation resistance of solid Mg alloys because of the sluggish accumulation of Sr on the surface through segregation in the solid state. In contrast, due to the surface activity in liquid Mg, small additions of Sr effectively increase the oxidation resistance of molten Mg alloys. In addition, the ignition temperature is increased with higher Sr contents. Hence, development of Sr-containing Mg alloys is a promising approach for ignition-proof applications.

6.5 Nano-sized or micro-sized particles

Some Mg alloys containing nano-sized or micro-sized ceramic particles, such as graphene, chromium oxide (Cr_2O_3), aluminium oxide (Al_2O_3) and silicon dioxide (SiO_2) have shown improved mechanical properties, and decreased corrosion rates [182-187]. The use the ceramic particles to enhance the oxidation resistance in Mg alloys was first reported by Nguyen and co-workers [188]. AZ31B containing 1.5 vol.% Al_2O_3 particles exhibited a lower oxidation rate at 400 °C than that of AZ31B, due to the uniform distribution of nano-Al_2O_3

particles in the AZ31B matrix, restricting the migration of Mg ions [188]. However, non-protective oxidation occurred at 450 °C. The alloy containing nano-Al_2O_3 particles did not have a longer transition from parabolic to linear oxidation kinetics at the higher temperature, indicating no improvement in forming a compact protective oxide film.

SiC particles have been used to enhance the mechanical properties and wear resistance [189-192]. An enhancement of oxidation resistance in AM60, AZ91D and ZC63 by adding micro-sized SiC particles was reported [40, 193, 194]. Nguyen et al. [194] studied the oxidation kinetics of the AZ91D-(0, 5, 10, 20) wt.% SiC particles reinforced composite at both 430 °C and 450 °C in air. At 430 °C, the alloy with 5 wt.% SiC particles had lower oxidation weight gain and the weight gain decreased continuously with increasing the content of SiC particles. However, at 450 °C, rapid oxidation occurred in all alloys except for the alloy containing 20 wt.% SiC particles.

Nguyen and Lee [193] reported a similar result for AM60 containing 10 wt.% SiC. The oxidation rate of AM60 at 450 °C was 0.068 mg cm^{-2} h^{-1}, while the AM60-10 wt.% SiC composite had a nearly 10 times lower oxidation rate of 0.0066 mg cm^{-2} h^{-1}. The ignition temperature was also increased from 523 °C to 603 °C. Because the SiC particles were homogeneously dispersed in the alloys without any decomposition or oxidation, the reduced specific areas for oxidation was considered as the major cause of decreased oxidation. In a Ti-Al alloy, Lee et al. [195] found that uniformly distributed SiC particles acted as heterogeneous nucleation sites for oxide grains. Thus, a continuous dense Ti oxide layer was quickly formed. However, this hypothesis is not valid in Mg alloys as MgO is not protective due to the low P-B ratio.

Addition of nano or micro-sized ceramic particles in Mg alloys shows a beneficial effect on the oxidation resistance in both the solid and molten state. Compared with conventional alloying elements, the increased oxidation resistance is attributed to reducing the specific areas for oxidation instead of forming compact oxide layers. This mechanism might be used as a new approach to develop new oxidation resistant Mg alloys.

7. Discussion on the incubation period

Table 1 summarizes the published data on incubation periods of Mg alloys at various temperatures. The term “over” in Table 1 indicates that the oxidation tests were

terminated within the incubation period. In this case, the incubation period is designated by the maximum test duration with the prefix of "over".

The data in Table 1 can be divided into 3 groups.

The first group has pure Mg as a reference alloy, and considers the alloying elements Al and Zn. At 500 °C, pure Mg had an incubation period of 440 min. Alloying with Al or Zn, such as the alloys AM50, AM60, AE42 and ZE41, decreased the incubation period at 500 °C. The reduction in oxidation resistance is attributed to the lowering of the melting temperatures of the alloy and formation of a low melting temperature eutectic microstructure consisting of α-Mg solid solution and intermetallic compound.

Alloying with RE elements and Sr increased the incubation period at 500 °C compared with pure Mg. Alloying with 0.5 wt.% Nd increased the incubation period to 670 min at 500 °C due to the formation of a dense Nd_2O_3 layer on the surface that suppressed further oxidation. Alloying with 2.5 wt.% Sr increased the incubation period to over 700 min at 500 °C. Fig. 24 compares Mg-Nd alloys and Mg-Sr alloys in terms of the oxidation resistance in the solid and molten states, respectively. Fig. 24a indicates that the oxidation kinetics for the Mg-Sr alloys in the solid state was similar to that of the Mg-Nd alloys. The weight gains of Mg-2.5Nd, Mg-2.5Sr and Mg-6Sr are similar within the test period. For the alloy with high content of Nd, the $Mg_{12}Nd$ intermetallic phases formed along the grain boundaries, oxidation preferentially occurs on the intermetallic phases [146]. Thus, the initial weight gain of Mg-6Nd increases significantly. The subsequent formation of Nd_2O_3 layer can protect the alloy from further oxidation, leading to an increase in the oxidation incubation period. In contrast, in molten Mg alloys, Fig. 24b indicates that there was an obvious difference between Nd and Sr. There was an increase in the ignition temperature when the Nd increased to 0.5 wt.%, but there was no further increase with further addition of Nd. In comparison, the effect of Sr was more remarkable. The ignition temperature of Mg increased continuously with increasing Sr content, and reached 854 °C for 6 wt.% Sr. In molten Mg, Sr accumulates on the surface because of its surface activity in liquid Mg. Thus, the formation of SrO is promoted, and the surface oxide can suppress Mg vaporisation.

Other reported incubation period data are listed in the five rows just below the Mg-6Sr in Table 1, showing the effect of the RE elements, such as Gd and Y, and Ca. Although no actual incubation period are reported, particularly at 500 °C, these alloying elements should

increase the oxidation resistance of pure Mg through the formation of denser combined oxide layers. Thereby, vaporisation of Mg is suppressed.

The third group of data compares the incubation period of AZ91-base alloys at either 400 or 450°C. Alloying with Ca, Y, Be and SiC nanoparticles increased the oxidation incubation period. Be was particularly effective. Alloying with 60 ppm (wt) Be extended the incubation period of AZ91 from 150 min to over 300 min. Fig. 25 presents the oxidation data of Cheng et al. [111] and Tan et al. [169] for AZ91-1.5Ca, AZ91-1.5Ca-0.5Y, AZ91-20 ppm (wt) Be and AZ91-60 ppm (wt) Be at 400 °C in air. AZ91 containing 20 ppm (wt) Be showed a lower oxidation rate than that of AZ91-1.5Ca. The incubation period of the AZ91 containing 60 ppm (wt) Be exceeded 300 min. For AZ91-1.5Ca, linear kinetics occurred after 270 min. In addition, the weight gain curve of AZ91 containing 60 ppm (wt) Be was lower and became flat after 220 min. Compared with AZ91-1.5Ca-0.5Y, the AZ91 containing 60 ppm (wt) Be had a lower weight gain at the end of the test, indicating a better oxidation resistance. In the molten state, a 0.3 wt.% Be-containing AZB910 was reported to be melted in air [166]. Thus, small addition of Be can increase the oxidation and ignition resistance of Mg alloys. But, the mechanism is still in controversial. The formation of BeO has been detected on molten Be-containing Mg alloys. However, in the solid state, there is a lack of evidence verifying the existence of a BeO layer. It appears that the oxidation in the solid or semi-solid state is controlled by the combined effects of Mg-ion diffusion, Mg vaporisation and the intermetallic phase. Thus, in the solid or semi-solid state, addition of Be may retard the diffusion of Mg-ions by the reactive element effect (REE). In addition, based on the analogy with Ca, Be may segregate along the grain boundaries and enhance the thermal stability of intermetallic phases.

8. Discussion on ignition temperature

The P-B ratio of the oxide of the main alloying element has been regarded as a key factor that controls the oxidation resistance and ignition temperature of Mg alloys. Table 2 summarizes the ignition temperatures (T_i) of Mg alloys with different shapes and the P-B ratio of the oxides of the main alloying elements. The ignition temperature varies significantly as a function of shape, indicating once again that the ignition temperature is critically dependant on how it is measured. With the same chemical composition, the ingot samples have higher ignition temperatures than chips and powders. For example, the ignition temperature of a

pure Mg ingot ranges from 620-650 °C [45-47] while pure Mg chip and powder ignite at lower temperatures of 504 °C [105] and 437 °C [82], respectively. Compared with ingot sample, the chip and powder samples have higher specific contact area with oxygen, leading to a lower ignition temperature. The ignition temperature also depends on the experimental condition. Lower ignition temperatures are measured for the test with slower heating rate and for samples with greater specific surface area, indicating the critical factor in ignition is the accumulation of a critical concentration of Mg vapour.

Table 2 shows that most alloying elements, except for Ca and Sr, are associated with the P-B ratio values for their oxides between 1 and 2, indicating the potential to protect the Mg matrix from oxidation. However, alloys with Al and Zn have decreased ignition resistance. For example, alloying with 3 wt.% Al decreased the ignition temperature of a pure Mg chip from 504 °C to 474 °C [105]. This decrease is attributed to the decreased melting temperature of the alloy. In addition, although some elements such as Ce and La have higher values of the P-B ratio, they do not noticeably increase the ignition temperature. This is attributed to their low solute solubility in Mg (1 wt.% for La and 0.52 wt.% for Ce) [105].

Fig. 26 presents the ignition temperatures (T_i) of some binary Mg alloys chips and the solute solubility of the alloying elements in Mg according to data from Kim et al. [105]. Mg alloys alloyed with alloying elements with high solubility have relatively high ignition temperatures. A high solubility enables the homogenization of solute elements in the matrix, and allows the formation of a dense oxide layer during oxidation [105]. Hence, despite the similar P-B ratios of Y_2O_3, La_2O_3, Ce_2O_3 and Gd_2O_3, Mg-3Y and Mg-3Gd have higher ignition temperatures due to their higher solubilities in Mg (11.4 wt.% for Y and 23.5 wt.% for Gd). In addition, although the solubility of Ca in Mg is only 1.34 wt.%, the dissolution of Mg-Ca eutectics increases the content of Ca in the Mg matrix, promoting the formation of CaO during heating. Hence, the presence of Ca can improve the ignition resistance of the Mg matrix. In the case of Sr, although its solubility in Mg is low (0.11 wt.%) and the P-B ratio of SrO is only 0.66, accumulation of Sr on the surface can be achieved due to its surface activity in liquid Mg. Thus, the formation of SrO is significantly promoted after melting. In the case of Be, even though the solute solubility of Be in Mg is almost zero [169], a Mg-0.15Be alloy exhibits an ignition temperature of 750 °C [198]. Furthermore, microalloying of Mg-Ca alloy with Be produced a significantly higher ignition temperature of 1050 °C [165] as shown in Table 2. Based on the analogy with Sr, the excellent ignition resistance by micro-alloying with Be

may also be attributed to a surface active effect. However, experimental evidence is required to verify this hypothesis.

In addition, melting temperature, localized melting temperature in particular, also defines the ignition temperature. Due to the low melting temperature of the Mg-Al eutectic microstructure, the ignition temperature of AZ91 is lower than that of pure Mg. However, alloying with Ca can partially consume the Al solute through forming Al-Ca intermetallics, and therefore reduce and even eliminate the Mg-Al eutectic microstructure. Hence, Ca alloying can significantly increase the ignition temperature of the AZ91 alloy.

9. Concluding discussion

Published work indicated that although the MgO formed on the surface of Mg alloys can protect Mg from oxidation at temperatures up to approximately 400 °C, rapid oxidation and ignition occurs at temperature above approximately 400 °C. This is attributed to the combined effects of the incompact structure of MgO, fast diffusion of Mg ions, Mg vaporisation and melting of intermetallic phases in the eutectic microstructure. The oxidation resistance is decreased by the common alloying elements, Al, Zn and Cu. For example, Al promotes Mg evaporation by the formation of the β-phase, which forms low melting temperature eutectic microstructure with α-Mg, and Zn tends to sublime leading to the formation of pores within both the matrix and the oxide.

The development of oxidation resistant Mg alloys is based on the chemical and microstructural modification of the surface oxide film by alloying elements to increase the P-B ratio of the oxides formed. For example, alloying with Ca and RE elements has been experimentally confirmed as an effective way to increase the oxidation resistance of Mg alloys. In addition, the “reactive element effect” (REE) and surface active effect should also be taken into consideration during the development of new alloys. For example, alloying with Be or Sr has good performance in improving the oxidation resistance of Mg alloys in both the solid and molten states.

10. Conclusions

i. Magnesium oxide, MgO, which has a low P-B ratio (0.81), provide little protection to Mg substrates from thermal oxidation at high temperatures.

ii. Lattice diffusion by a vacancy mechanism, which is a sluggish process, is assumed to dominate the Mg transport at temperatures below approximately 400 °C. Hence, the thin MgO is considered protective and the oxidation rate of Mg alloys at temperatures below approximately 400 °C is low, following parabolic kinetics.

iii. Non-protective oxidation with linear kinetics occurs at temperatures above approximately 400 °C after an incubation period. This is attributed to the combined effects of faster diffusion of Mg ions, Mg vaporisation and melting of intermetallic phases. The onset of non-protective oxidation is associated with the growth of oxide nodules.

iv. Further increasing the temperature and/or continuing oxidation at high temperatures above approximately 400 °C may cause ignition and burning of Mg alloys. Mg vapour is the burning species. The large amount of heat generated during burning makes Mg flames difficult to extinguish. The cauliflower surface morphology is regarded a result of burning of Mg alloys.

v. The ignition temperature depends on the experimental conditions. Lower ignition temperature are measured for the test with slower heating rate and for samples with greater specific surface area.

vi. Common alloying elements Al, Zn and Cu increase the oxidation rate and decrease the ignition temperature. The effect of Mn on the oxidation resistance of Mg alloys is small.

vii. The alloying elements Ca, Y, Ce, Nd, Gd, La, Be and Sr decrease the oxidation rate and increase the ignition temperature in both pure Mg and Mg alloys through the formation of compact layers on the surface and/or the formation of thermally stable intermetallic phases. Alloying with nano-sized and/or micro-sized Al_2O_3 and SiO_2 particles decrease the oxidation rate of Mg alloys in the solid and semi-solid state. This is attributed to the reduced specific areas for oxidation.

Acknowledgement

The authors are very grateful to the Australian Research Council for funding support.

References

[1] H. Davy, Electron-chemical researches on the decomposition of the earths; with observations on the metals obtained from the alkaline earths, and on the amalgam procured from ammonia, Philos. Trans. R. Soc. Lond., 98 (1808) 333–370.

[2] M.T. Weller, T. Overton, J. Rourke, F.A. Armstrong, Inorganic Chemistry, sixth ed., Oxford University Press, Oxford, 2006.

[3] E. Lee Bray, Magnesium, in: Minerals Yearbook, United States Geological Survey, < http://minerals.usgs.gov/minerals/pubs/commodity/magnesium/>, 2013 (accessed 20.12.15).

[4] J. Buha, Mechanical properties of naturally aged Mg–Zn–Cu–Mn alloy, Mater. Sci. Eng.: A 489 (2008) 127-137.

[5] J. Jeon, S. Lee, B. Kim, B. Park, Y. Park, I. Park, Effect of Sb and Sr addition on corrosion properties of Mg-5Al-2Si alloy, J. Korean Inst. Met. Mater. 46 (2008) 304-309.

[6] J.H. Jun, J.M. Kim, B.K. Park, K.T. Kim, W.J. Jung, Effects of rare earth elements on microstructure and high temperature mechanical properties of ZC63 alloy, J. Mater. Sci. 40 (2005) 2659-2661.

[7] B.S. Shin, Y. Kim, D.H. Bae, Deformation behavior of a wrought Mg-Zn-RE alloy at the elevated temperatures, J. Korean Inst. Met. Mater. 46 (2008) 1-5.

[8] G.L. Song, A. Atrens, Corrosion Mechanisms of Magnesium Alloys, Advanced Engineering Materials 1 (1999) 11-33.

[9] I. Toda-Caraballo, E.I. Galindo-Nava, P.E.J. Rivera-Diaz-del-Castillo, Understanding the factors influencing yield strength on Mg alloys, Acta Mater. 75 (2014) 287-296.

[10] W.Q. Xu, N. Birbilis, G. Sha, Y. Wang, J.E. Daniels, Y. Xiao, M. Ferry, A high-specific-strength and corrosion-resistant magnesium alloy, Nat. Mater. 14 (2015) 1229-1235.

[11] A. Atrens, G.L. Song, M. Liu, Z.M. Shi, F.Y. Cao, M.S. Dargusch, Review of Recent Developments in the Field of Magnesium Corrosion, Adv. Eng. Mater. 17 (2015) 400-453.

[12] S. Abaspour and C.H. Cáceres, Thermodynamics-Based Selection and Design of Creep-Resistant Cast Mg Alloys, Metall. Mater. Trans. A 46 (2015) 5972-5988.

[13] S. Johnston, Z.Shi, A. Atrens, The influence of pH on the corrosion rate of high-purity Mg, AZ91 and ZE41 in bicarbonate buffered Hanks' solution, Corros. Sci. 101 (2015) 182-192.

[14] F. Cao, Z.Shi, G.L. Song, M. Liu, M.S. Dargusch, A. Atrens, Influence of hot rolling on the corrosion behaviour of several Mg-X alloys, Corros. Sci. 90 (2015) 176-191.

[15] F. Cao, Z.Shi, G.L. Song, M. Liu, A. Atrens, Corrosion behaviour in salt spray and in 3.5 % NaCl solution saturated with $Mg(OH)_2$ of as-cast and solution heat-treated binary Mg-X alloys: X = Mn, Sn, Ca, Zn, Al, Zr, Si, Sr, Corros. Sci. 76 (2013) 60-97.

[16] K. Schlüter, Z.Shi, C. Zamponi, F. Cao, E. Quandt, A. Atrens, Corrosion performance and mechanical properties of sputter-deposited MgY and MgGd alloys, Corros. Sci. 78 (2014) 43-54.

[17] Z. Shi, F.Cao, G.L. Song, M. Liu, A. Atrens, Corrosion behaviour in salt spray and in 3.5 % NaCl solution saturated with $Mg(OH)_2$ of as-cast and solution heat-treated binary Mg-RE alloys: RE = Ce, La, Nd, Y, Gd, Corros. Sci. 76 (2013) 98-118.

[18] M.M. Avedesian, Magnesium and magnesium alloys, ASM international, Materials Park, OH, 1999.

[19] X. Yu, B. Jiang, H. Yang, Q. Yang, X. Xia, F. Pan, High temperature oxidation behavior of Mg-Y-Sn, Mg-Y, Mg-Sn alloys and its effect on corrosion property, Appl. Surf. Sci. 353 (2015) 1013-1022.

[20] B. Kondori, R. Mahmudi, Impression creep characteristics of a cast Mg alloy, Metall. Mater. Trans. A 40 (2009) 2007-2015.

[21] A.A. Luo, Recent magnesium alloy development for elevated temperature applications, Int. Mater. Rev. 49 (2004) 13-30.

[22] M.O. Pekguleryuz, A.A. Kaya, Creep resistant magnesium alloys for powertrain applications, Adv. Eng. Mater. 5 (2003) 866-878.

[23] F. Czerwinski, Overcoming Barriers of Magnesium Ignition and Flammability, Adv. Mater. Process. 172 (2014) 28-31.

[24] C.C. Liu, S. Lu, Y.T. Fu, H.P. Zhang, Flammability and the oxidation kinetics of the magnesium alloys AZ31, WE43, and ZE10, Corros. Sci. 100 (2015) 177-185.

[25] J.F. Fan, C.L. Yang, G. Han, S. Fang, W.D. Yang, B.S. Xu, Oxidation behavior of ignition-proof magnesium alloys with rare earth addition, J. Alloys Compd. 509 (2011) 2137-2142.

[26] F. Czerwinski, Oxidation Characteristics of Magnesium Alloys, JOM 64 (2012) 1477-1483.

[27] F. Czerwinski, The reactive element effect on high-temperature oxidation of magnesium, Int. Mater. Rev. 60 (2015) 264-296.

[28] A.P. Chermyshev, V.A. Petrov, V.E. Titov, A. Vorobyev, Thermal radiative properties of magnesium oxide at high temperatures, Thermochim. Acta 218 (1993) 195-209.

[29] V. Fournier, P. Marcus, I. Olefjord, Oxidation of magnesium, Surf. Interface Anal. 34 (2002) 494-497.

[30] G. Song, A. Atrens, Understanding magnesium corrosion. A framework for improved alloy performance, Adv. Eng. Mater. 5 (2003) 837-858.

[31] F. Czerwinski, Factors affecting the oxidation nature of magnesium alloys, JOM 56 (2004) 29-31.

[32] F. Czerwinski, The oxidation behaviour of an AZ91D magnesium alloy at high temperatures. Acta Mater. 50 (2002) 2639-2654.

[33] N.E. Hakiki, Comparative study of structural and semiconducting properties of passive films and thermally grown oxides on AISI 304 stainless steel, Corros. Sci. 53 (2011) 2688-2699.

[34] V. Maurice, H. Peng, L.H. Klein, A. Seyeux, S. Zanna, P. Marcus, Effects of molybdenum on the composition and nanoscale morphology of passivated austenitic stainless steel surfaces, Faraday Discuss. 180 (2015) 151-170.

[35] G. Okamoto, Passive film of 18-8 stainless steel structure and its function, Corros. Sci. 13 (1973) 471-489.

[36] P. Marcus, C. Hinnenn, I. Olefjord, Determination of attenuation lengths of photoelectrons in aluminium and aluminium oxide by angle-dependent x-ray photoelectron spectroscopy, Surf. Interface Anal. 20 (1993) 923-929.

[37] K. Mizuno, A. Nylund, I. Olefjord, Influence of Mg and Si on the oxidation of aluminum, Oxid. Met. 50 (1998) 309-325.

[38] J. Medved, P. Mrvar, M. Vončina, Oxidation Resistance of Cast Magnesium Alloys, Oxid. Met. 71 (2009) 257-270.

[39] L.P.H. Jeurgens, M.S. Vinodh, E.J. Mittemeijer, Initial oxide-film growth on Mg-based MgAl alloys at room temperature, Acta Mater. 56 (2008) 4621-4634.

[40] D. Lee, T. Nguyen, Y. Kim, Oxidation of ZC63 Mg alloys reinforced with SiC particles between 390 °C and 500 °C in air, Met. Mater. Int. 16 (2010) 761-766.

[41] M.D. López, C.J. Múnez, M. Carboneras, P. Rodrigo, M.D. Escalera, E. Otero, Influence of temperature on oxidation behaviour of ZE41 magnesium alloy, J. Alloys Compd. 491 (2010) 131-136.

[42] T. Leontis, F. Rhines, Rates of High Temperature Oxidation Of Magnesium And Magnesium Alloys, Trans. Am. Inst. Min. Metall. Eng. 166 (1946) 265-294.

[43] F. Czerwinski, Controlling the ignition and flammability of magnesium for aerospace applications, Corros. Sci. 86 (2014) 1-16.

[44] E.A. Gulbransen, The Oxidation and Evaporation of Magnesium at Temperatures from 400 °C to 500 °C, J. Electrochem. Soc. 87 (1945) 589-599.

[45] B.L. Bobryshev, Y.P. Aleksandrova, Ignition of Magnesium and its alloys, Met. Sci. heat Treat. 30 (1988) 219-222.

[46] D.S. Aydin, Z. Bayindir, M. Hoseini, M.O. Pekguleryuz, The high temperature oxidation and ignition behavior of Mg–Nd alloys part I: The oxidation of dilute alloys, J. Alloys Compd. 569 (2013) 35-44.

[47] W.M. Fassel, L.B. Gulbransen, J.R. Lewis, J.H. Hamilton, Ignition temperatures of magnesium and magnesium alloys. J. Met. 3 (1951) 522-528.

[48] M. Liu, Shih, S. Donald, C. Parish, A. Atrens, The ignition temperature of Mg alloys WE43, AZ31 and AZ91, Corros. Sci. 54 (2012) 139-142.

[49] N. Mebarki, N.V.R. Kumar, J.J Blandin, M. Suery, F. Pelloux, G. Khelifati, Correlation between ignition and oxidation behaviours of AZ91 magnesium alloy, Mater. Sci. Technol. 21 (2005) 1145-1151.

[50] P. Boris, A Study of the Flammability of Magnesium, Federal Aviation Agency, Washington, 1964.

[51] E.L. Dreizin, C.H. Berman, E.P. Vicenzi, Condensed-phase modifications in magnesium particle combustion in air, Combust. Flame 122 (2000) 30-42.

[52] F.J. Zong, C.Z. Meng, Z.M. Guo, F. Ji, H.D. Xiao, X.J. Zhang, J. Ma, H.L. Ma, Synthesis and characterization of magnesium nitride powder formed by Mg direct reaction with N_2, J. Alloys Compd. 508 (2010) 172-176.

[53] M.I. Barrena, J.M. Gómez de Salazar, J.M. Vázquez, I. García-Cano, J.M. Guilemany, Protection behaviour of surface films formed on AZ91D magnesium alloy in nitrogen/1,1,1,2-tetrafluoroethane atmospheres, Met. Mater. Int. 20 (2014) 613-618.

[54] I.J. Polmear, Light alloys, third ed., Arnold, London, 1995.

[55] N.V.R. Kumar, J.J. Blandin, M. Suéry, E. Grosjean, Effect of alloying elements on the ignition resistance of magnesium alloys, Scripta Mater. 49 (2003) 225-230.

[56] M.J. Balart, Z. Fan, Surface oxidation of molten AZ91D magnesium alloy in air, Int. J. Cast Met. Res. 27 (2014) 167-175.

[57] J. Liu, H. Chen, L. Zhao, W. Huang, Oxidation behaviour of molten magnesium and AZ91D magnesium alloy in 1,1,1,2-tetrafluoroethane/air atmospheres, Corros. Sci. 51 (2009) 129-134.

[58] A. Prasad, Z. Shi, A. Atrens, Influence of Al and Y on the ignition and flammability of Mg alloys, Corros. Sci. 55 (2012) 153-163.

[59] A. Prasad, Z. Shi, A. Atrens, Flammability of Mg-X Binary Alloys, Adv. Eng. Mater. 14 (2012) 772-784.

[60] T. Marker, Evaluating the flammability of various magnesium alloys during laboratory- and full-scale aircraft fire tests, DOT/FAA/AR-11/3, US Department of Transportation, Federal Aviation Administration, Atlantic City, New Jersey, 2013.

[61] T. Marker, Development of a laboratory-scale flammability test for magnesium alloys used in aircraft seat construction, DOT/FAA/TC-13/52, US Department of Transportation, Federal Aviation Administration, Atlantic City, New Jersey, 2014.

[62] N. B. Pilling, R. E. Bedworth, The Oxidation of Metals at High Temperatures, J. Inst. Met. 29 (1923) 529-591.

[63] D. Alfè, M.J. Gillan, Schottky defect formation energy in MgO calculated by diffusion Monte Carlo, Phys. Rev. B 71 (2005) 220101.

[64] N. Birks, G.H. Meier, F.S. Pettit, Introduction to the high-temperature oxidation of metals, second ed., Cambridge University Press, Cambridge, New York 2006.

[65] F.A. Kroger, The chemistry of imperfect crystals, North-Holland Pub. Co., Amsterdam, 1964.

[66] P. Kofstad, High temperature corrosion, Elsevier Applied Science Publishers Ltd., New York, 1988.

[67] F. Czerwinski, Z. Kedzierski, On the mechanism of microcrack formation in nanocrystalline Fe-Ni electrodeposits, J. Mater. Sci. 32 (1997) 2957-2961.

[68] W.W. Smeltzer, The influence of short-circuit grain boundary diffusion on the growth of oxide layers on metals, Mater. Sci. Forum 29 (1988) 151-172.

[69] W.W. Smeltzer, Oxidation of An Aluminum-3 Per Cent Magnesium Alloy in the Temperature Range 200°C-550°C, J. Electrochem. Soc., 105 (1958) 67-71.

[70] J. Perrow, W.W. Smeltzer, J. Embury, The role of structural defects in the growth of nickel oxide films, Acta Metall. 16 (1968) 1209-1218.

[71] R. Rapp, The high temperature oxidation of metals forming cation-diffusing scales, Metall. Trans. A 15 (1984) 765-782.

[72] C. Lea, C. Molinari, Magnesium diffusion, surface segregation and oxidation in Al-Mg alloys, J. Mater. Sci. 19 (1984) 2336-2352.

[73] G.I. Finch, A.G. Quarrell, The Structure of Magnesium, Zinc and Aluminium Films, P. Roy. Soc. Lond. A: Mat. 141 (1933) 398-414.

[74] A.G. Quarrell, G.I. Finch, Crystal Structure and Orientation in Thin Films, Nature 131 (1933) 877-877

[75] O. Kubaschewske, B. Hopkins, Oxidation of metals and alloys, Butterworths, London, 1953.

[76] Properties of the Elements and Inorganic Compounds; Vapor Pressure of the Metallic Elements, in: David R. Lide (Eds), CRC Handbook of Chemistry and Physics, 84th ed., CRC Press, Boca Raton, Florida, 2003.

[77] X. Wang, S. Xiong, Protection behavior of SO_2-containing cover gases to molten magnesium alloy, Trans. Nonferrous Met. Soc. China 21 (2011) 807-813.

[78] H. Okamoto, Phase Diagrams for Binary Alloys, ASM international, Material Park, OH, 2000.

[79] F.S. Pan, J. Peng, P.D. Ding, L.Y. Wnag, A novel hot extrusion method to improve the plastic of magnesium alloy profiles, China Patent Application, CN101269387 A, 24 September 2008.

[80] R. Arrabal, A. Pardo, M.C. Merino, M. Mohedano, P. Casajús, K. Paucar, E. Matykina, Oxidation Behavior of AZ91D Magnesium Alloy Containing Nd or Gd, Oxid. Met. 76 (2011) 433-450.

[81] Brown, C., The Determination of the Ignition Temperature of Solid Materials. Thesis, Catholic University of America, 1934.

[82] C.M. Yuan, D.Z. Huang, C. Li, G. Li, Ignition behavior of magnesium powder layers on a plate heated at constant temperature, J. Hazard. Mater. 246 (2013) 283-290.

[83] A. Luo, M.O. Pekguleryuz, Cast magnesium alloys for elevated temperature applications, J. Mater. Sci. 29 (1994) 5259-5271.

[84] D. StJohn, M. Qian, M. Easton, P. Cao, Z. Hildebrand, Grain refinement of magnesium alloys, Metall. Mater. Trans. A 36 (2005) 1669-1679.

[85] A.D. Südholz, N. Birbilis, C.J. Bettles, M.A. Gibson, Corrosion behaviour of Mg-alloy AZ91E with atypical alloying additions, J. Alloys Compd. 471 (2009) 109-115.

[86] M.X. Zhang, P.M. Kelly, Surface alloying of AZ91D alloy by diffusion coating, J. Mater. Res. 17 (2002) 2477-2479.

[87] J. Jedlinski, G. Borchardt, On the oxidation mechanism of alumina formers, Oxid. Met. 36 (1991) 317-337.

[88] M. Barrena, J. Gomez de Salazar, L. Matesanz, A. Soria, Effect of heat treatment on oxidation kinetics in AZ91 and AM60 magnesium alloys. Mater. Char. 62 (2011) 982–986.

[89] S. Feliu, C. Maffiotte, A. Samaniego, J. Galvan, V. Barranco, Effect of the chemistry and structure of the native oxide surface film on the corrosion properties of commercial AZ31 and AZ61 alloys, Appl. Surf. Sci. 257 (2011) 8558–8568.

[90] T.S. Shih, J.B. Liu, P.S. Wei, Oxide films on magnesium and magnesium alloys, Mater. Chem. Phys. 104 (2007) 497-504.

[91] J. Geng, X. Gao, X. Fang, J. Nie, Enhanced age-hardening response of Mg–Zn alloys via Co additions, Scripta Mater. 64 (2011) 506-509.

[92] X. Gao, J. Nie, Characterization of strengthening precipitate phases in a Mg–Zn alloy, Scripta Mater. 56 (2007) 645-648.

[93] C.L. Mendis, K. Hono, Understanding precipitation processes in magnesium alloys, in: Fundamentals of Magnesium Alloy Metallurgy, M.O. Pekguleryuz, K.U. Kainer, A.A. Kaya (Eds.), Woodhead Publishing, Cambridge, 2013, pp. 125-151.

[94] H. Huang, G.Y. Yuan, Z.H. Chu, W.J. Ding, Microstructure and mechanical properties of double continuously extruded Mg-Zn-Gd-based magnesium alloys, Mater. Sci. Eng.: A 560 (2013) 241-248.

[95] B. Mordike, K.U. Kainer, Magnesium Alloys and their Application, Werkstoff-Informationsgesellschaft, Frankfurt, 1998.

[96] H. Pan, F. Pan, X. Wang, J. Peng, High conductivity and high strength Mg-Zn-Cu alloy, Mater. Sci. Technol. 30 (2014) 759-764.

[97] W. Unsworth, J.F. King, Magnesium Technology, Institute of Metals, London, 1987.

[98] H.G. Paris, W.H. Hunt, Advances in Magnesium Alloys and Composites, International Magnesium Association and the Non-Ferrous Metals Committee, Arizona, 1988.

[99] G. L. Makar, J. Kruger, Corrosion of magnesium, Int. Mater. Rev. 38 (1993) 138-153.

[100] J.E. Hillis, The effects of heavy metal contamination on magnesium corrosion performance, SAE Technical Papers 830523 (1983) 1-12.

[101] J.E. Gray, B. Luan, Protective coatings on magnesium and its alloys-A critical review, J. Alloys Compd. 336 (2002) 88-113.

[102] F.S. Pan, X.H. Chen, T. Yan, T.T. Liu, J.J. Mao, W. Luo, Q. Wang, J. Peng, A. Tang, B. Jiang, A novel approach to melt purification of magnesium alloys, JMA 4 (2016) 8-14.

[103] P. Pérez, G. Garcés, P. Adeva, Oxidation Behavior of a PVD-Processed Mg–10.6Zr Alloy, Oxid. Met. 58 (2002) 607-621.

[104] C. Xu, W. Gao, Pilling-bedworth ratio for oxidation of alloys, Mater. Res. Innov. 3 (2000) 231-235.

[105] H.S. Kim, Y.M. Kim, C.D. Yim, B.S. You, Key factor influencing the ignition resistance of magnesium alloys at elevated temperatures, Scripta Mater. 65 (2011) 958-961.

[106] L.L. Rokhlin, T.V. Dobatkina, N.I. Nikitina, I.E. Tarytina, Calcium-alloyed magnesium alloys, Met. Sci. heat Treat. 51 (2009) 164-169.

[107] C.L. Mendis, K. Oh-ishi, K. Hono, Enhanced age hardening in a Mg–2.4 at.% Zn alloy by trace additions of Ag and Ca, Scripta Mater. 57 (2007) 485-488.

[108] P. Li, B. Tang, E.G. Kandalova, Microstructure and properties of AZ91D alloy with Ca additions, Mater. Lett. 59 (2005) 671-675.

[109] B. Jiang, W. Liu, D. Qiu, M.X. Zhang, F. Pan, Grain refinement of Ca addition in a twin-roll-cast Mg–3Al–1Zn alloy, Mater. Chem. Phys. 133 (2012) 611-616.

[110] B.S. You, W.W. Park, I.S. Chung, The effect of calcium additions on the oxidation behavior in magnesium alloys, Scripta Mater. 42 (2000) 1089-1094.

[111] S. Cheng, G. Yang, J. Fan, Y. Li, Y. Zhou, Effect of Ca and Y additions on oxidation behavior of AZ91 alloy at elevated temperatures, Trans. Nonferrous Met. Soc. China 19 (2009) 299-304.

[112] M. Sakamoto, S. Akiyama, K. Oqi, Suppression of ignition and burning of molten Mg alloys by Ca bearing stable oxide film, J. Mater. Sci. Lett. 16 (1997) 1048-1050.

[113] D.B. Lee, High temperature oxidation of AZ31+0.3wt.%Ca and AZ31+0.3wt.%CaO magnesium alloys, Corros. Sci. 70 (2013) 243-251.

[114] X.G. Min, W.W. Du, F. Xue, Y.S. Sun, Analysis of EET on Ca increasing the melting point of $Mg_{17}Al_{12}$ phase, Chin. Sci. Bull. 47 (2002) 1082-1086.

[115] J.F. Fan, G.C. Yang, Y.H. Zhou, Y.H. Wei, B.S. Xu, Selective oxidation and the third-element effect on the oxidation of Mg-Y alloys at high temperatures, Metall. Mater. Trans. A 40 (2009) 2184-2189.

[116] M. Sakamoto, S. Akiyama, T. Hagio, K. Ogi, Control of oxidation surface film and suppression of ignition of molten Mg-Ca alloy by Ca addition, J. Jpn. Foundry Eng. Soc. 69 (1997) 227-233.

[117] B.H. Choi, B.S. You, I.M. Park, Characterization of protective oxide layers formed on molten AZ91 alloy containing Ca and Be, Met. Mater. Int. 12 (2006) 63-67.

[118] F. Li, W.Y. Peh, V. Nagarajan, M.K. Ho, A. Danno, B.W. Chua, M.J. Tan, Development of non-flammable high strength AZ91+Ca alloys via liquid forging and extrusion, Mater. Design 99 (2016) 37-43.

[119] M. Li, High temperature corrosion of metals, Metallurgical Industry Press, Beijing, 2001.

[120] D. Eliezer, H. Alves, Corrosion and Oxidation of Magnesium alloys, In: M. Kutz (eds.), Handbook of Materials Selection, John Wiley and Sons, Inc., New York, 2007, pp. 267-291.

[121] S. Golmakaniyoon, R. Mahmudi, Comparison of the effects of La- and Ce-rich rare earth additions on the microstructure, creep resistance, and high-temperature mechanical properties of Mg-6Zn-3Cu cast alloy, Mater. Sci. Eng.: A 528 (2011) 5228-5233.

[122] S. Golmakaniyoon, R. Mahmudi, Microstructure and creep behavior of the rare-earth doped Mg-6Zn-3Cu cast alloy, Mater. Sci. Eng.: A 528 (2011) 1668-1677.

[123] V. Neubert, I. Stulíková, B. Smola, B.L. Mordike, M. Vlach, A. Bakkar, J. Pelcová, Thermal stability and corrosion behaviour of Mg–Y–Nd and Mg–Tb–Nd alloys, Mater. Sci. Eng.: A 462 (2007) 329-333.

[124] Y.B. Hu, J. Deng, C. Zhao, F.S. Pan, J. Peng, Microstructure and mechanical properties of Mg-Gd-Zr alloys with low gadolinium contents, J. Mater. Sci. 46 (2011) 5838-5846.

[125] J.G. Wang, P.F. Song, S. Huang, F.S. Pan, High-strength and good-ductility Mg-RE-Zn-Mn magnesium alloy with long-period stacking ordered phase, Mater. Lett. 93 (2013) 415-418.

[126] X.M. Wang, X.Q. Zeng, G.S. Wu, S.S. Yao, Yttrium ion implantation on the surface properties of magnesium, Appl. Surf. Sci. 253 (2006) 2437-2442.

[127] X. Wang, X. Zeng, G. Wu, S. Yao, Y. Lai, Effects of tantalum ion implantation on the corrosion behavior of AZ31 magnesium alloys, J. Alloys Compd. 437 (2007) 87-92.

[128] Z. Chen, X. Ren, Y. Zhang, Effect of RE on the ignition proof, microstructure and properties of AZ91D magnesium alloy, J. Univ. Sci. Technol. B. 12 (2005) 540–544.

[129] J.F. Fan, S.L. Cheng, H. Xie, W.X. Hao, M. Wang, G.C. Yang, Y.H. Zhou, Surface oxidation behavior of Mg-Y-Ce alloys at high temperature, Metall. Mater. Trans. A 36 (2005) 235-239.

[130] J.F. Fan, G.C. Yang, S.L. Chen, H. Xie, M. Wang, Y.H. Zhou, Effect of rare earths (Y, Ce) additions on the ignition points of magnesium alloys, J. Mater. Sci. 39 (2004) 6375-6377.

[131] B.A. Pint, Experimental observations in support of the dynamic-segregation theory to explain the reactive-element effect, Oxid. Met. 45 (1996) 1-37.

[132] Z. Ning, W. Liang, F. Cao, J. Sun, The Effect of Y On The Oxidation of Mg-Zn-Zr Alloys, Int. J. Mod. Phys. B 23 (2009) 796-801.

[133] S.H. Bak, D.B. Lee, Effect of Y and Y_2O_3 on oxidation of AZ91D Mg alloys between 400 °C and 500 °C, Trans. Nonferrous Met. Soc. China 19 (2009) 871-874.

[134] X.W. Yu, S.J. Shen, B. Jiang, Z.T. Jiang, H. Yang, F.S. Pan, The effect of the existing state of Y on high temperature oxidation properties of magnesium alloys, Appl. Surf. Sci. 370 (2016) 357-363.

[135] B.S. You, Y.M. Kim, C.D. Yim, H.S. Kim, Oxidation and corrosion behavior of non-flammable magnesium alloys containing Ca and Y, in: M. Alderman, M.V. Manuel, N. Hort, N.R. Neelameggham (Eds), Magnesium Technology 2014, John Wiley & Sons Inc., New York, 2014, pp.325-329.

[136] B. Jiang, X.W. Yu, F.S. Pan, Q.S. Yang, X. Li, A high temperature anti-oxidation magnesium alloy, China Patent Application, CN104060140A, 24 September 2014.

[137] S. Cheng, G. Yang, J. Fan, Y. Li, Y. Zhou, Effect of Ca and Y on microstructure and mechanical properties of AZ91 alloy, Rare Met. Mater. Eng. 35 (2006) 1400-1403.

[138] T.S. Shih, J.H. Wang, K.Z. Chong, Combustion of magnesium alloys in air, Mater. Chem. Phys. 85 (2004) 302-309.

[139] W. Ding, X. Wang, X. Zeng, G. Wu, S. Yao, Y. Lai, Cyclic oxidation behaviour of cerium implanted AZ31 magnesium alloys, Mater. Lett. 61 (2007) 1429-1432.

[140] M. Laleh, F. Kargar, A. Sabour Rouhaghdam, Formation of a compact oxide layer on AZ91D magnesium alloy by microarc oxidation via addition of cerium chloride into the MAO electrolyte, J. Coating Technol. Res. 8 (2011) 765-771.

[141] A.A. Luo, R.K. Mishra, A.K. Sachdev, High-ductility magnesium–zinc–cerium extrusion alloys. Scripta Mater. 64 (2011) 410-413.

[142] Wang, X.M, X.Q. Zeng, G.S. Wu, S.S. Yao, Y.J. Lai, The effects of cerium implantation on the oxidation behavior of AZ31 magnesium alloys, J. Alloys Compd. 456 (2008) 384-389.

[143] P. Lin, H. Zhou, W. Li, W.P. Li, N. Sun, R. Yang, Interactive effect of cerium and aluminum on the ignition point and the oxidation resistance of magnesium alloy, Corros. Sci. 50 (2008) 2669-2675.

[144] W.P. Li, W. Li, H. Zhou, W. Zhou, M.X. Wang, Effect of cooling rate on ignition point of AZ91D-0.98 wt.% Ce magnesium alloy, Mater. Lett. 61 (2007) 2772-2774.

[145] X.M. Wang, X.Q. Zeng, G.S. Wu, S.S. Yao, L.B. Li, Surface oxidation behavior of MgNd alloys, Appl. Surf. Sci. 253 (2007) 9017-9023.

[146] D.S. Aydin, Z. Bayindir, M.O. Pekguleryuz, The high temperature oxidation behavior of Mg–Nd alloys. Part II: The effect of the two-phase microstructure on the on-set of oxidation and on oxide morphology, J. Alloys Compd. 584 (2014) 558-565.

[147] D.S. Aydin, M. Hoseini, M.O. Pekguleryuz, Understanding the high temperature oxidation and ignition behaviour of two-phase Mg-Nd alloys and a comparison to single phase Mg-Nd, Philos. Mag. 95 (2015) 259-274.

[148] W.M. Zhao, Y. Zhao, Z.F. Wang, Y.Y. Li, J. Ding, H.T. Xue, Effect of Mg-Nd master alloys on ignition-proof performance of AZ91D magnesium alloy, Adv. Mater. Res. 214 (2011) 118-121.

[149] S.M. He, X.Q. Zeng, L.M. Peng, X. Gao, J.F. Nie, W.J. Ding, Microstructure and strengthening mechanism of high strength Mg-10Gd-2Y-0.5Zr alloy, J. Alloys Compd. 427 (2007) 316-323.

[150] J. Liu, Y. Li, F. Wang, The High Temperature Oxidation Behavior of Mg–Gd–Y–Zr Alloy, Oxid. Met. 71 (2009) 319-334.

[151] X. Wang, W. Wu, Y. Tang, X. Zeng, S. Yao, Early high temperature oxidation behaviors of Mg–10Gd–3Y alloys, J. Alloys Compd. 474 (2009) 499-504.

[152] Y.J. Wu, L.M. Peng, S. Zhao, D.J. Li, F. Huang, W.J. Ding, Ignition-Proof Properties of a High-Strength Mg-Gd-Ag-Zr Alloy, Journal of Shanghai Jiaotong University (Science) 17 (2012) 643-647.

[153] D. Yao, W. Zhao, H. Zhao, F. Qiu, Q. Jiang, High creep resistance behavior of the casting Al-Cu alloy modified by La, Scripta Mater. 61 (2009) 1153-1155.

[154] D. Yao, Y. Xia, F. Qiu, Q. Jiang, Effects of La addition on the elevated temperature properties of the casting Al-Cu alloy, Mater. Sci. Eng.: A 528 (2011) 1463-1466.

[155] S. Zhao, H. Zhou, T. Zhou, Z. Zhang, P. Lin, L. Ren, The oxidation resistance and ignition temperature of AZ31 magnesium alloy with additions of La_2O_3 and La, Corros. Sci. 67 (2013) 75-81.

[156] J.A. Dean, N.A. Lange, Lange's Handbook of Chemistry, fifteenth ed., McGraw-Hill, New York, 1999.

[157] H. Fan, S. Li, Z. Zhao, H. Wang, Z. Shi, Improving the formation and protective properties of La-conversion coatings on brass by use of La_2O_3 nanoparticle incorporation with electrodeposition, Corros. Sci. 53 (2011) 3821-3831.

[158] G. Zhang, Z. Luo, H. Zhang, R. Chu, Ignition-proof mechanism of magnesium alloy added with rare earth La from first-principle study, J. Rare Earth. 30 (2012) 573-578.

[159] W.Y. Youdelis, C.S. Yang, Beryllium-enhanced grain refinement of aluminium–titanium alloys, Met. Sci. 16 (1982) 275-281.

[160] J.C. Harkness, W.D. Spiegelberg, W.R. Cribb, Beryllium-Copper and other Beryllium-Containing Alloys, in: ASM Metals Handbook Vol. 2: Properties and Selection: Nonferrous Alloys and Special-Purpose Materials, ASM international, Materials Park, OH, 1990, pp. 403-427.

[161] C. Houska, Beryllium in alumium and magnesium alloys, Met. Mater. 4 (1988) 100-104.

[162] J.R. Davis, Aluminum and aluminum alloys, ASM International, Material Park, OH, 1993.

[163] G. Foerster, HiLoN: A new approach to magnesium die casting, Adv. Mater. Process. 154 (1998) 79-81.

[164] K.G. Wikle, Improving aluminum castings with beryllium, AFS Trans. 119 (1978) 513-518.

[165] Y.B. Huang, I.S. Chung, B.S. You, W.W. Park, B.H. Choi, Effect of Be addition on the oxidation behavior of Mg−Ca alloys at elevated temperature, Met. Mater. Int. 10 (2004) 7-11.

[166] X. Zeng, Q. Wang, Y. Lü, W. Ding, Y. Zhu, C. Zhai, C. Lu, X. Xu, Behavior of surface oxidation on molten Mg–9Al–0.5Zn–0.3Be alloy, Mater. Sci. Eng.: A 301 (2001) 154-161.

[167] X.Q. Zeng, Q.D. Wang, Y.Z. Lü, W.J. Ding, C. Lu, Y.P. Zhu, C.Q. Zhai, X.P. Xu, Study on ignition proof magnesium alloy with beryllium and rare earth additions, Scripta Mater. 43 (2000) 403-409.

[168] F. Czerwinski, The early stage oxidation and evaporation of Mg-9%Al-1%Zn alloy, Corros. Sci. 46 (2004) 377-386.

[169] Q.Y. Tan, N. Mo, B. Jiang, F.S. Pan, A. Atrens, M.X. Zhang, Oxidation resistance of Mg-9Al-1Zn alloys micro-alloyed with Be, Scripta Mater. 115 (2016) 38-41.

[170] F. Czerwinski, J.A. Szpunar, The influence of crystallographic orientation of nickel surface on oxidation inhibition by ceria coatings, Acta Mater. 46 (1998) 1403-1417.

[171] F. Czerwinski, On the use of the micromarker technique for studying the growth mechanism of thin oxide films, Acta Mater. 48 (2000) 721-733.

[172] E. Clementi, D.L. Raimondi, W.P. Reinhardt, Atomic Screening Constants from SCF Functions. II. Atoms with 37 to 86 Electrons, J. Chem. Phys. 47 (1967) 1300-1307.

[173] P. Cao, Q. Ma, D.H. StJohn, Grain coarsening of magnesium alloys by beryllium, Scripta Mater. 51 (2004) 647-651.

[174] P. Cao, Q. Ma, D.H. StJohn, Mechanism for grain refinement of magnesium alloys by superheating, Scripta Mater. 56 (2007) 633-636.

[175] M.O. Pekguleryuz, Alloying behavior of magnesium and alloy design in: M.O. Pekguleryuz, K.U. Kainer, A.A. Kaya (Eds.), Fundamentals of Magnesium Alloy Metallurgy, Woodhead Publishing, Cambridge, 2013, pp. 152-196.

[176] K. Dennis, Effects of magnesium, silicon, and strontium on the oxidation of molten aluminum, Thesis, McGill University (Canada), 1999.

[177] O. Ozdemir, Effect of strontium on the oxidation behavior of molten aluminum-magnesium alloys, Thesis, McGill University (Canada), 2006.

[178] D.S. Aydin, Z. Bayindir, M.O. Pekguleryuz, High Temperature Oxidation Behavior of Hypoeutectic Mg-Sr Binary Alloys: The Role of the Two-Phase Microstructure and the Surface Activity of Sr, Adv. Eng. Mater. 17 (2015) 697-708.

[179] M. Pekguleryuz, P. Vermette, Strontium for melt oxidation reduction of magnesium and a method for adding strontium to magnesium, US Patent Application, US20040159188 A1, 19 Augest 2004.

[180] D.S. Aydin, Z. Bayindir, M.O. Pekguleryuz, The effect of strontium (Sr) on the ignition temperature of magnesium (Mg): a look at the pre-ignition stage of Mg–6 wt% Sr, J. Mater. Sci. 48 (2013) 8117-8132.

[181] M. Pekguleryuz, M. Avedesian, Magnesium Alloying-Some Metallurgical Aspects, In: F. Hehman, B.L. Mordike, (Eds.), Magnesium alloys and their applications, DGM, Germisch, 1992, pp. 213-220.

[182] F. Mansfeld, Corrosion Mechanisms, Marcel Dekker Inc., New York, 1987.

[183] M. Rashad, F.S. Pan, D. Lin, M. Asif, High temperature mechanical behavior of AZ61 magnesium alloy reinforced with graphene nanoplatelets, Mater. Design 89 (2016) 1242-1250.

[184] M. Rashad, F.S. Pan, M. Asif, Exploring mechanical behavior of Mg-6Zn alloy reinforced with graphene nanoplatelets, Mater. Sci. Eng.: A 649 (2016) 263-269.

[185] M. Rashad, F.S. Pan, W. Guo, H. Lin, M. Asif, M. Irfan, Effect of alumina and silicon carbide hybrid reinforcements on tensile, compressive and microhardness behavior of Mg-3Al-1Zn alloy, Mater. Char. 106 (2015) 382-389.

[186] M. Rashad, F.S. Pan, A.T. Tang, M. Asif, M. Aamir, Synergetic effect of graphene nanoplatelets (GNPs) and multi-walled carbon nanotube (MW-CNTs) on mechanical properties of pure magnesium, J. Alloys Compd. 603 (2014) 111-118.

[187] M. Rashad, F.S. Pan, A.T. Tang, M. Asif, S. Hussain, J. Gou, J.J. Mao, Improved strength and ductility of magnesium with addition of aluminum and graphene nanoplatelets (Al plus GNPs) using semi powder metallurgy method, J. Ind. Eng. Chem. 23 (2015) 243-250.

[188] Q.B. Nguyen, M. Gupta, T.S. Srivatsan, On the role of nano-alumina particulate reinforcements in enhancing the oxidation resistance of magnesium alloy AZ31B, Mater. Sci. Eng.: A 500 (2009) 233-237.

[189] X.J. Wang, C.Y. Wang, X.S. Hu, K. Wu, K.K. Deng, W.M. Gan, M.Y. Zheng, Hot deformation behavior of SiCp/AZ91 magnesium matrix composite fabricated by stir casting, Mater. Sci. Eng.: A 492 (2008) 481-485.

[190] J.Q. Li, L. Wang, H.W. Cheng, H.F. Zhang, Z.Q. Hu, H.N. Cai, Synthesis and compressive deformation of rapidly solidified magnesium alloy and composites reinforced by SiCp, Mater. Sci. Eng.: A 474 (2008) 24-29.

[191] W. Yang, G.C. Weatherly, D.W. McComb, D.J. Lloyd, The structure of SiC-reinforced Mg casting alloys, J. Microsc. 185 (1997) 292-302.

[192] B. Inem, G. Pollard, Interface structure and fractography of a magnesium-alloy, metal-matrix composite reinforced with SiC particles, J. Mater. Sci. 28 (1993) 4427-4434.

[193] T. Nguyen, D. Lee, Oxidation of AM60B Mg Alloys Containing Dispersed SiC Particles in Air at Temperatures Between 400 and 550 °C, Oxid. Met. 73 (2010) 183-192.

[194] T.D. Nguyen, Y.J. Kim, J.C. Lee, S.J. Kim, D.B. Lee, Effect Of Dispersed Sic Particles On The Oxidation Of AZ91D Magnesium Alloys Between 420 And 500°C In Air, Surf. Rev. Lett. 17 (2010) 9-14.

[195] D.B. Lee, J.H. Park, Y.H. Park, Y.J. Kim, High temperature oxidation of TiAl/SiCp composites manufactured by MA-SPS process, Mater. Trans. Jim 38 (1997) 306-311.

[196] P.Y. Lin, H. Zhou, W.P. Li, S.Z. Zhao, J.G. Su, Effect of yttrium addition on the oxide scale of AM50 magnesium alloy, Corros. Sci. 51 (2009) 1128-1133.

[197] B.H. Choi, B.S. You, W.W. Park, Y.B. Huang, L.M. Park, Effect of Ca addition on the oxidation resistance of AZ91 magnesium alloys at elevated temperatures, Met. Mater. Int. 9 (2003) 395-398.

[198] W. Zhao, Y. Sun, H. Li, C. Liang, The effects of some elements on the igniting temperature of magnesium alloys, Mater. Sci. Eng.: B 127 (2006) 105-107.

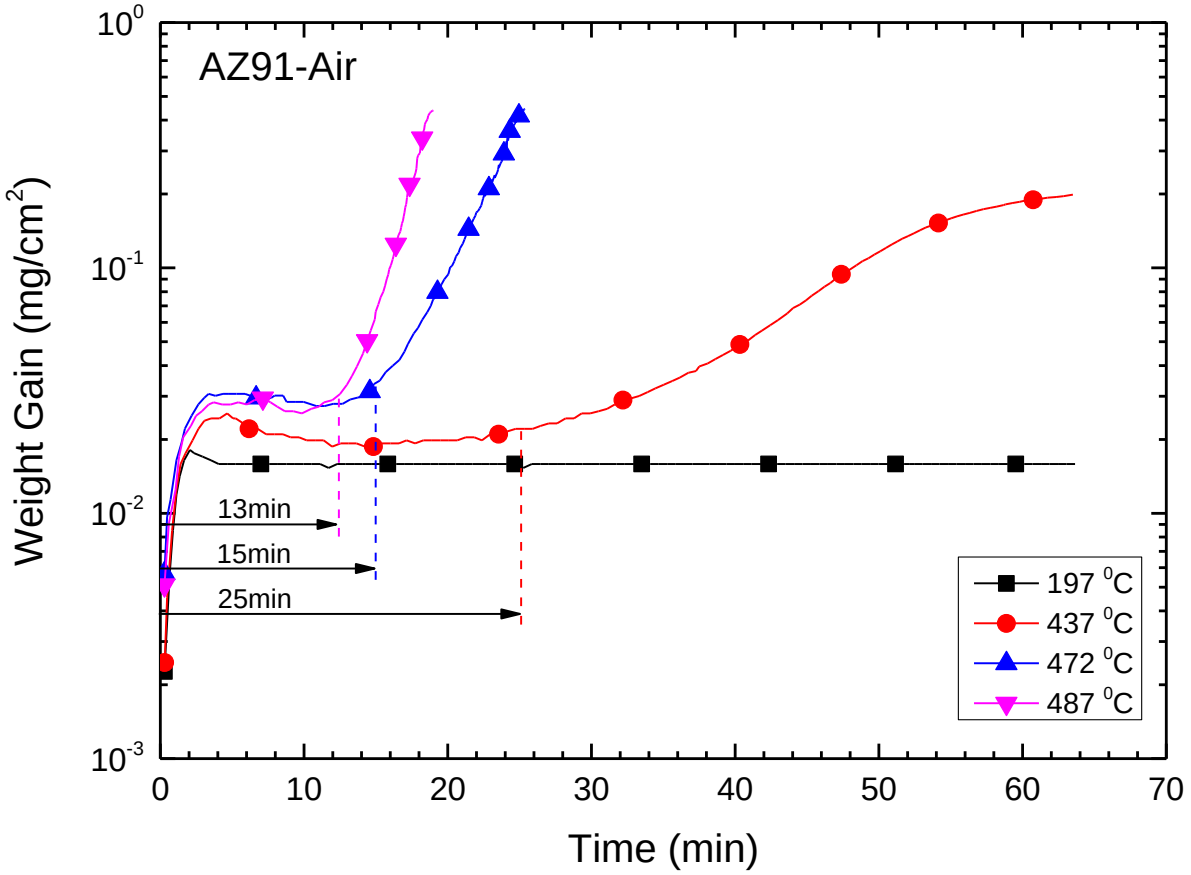

Figure 1: The thermogravimetric measurements of weight change versus time for as-cast Mg-9Al-1Zn in air at 197 °C, 437 °C, 472 °C and 487 °C. The small weight gain at 197 °C represented a slow oxidation speed. The oxidation rate dramatically increased at temperatures above 400 °C and indicated a rapid oxidation stage, after an incubation period. Redrawn from Czerwinski [32] and used with permission from Elsevier.

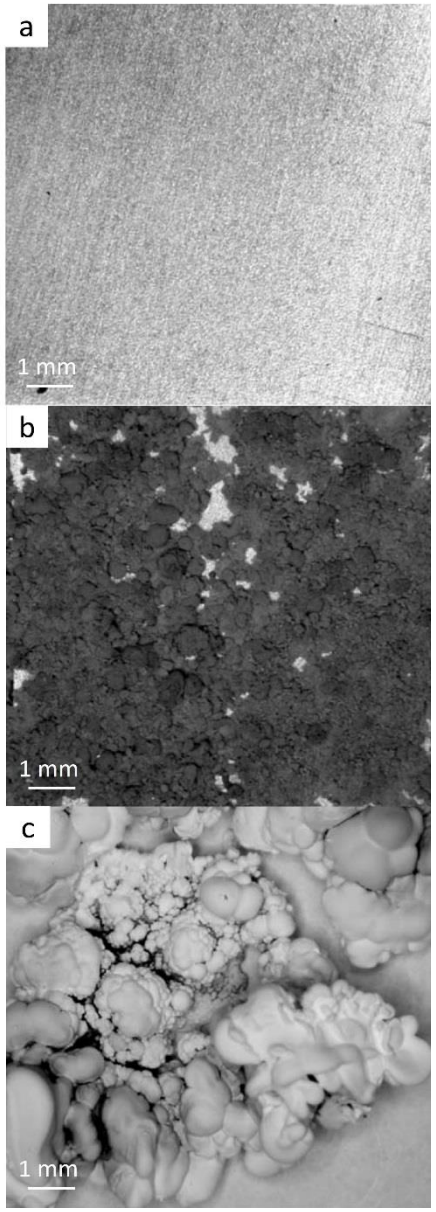

Figure 2: Macroscopic surface morphologies of AZ91 after oxidation in air for the following conditions. (a) After 10 hour at 387 ℃, the surface was flat and a change of colour from bright metallic to matte grey indicated the formation of a uniform surface layer. (b) After one hour at 497 ℃, the surface was covered with black oxide nodules. This was typical of a catastrophic oxidation and a non-protective surface layer. (c) After 10 min at 547 ℃, the cauliflower morphology was typical of burning Mg. Reproduced from Czerwinski [32] with permission from Elsevier.

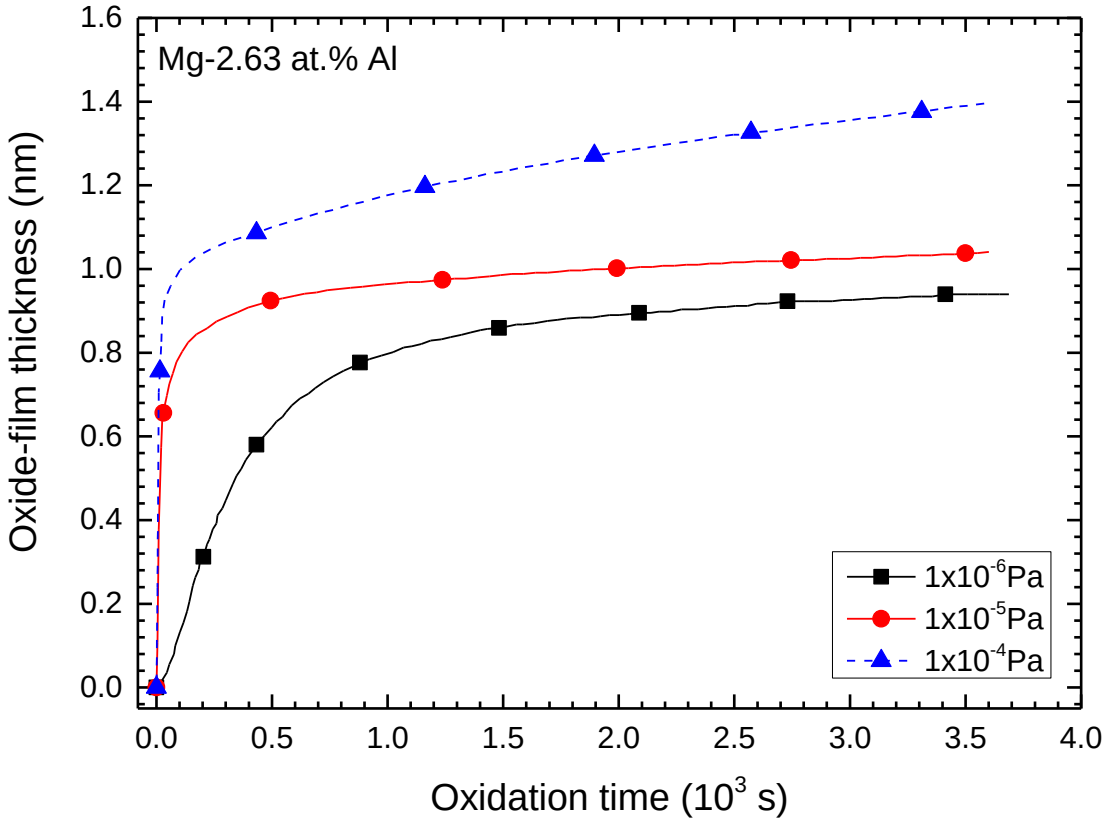

Figure 3: Oxidation kinetics of Mg-2.63 at.% Al at 31 ℃ and indicated oxygen pressures, as-measured by real-time in situ spectroscopic ellipsometry (RISE). Parabolic kinetics were obtained. Initially, the oxide film grew rapidly and a higher oxygen pressure led to a higher growth rate and shorter duration. Subsequently, the growth rate was constant and independent on the oxygen pressure, indicating a protective surface film that controlled the oxidation rate by transport of species through the surface film. Redrawn from Jeurgens [39] and used with permission from Elsevier.

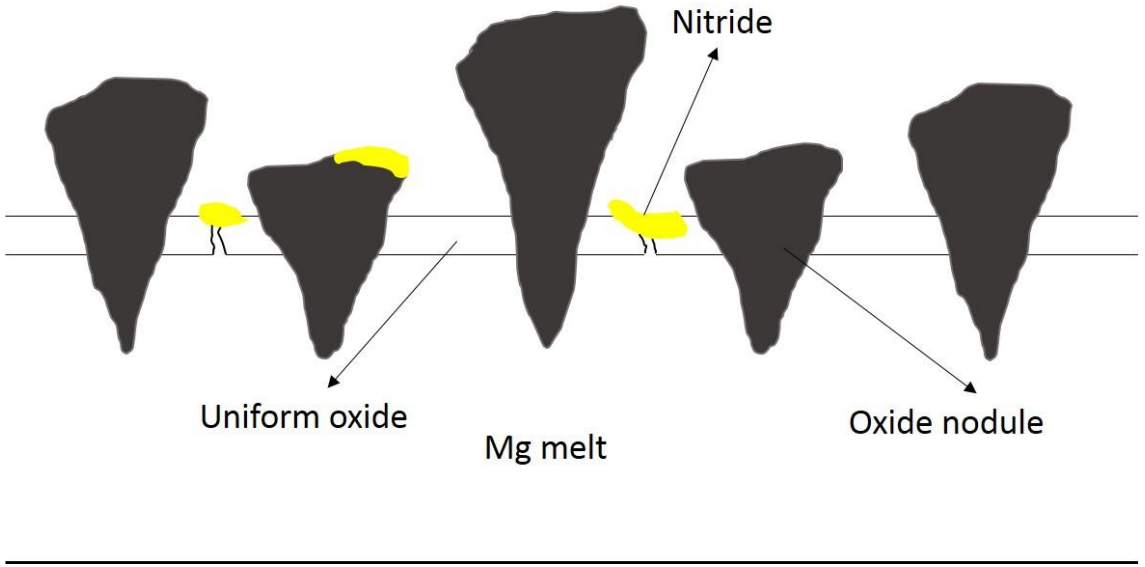

Figure 4: Schematic oxidation behaviour of molten Mg alloys. The uniform layer formed at the initial stage is quickly replaced by oxide nodules and subsequent ignition and burning. The uniform oxide layer, oxide nodules and nitrides are marked.

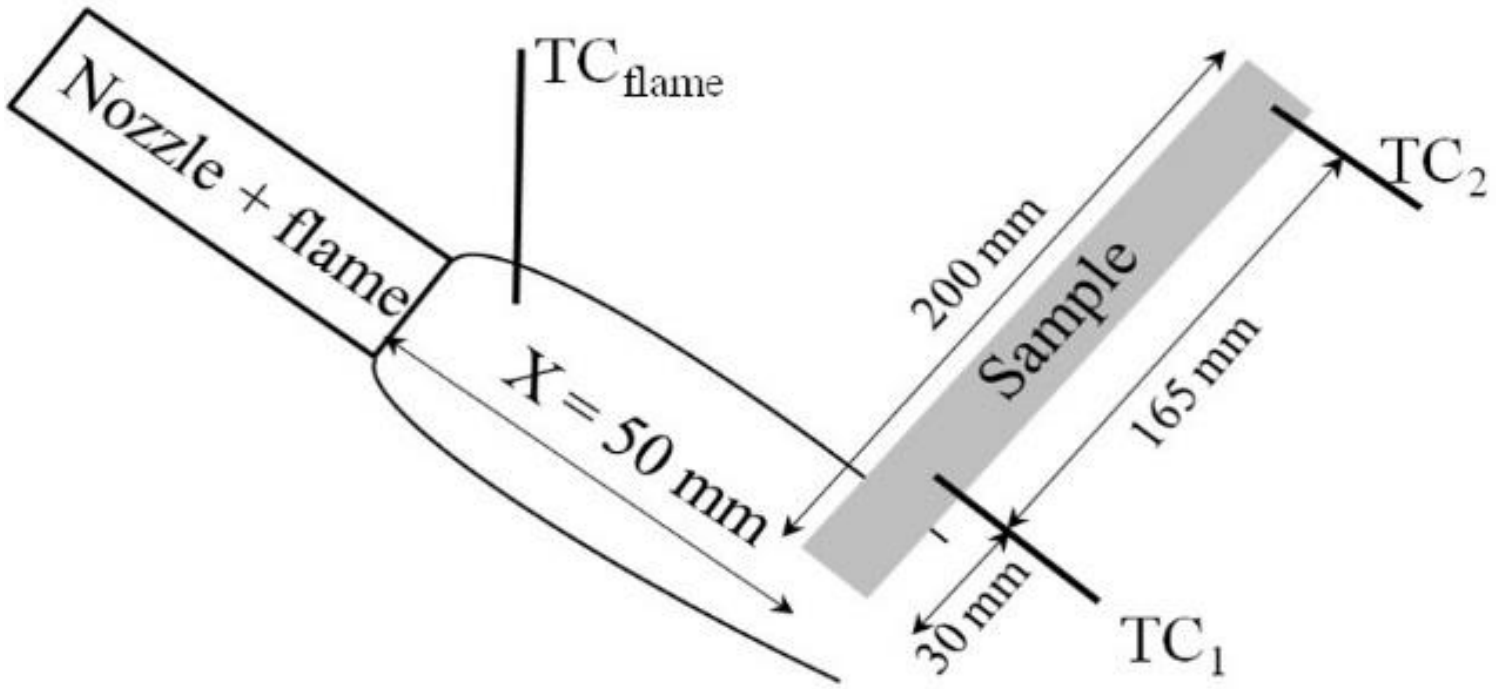

Figure 5: The flame test to study the oxidation of Mg-X (X = Al, Ca, Si, Sn, Sr, La, Mn, Zn, Zr, Ce, Gd, and Nd) and two typical Mg alloys-AZ61 and AZ91 is shown schematically in a top view. One end of the Mg alloy sample (typically 20 mm in diameter and 200 mm in length) was subjected to a liquefied petroleum gas (LPG) flame with a temperature of ~1100 °C. Thermo-couples allowed estimation of the flame temperature and the temperature at the ends of the Mg alloy sample. Reproduced from Prasad [58] with permission from Elsevier.

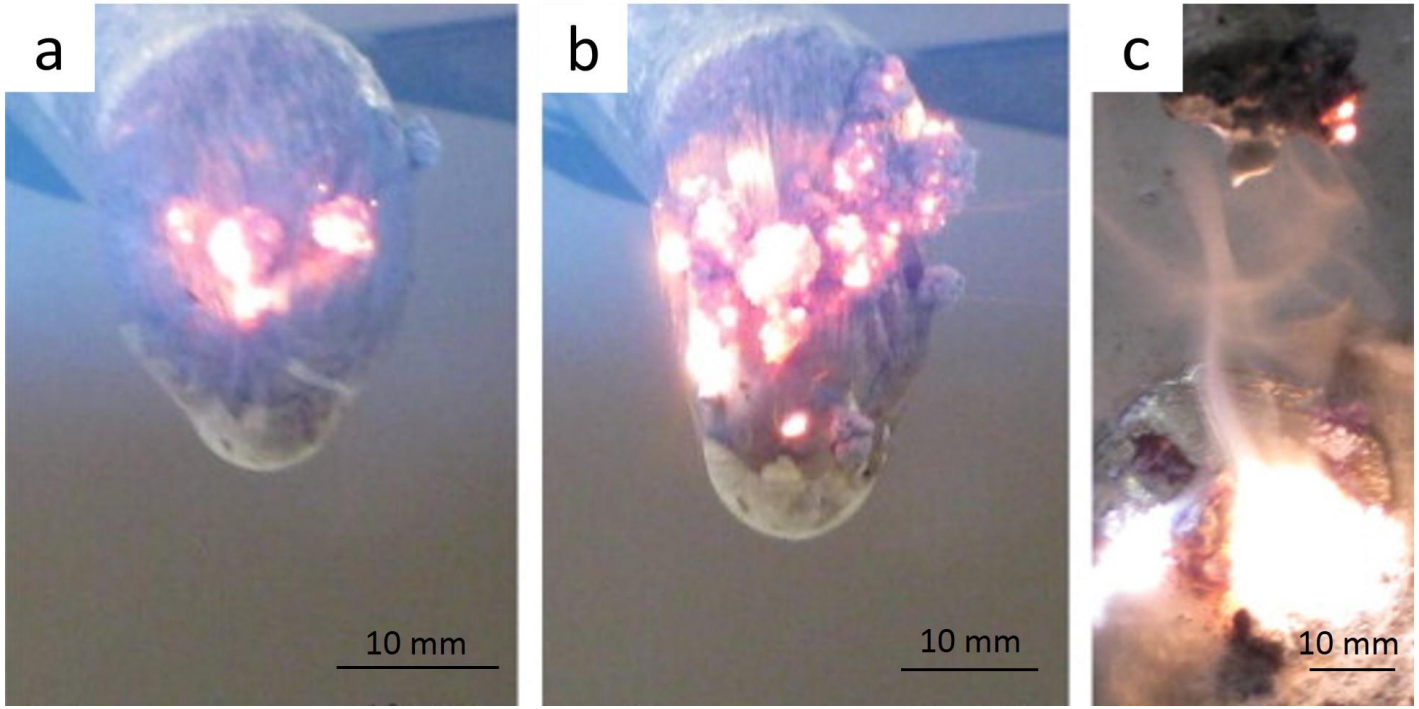

Figure 6: Flame melting test using AZ61. (a) The specimen tip exposed to the LPG flame melted and partially ignited; (b) Subsequent burning of specimen tip. (c) The detached ignited blob continued to burn whereas the flame of the specimen tip extinguished in the absence of the LPG flame. Reproduced from Prasad [58] with permission from Elsevier.

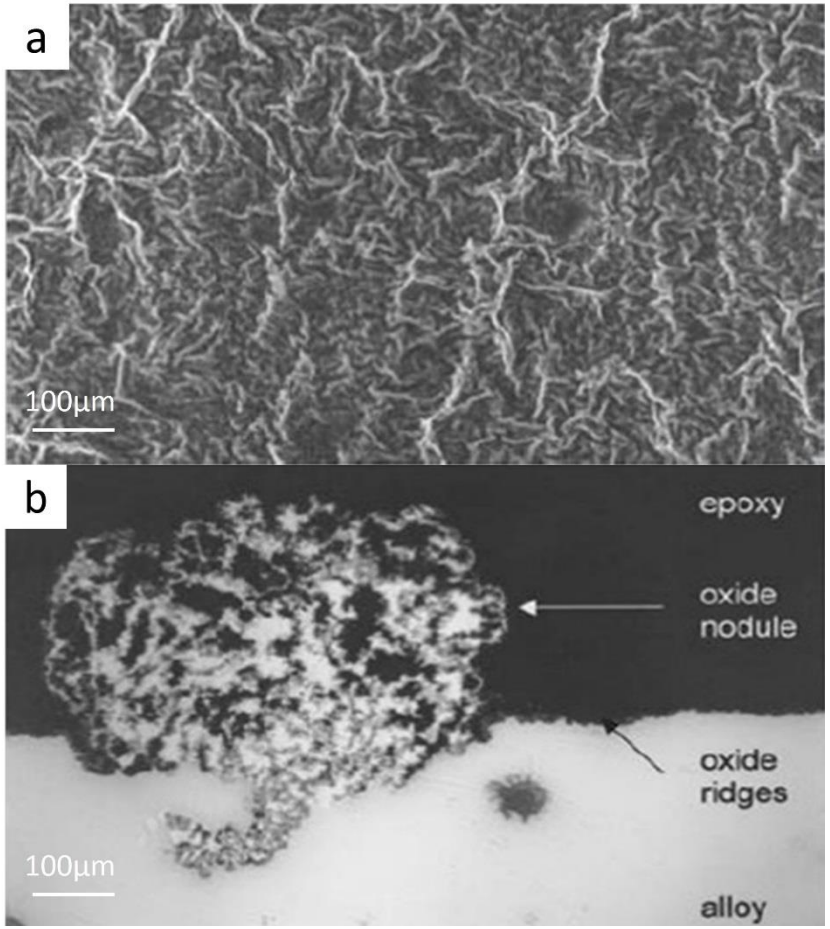

Figure 7: Typical morphologies on the Mg surface during oxidation at high temperatures: (a) The oxide ridge morphology formed on Mg-9Al-1Zn after oxidation at 487 ℃ for 1 min; (b) a cross-sectional view of individual oxide nodule formed at 527 ℃ after 5 min. Reproduced from Czerwinski [31] with permission of Springer.

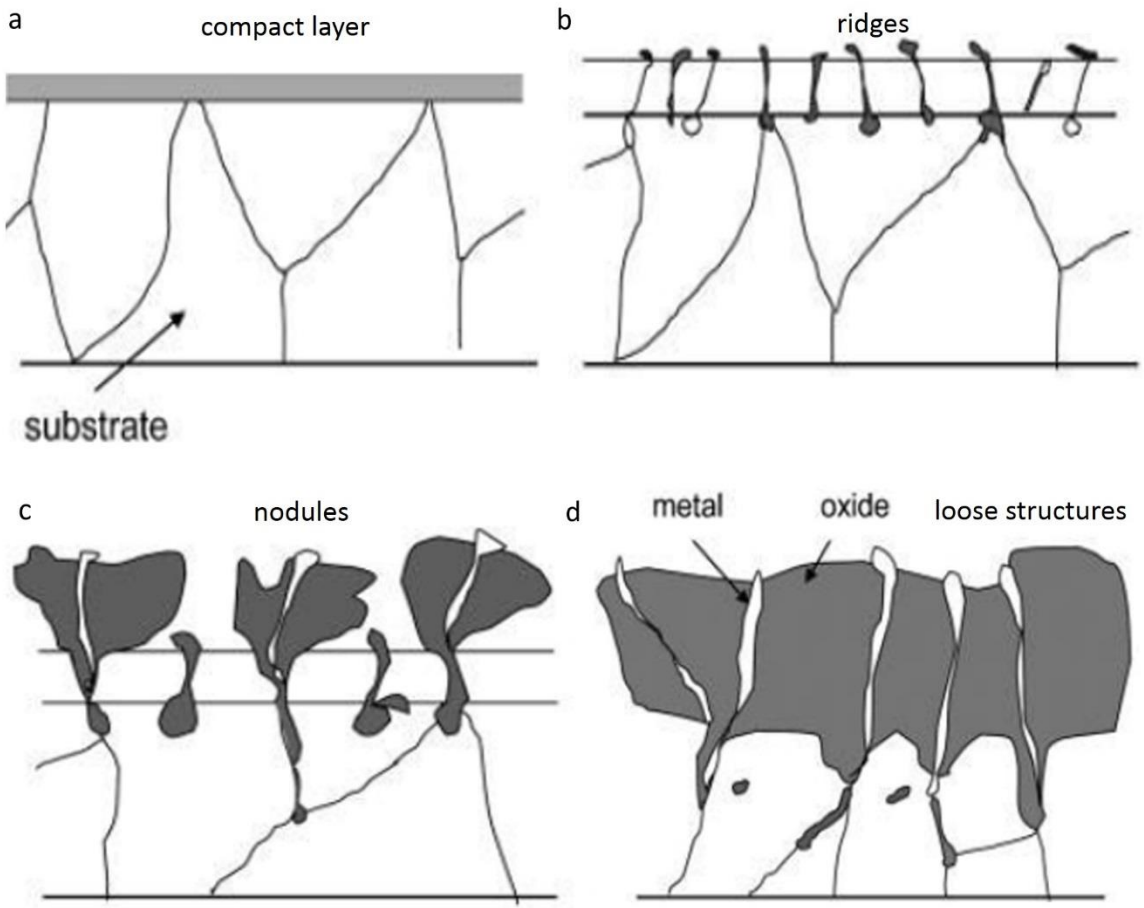

Figure 8: Schematic of the stages for MgO growth on AZ91 at high temperature: (a) a compact layer showing protective properties; (b) cracking of the layer and growth of oxide ridges; (c) nodular growth accompanied with linear kinetics; (d) coalescence of nodules and the formation of loose layer with pores. Reproduced from Czerwinski [31] with permission of Springer.

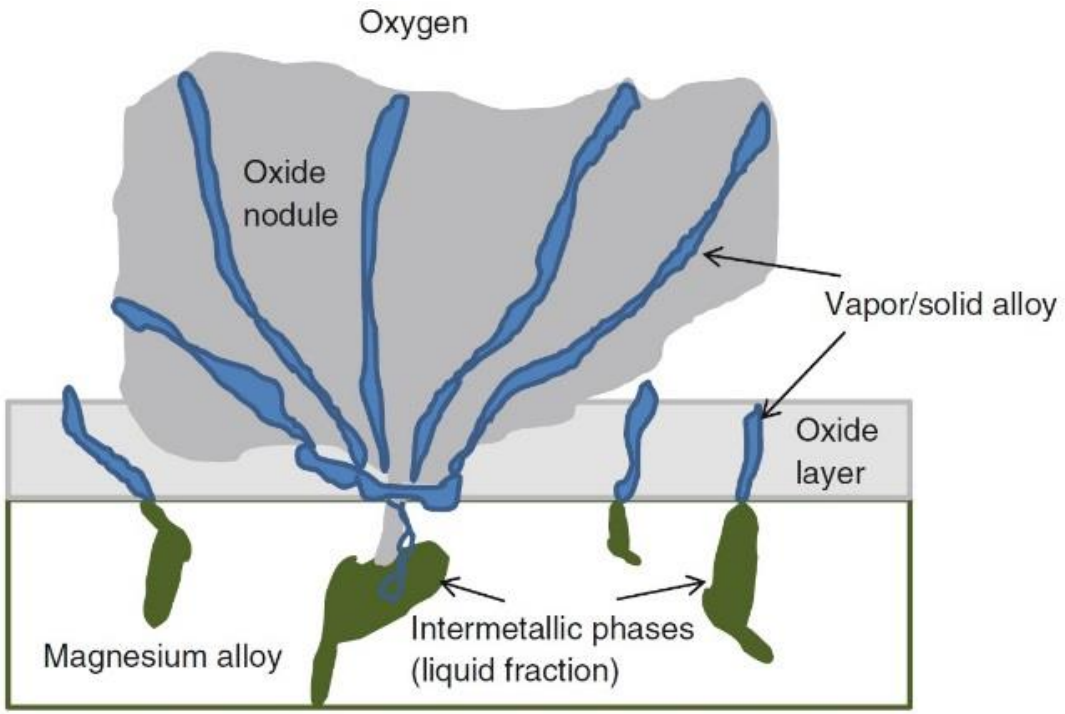

Figure 9: Schematics of the formation mechanism and internal structure of an oxide nodule. Melting of the intermetallic phases can produce locally high vapour pressures of Mg vapour. If such a region is associated with cracks in the oxide, Mg vapour can diffuse through the cracks, be oxidized at the oxide surface, and contribute to the growth of the oxide nodule. Reproduced from Czerwinski [26] with permission of Springer.

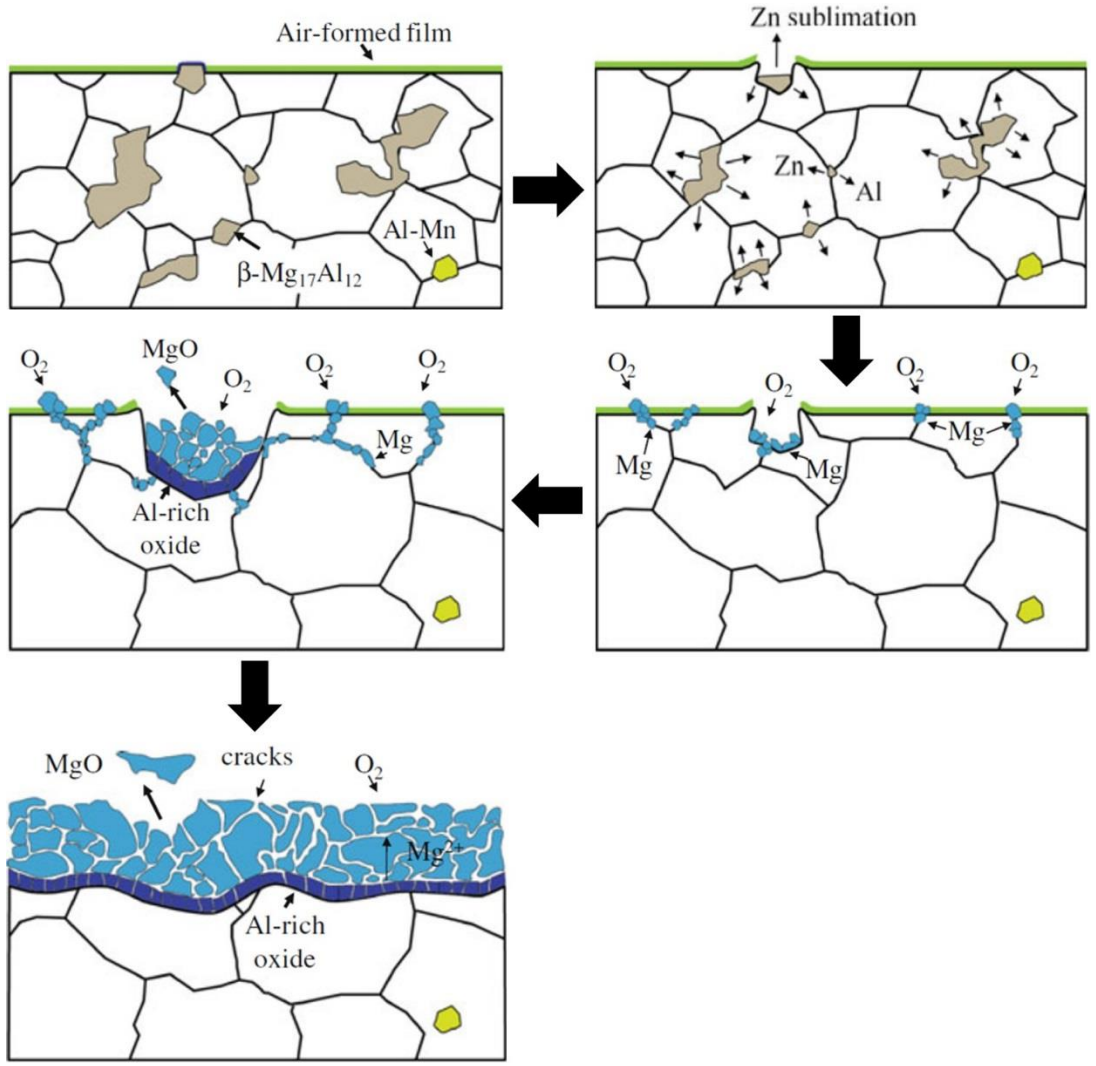

Figure 10: Proposed oxidation mechanism of AZ91 at 410℃. Selective oxidation accompanied with Zn sublimation leads to a pit. Further oxidation enlarges the pit, resulting in formation of loose oxide nodules. The consumption of Mg by oxidation leads to a local increase in the Al content at the oxide/substrate interface. Reproduced from Arrabal [80] with permission of Springer.

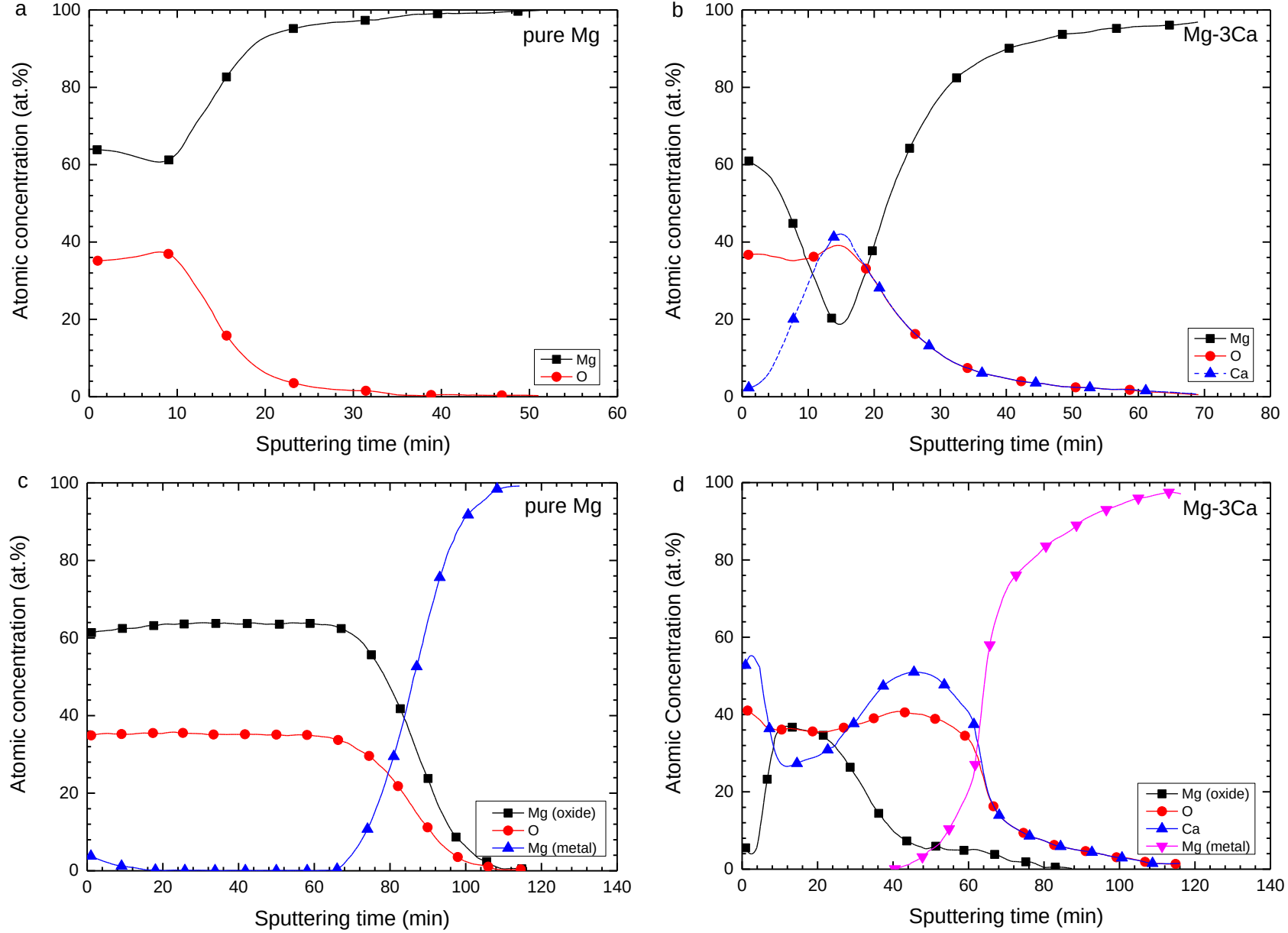

Figure 11: AES depth profiles sputtered from the surface of (a) pure Mg at 440 °C; (b) Mg-3Ca at 440 °C; (c) pure Mg at 500 °C and (d) Mg-3Ca at 500 °C for 1 h. In pure Mg, the Mg and O content at the surface were constant at both 440 and 500 °C. In Ca-containing alloys, Ca tended to segregate near the surface with increasing the temperature. Redrawn from You [110] and used with permission from Elsevier.

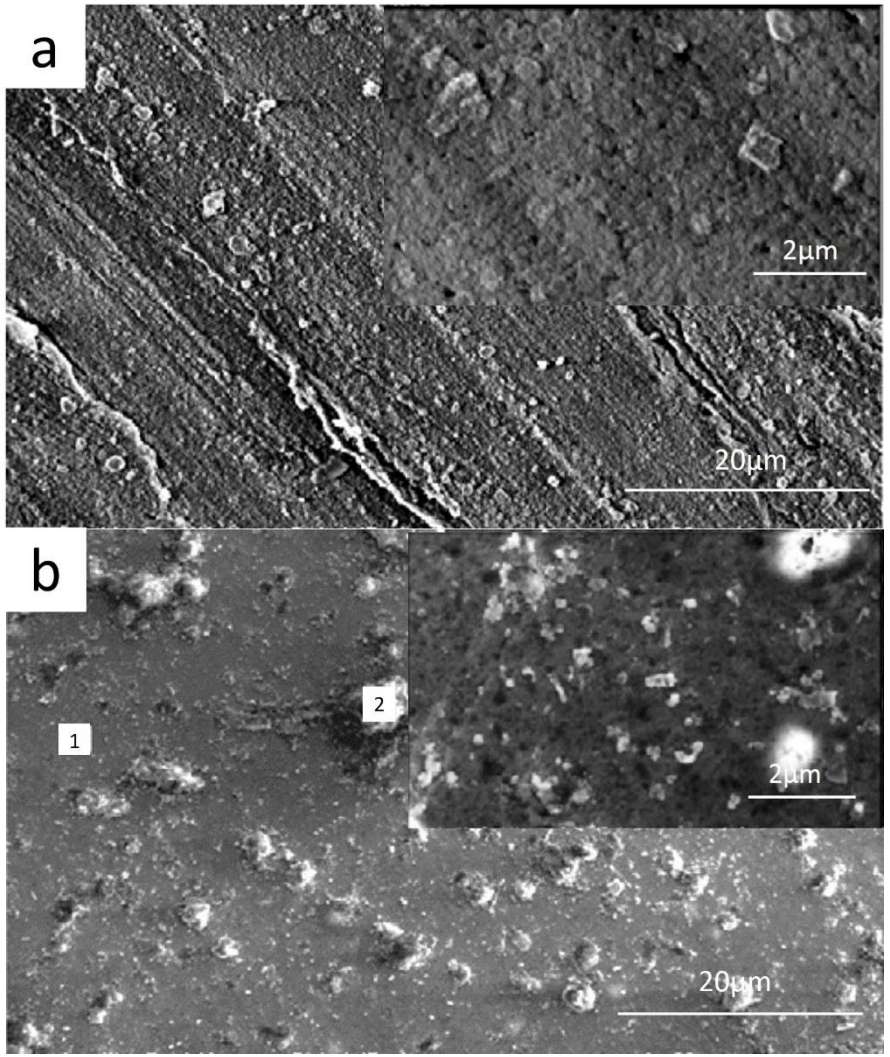

Figure 12: The surface morphology of the oxide scale on Mg at 500 °C for 90 min: (a) non-implanted surface: large cracks and cavities were produced on the surface; (b) implanted surface (Y ions of 90 keV with a dose of $5\times10^{17}cm^{-2}$ for 1h): the surface was dense with no cracks, the nodules on the surface shows a so-called reactive element effect. Reproduced from Wang [126] with permission from Elsevier.

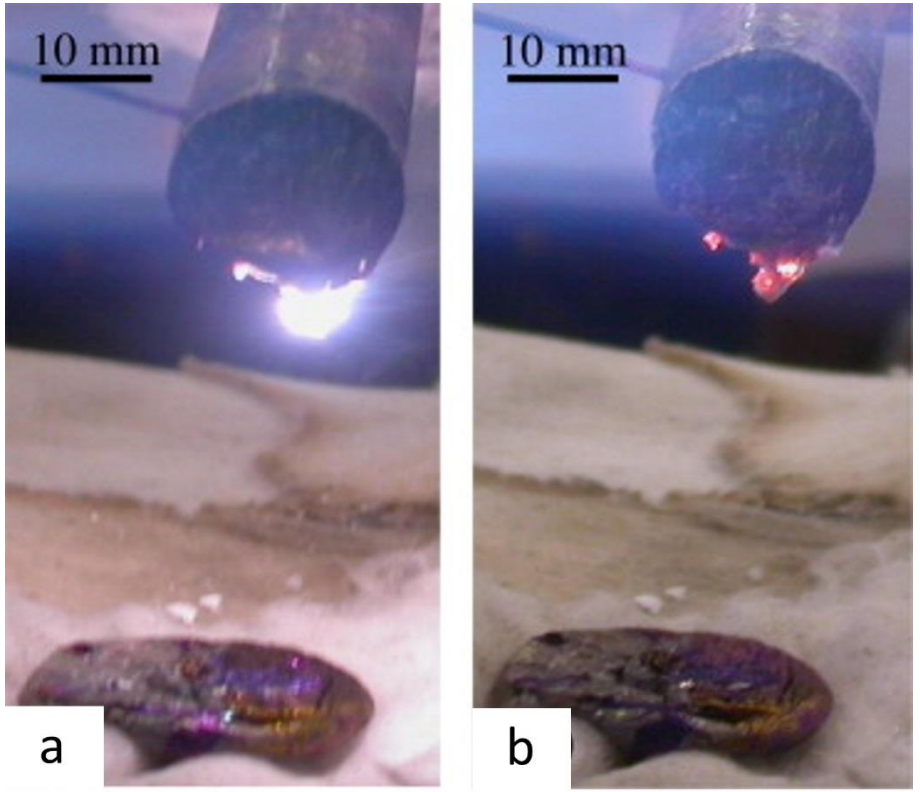

Figure 13: Images showing the behaviour of a Mg-5Y specimen exposed to a flame test as illustrated in Fig. 5: (a) specimen melted and a minor ignition occurred at the end of the specimen; (b) the incipient ignition was extinguished readily even in the presence of the LPG flame. Reproduced from Prasad [59] with permission from Elsevier.

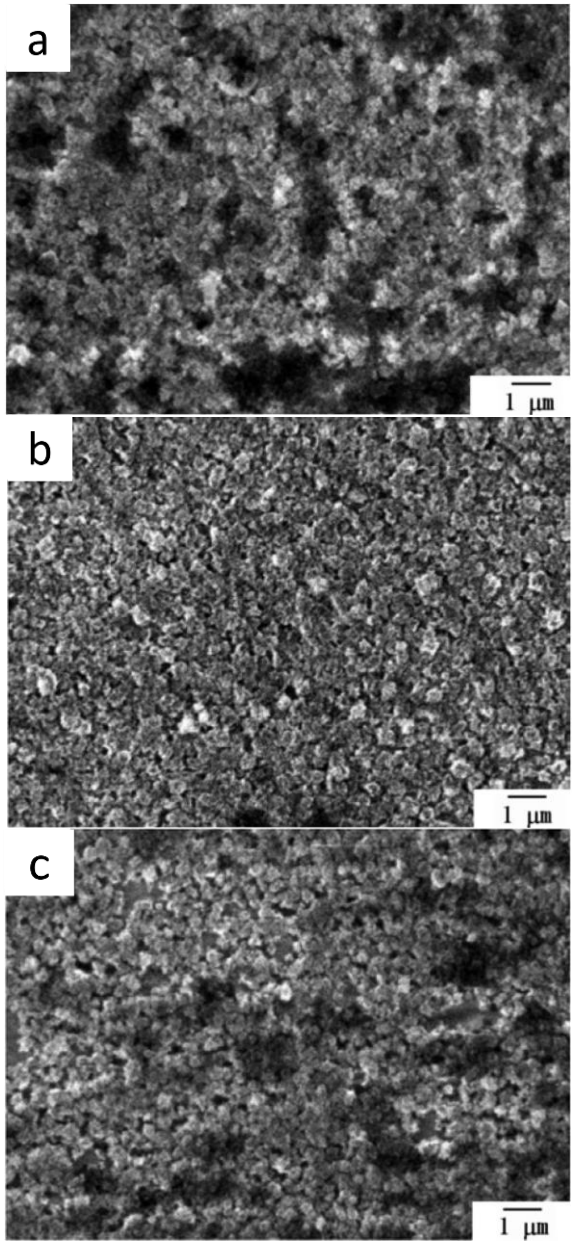

Figure 14: SEM micrographs on the surface of the AM50 Mg alloy after isothermal oxidation in air at 500℃ for 60 min: (a) 0 wt.% Ce with high porosity; (b) 0.25 wt.% Ce showing dense oxide layer; (c) 0.45 wt.% Ce showing porous oxide layer. Reproduced from Lin [143] with permission from Elsevier.

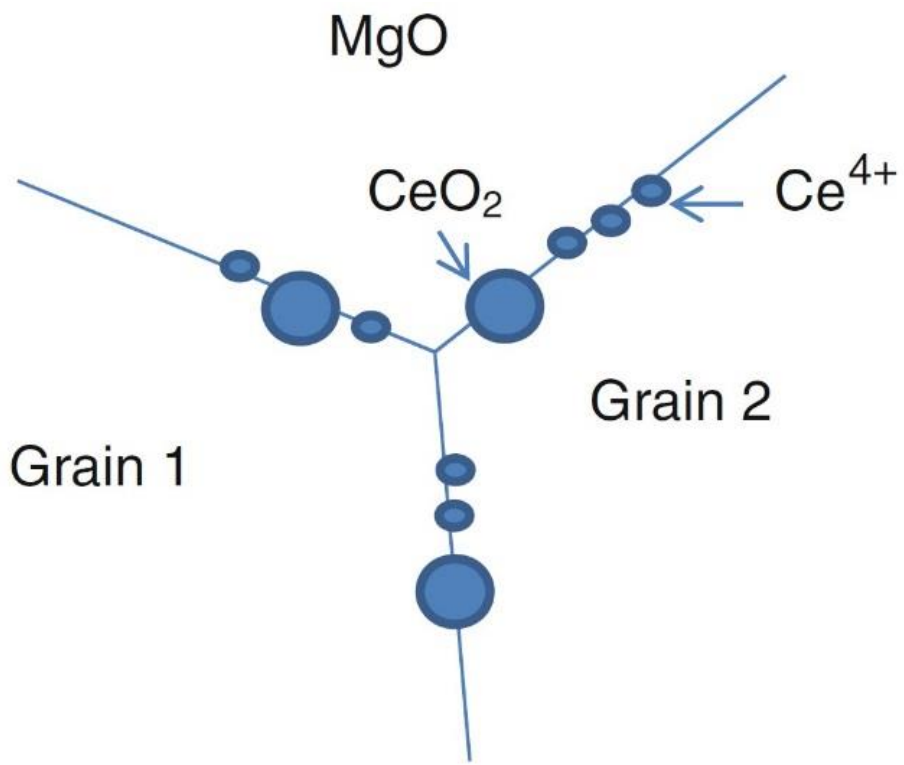

Figure 15: The proposed REE of Ce in MgO. The Ce oxide and Ce cations in MgO grain boundaries block the diffusion of Mg cations. Reproduced from Czerwinski [26] with permission of Springer.

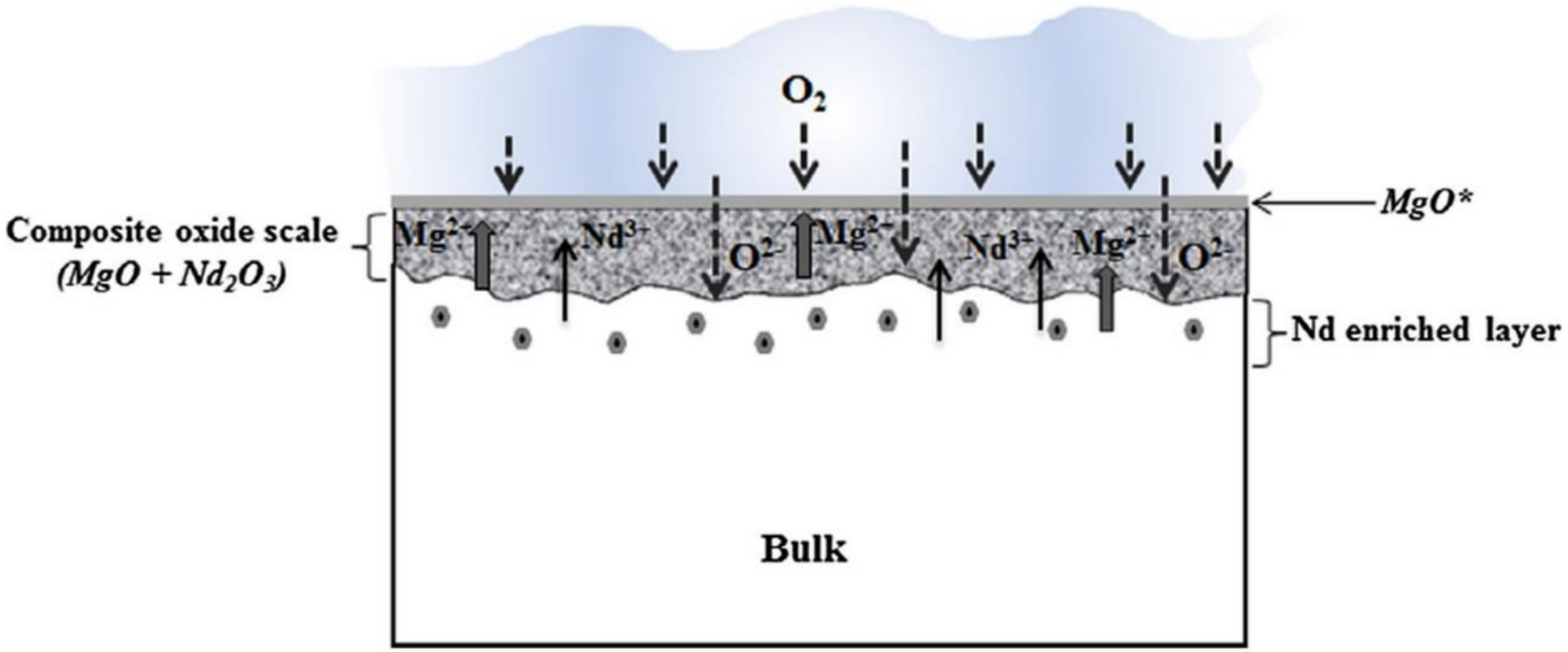

Figure 16: Proposed composite oxide layer formed during the oxidation of the α-Mg solid solution phase. The consumption of Mg during oxidation increased the concentration of Nd at the surface, leading Nd_2O_3 to form. Reproduced from Aydin [46] with permission from Elsevier.

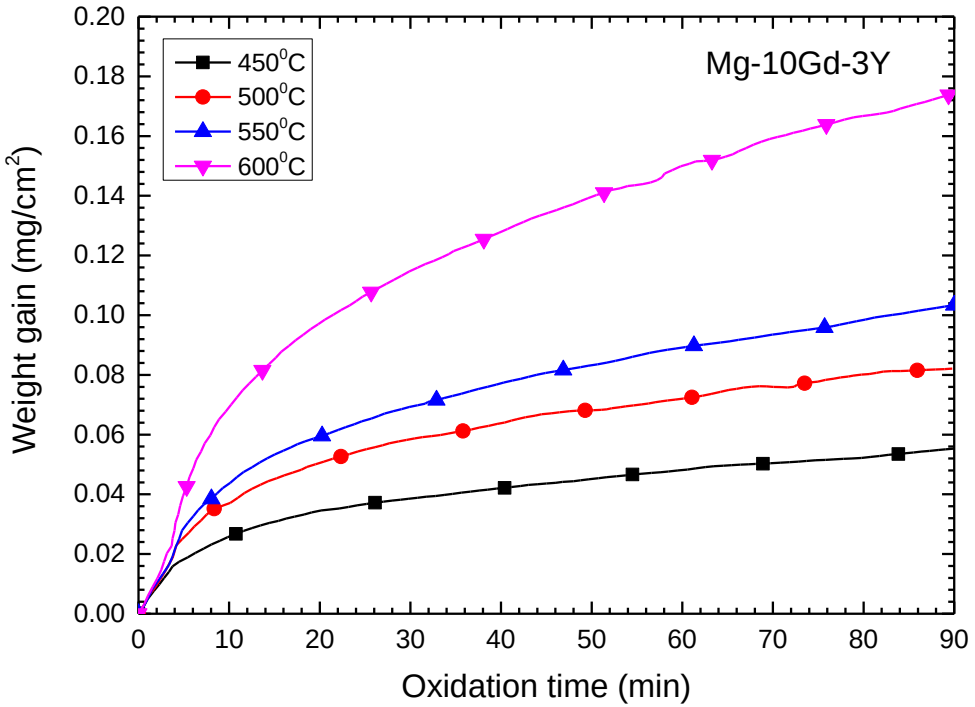

Figure 17: Weight gain curves of the Mg–10Gd–3Y alloys oxidized at different temperatures for up to 90 min. The oxide growth kinetics obeyed the parabolic law from 450 °C to 600 °C. Redrawn from Wang [151] and used with permission from Elsevier.

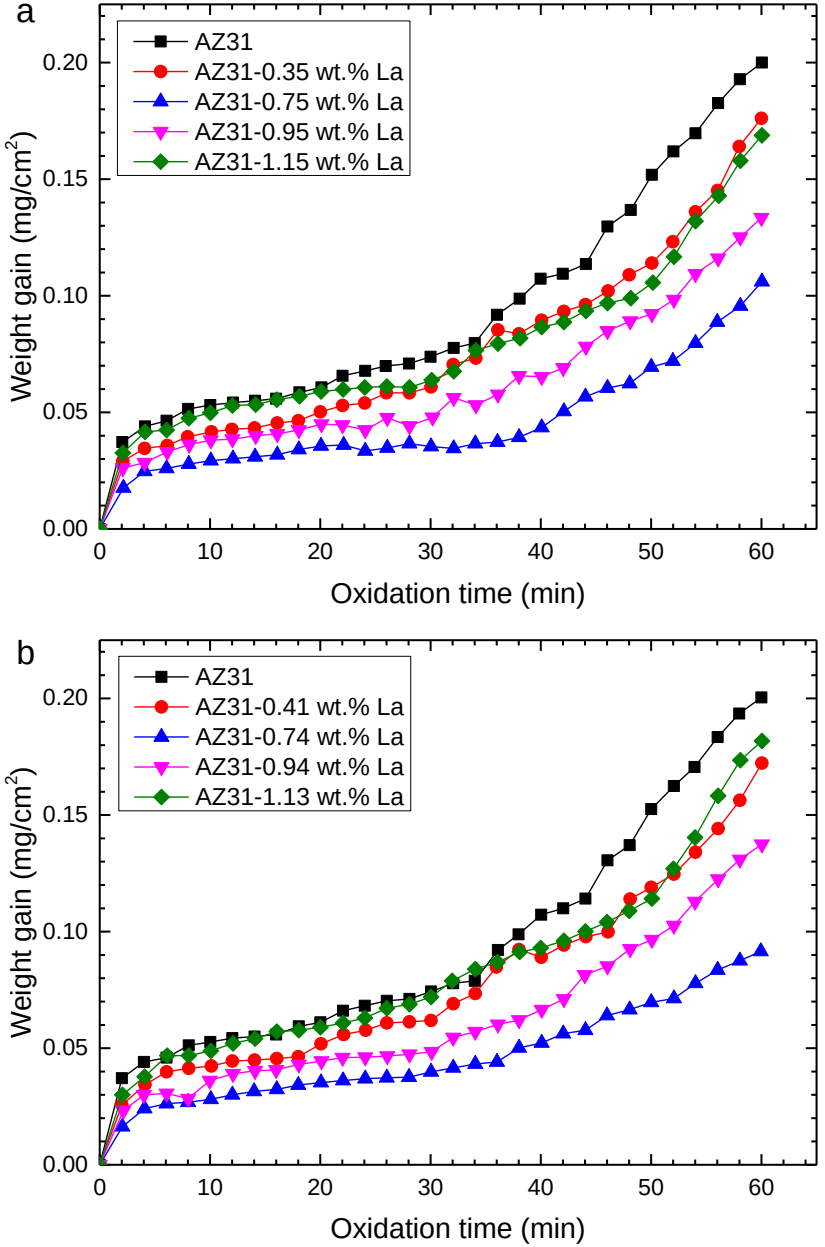

Figure 18: Oxidation kinetic curves of AZ31 at 450 ℃ alloyed with (a) La: the lowest oxidation rate was obtained by alloying 0.75 wt.% La, higher La content increased the oxidation rate; (b) La_2O_3: lowest oxidation rate was obtained by alloying 0.74 wt.% La (converted from La_2O_3), higher La_2O_3 addition increased the oxidation rate. Redrawn from Zhao [155] and used with permission from Elsevier.

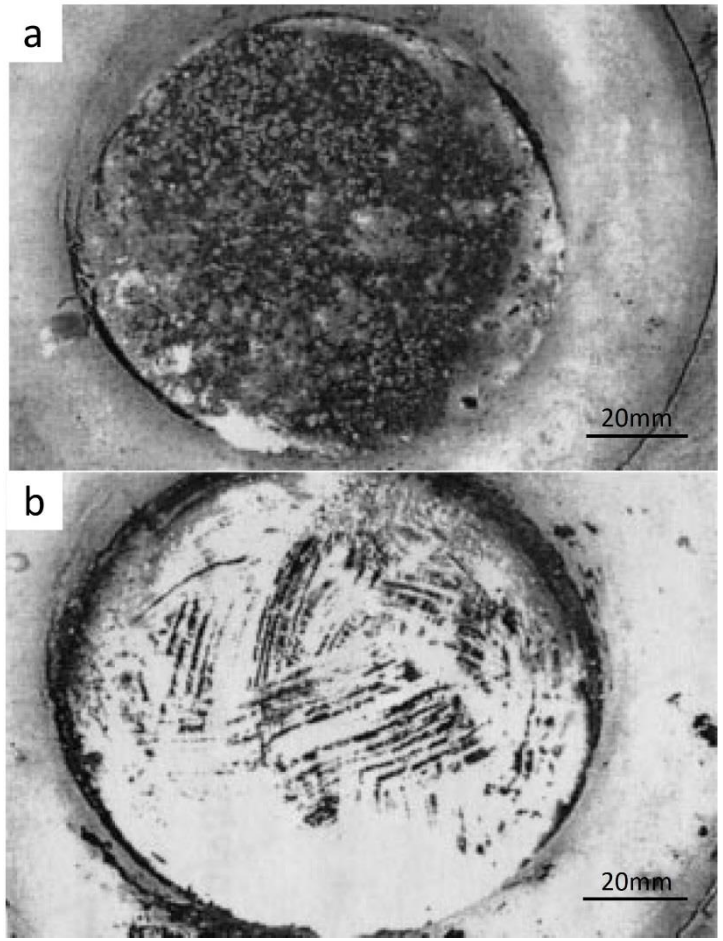

Figure 19: Top view of molten AZ91 and AZB910 alloy held at 650 °C: (a) the AZ91 melt surface was covered by lots of oxides; and (b) the AZB910 melt was smooth and clear. Reproduced from Zeng [166] with permission from Elsevier.

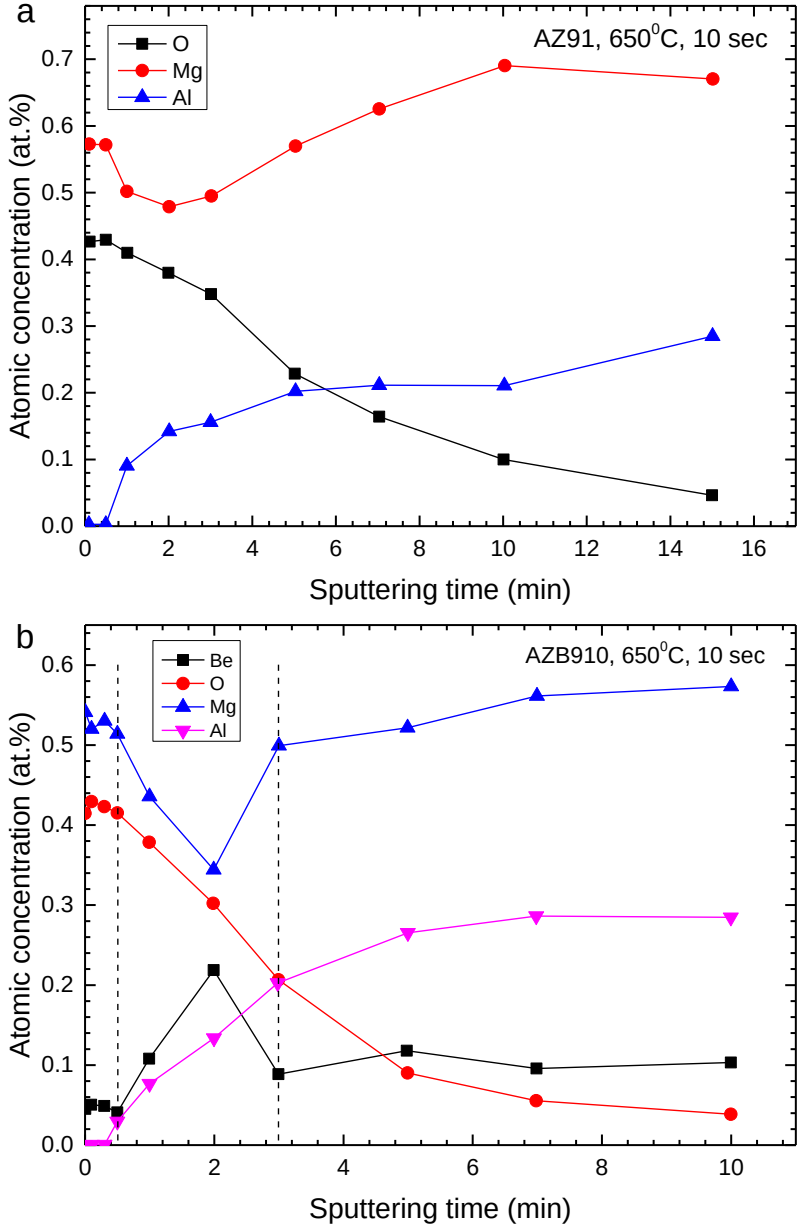

Figure 20: Auger depth profiles of: (a) AZ91; (b) AZB910 after oxidation at 650℃ for 10 seconds. The high concentration of Mg and O indicates MgO layers on the outmost surface of both alloys. For AZB910, the decreasing Mg concentration was accompanied with an increasing of Be content, indicating the appearance of BeO in the inner layer. Redrawn from Zeng [166] and used with permission from Elsevier.

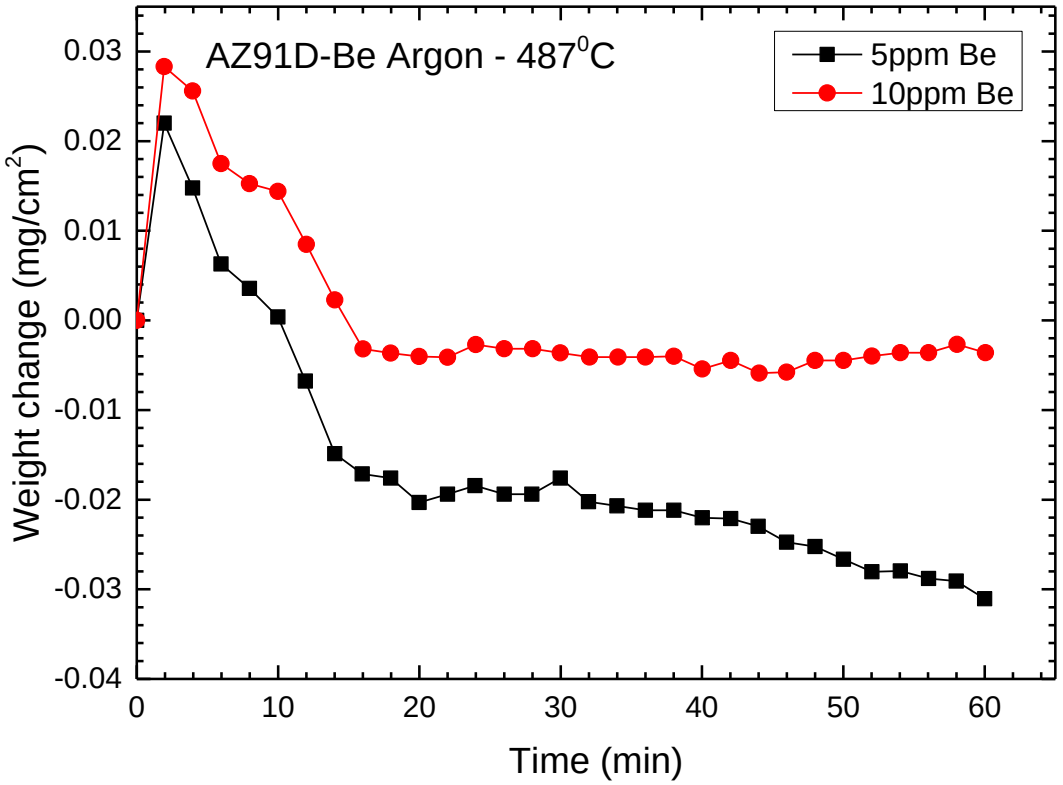

Figure 21: The influence of the Be content on weight change kinetics of AZ91D in argon. This weight loss for the 10 ppm (wt) Be-containing alloy was lower than that of the 5 ppm (wt) Be-containing alloy, implying an evaporation suppression by the higher amount of beryllium. Redrawn from Czerwinski [168] and used with permission from Elsevier.

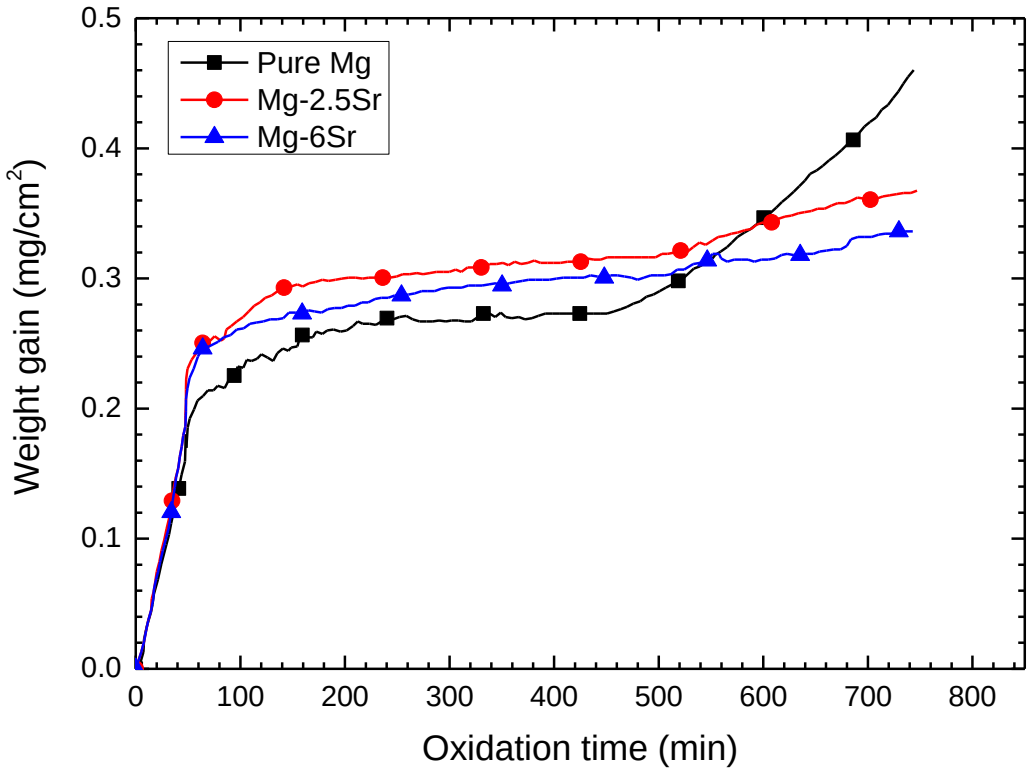

Figure 22: The oxidation kinetics at 500℃ for 12 hour in air of the alloys (a): pure Mg; (b): Mg-2.5 wt.% Sr and (c): Mg-6 wt.% Sr. There were two stages: (i) the initial parabolic-oxidation stage which can also be considered as the incubation period and (ii) the accelerated oxidation stage. Sr delayed the onset of accelerated oxidation. Redrawn from Aydin [178] and used with permission of John Wiley and Sons.

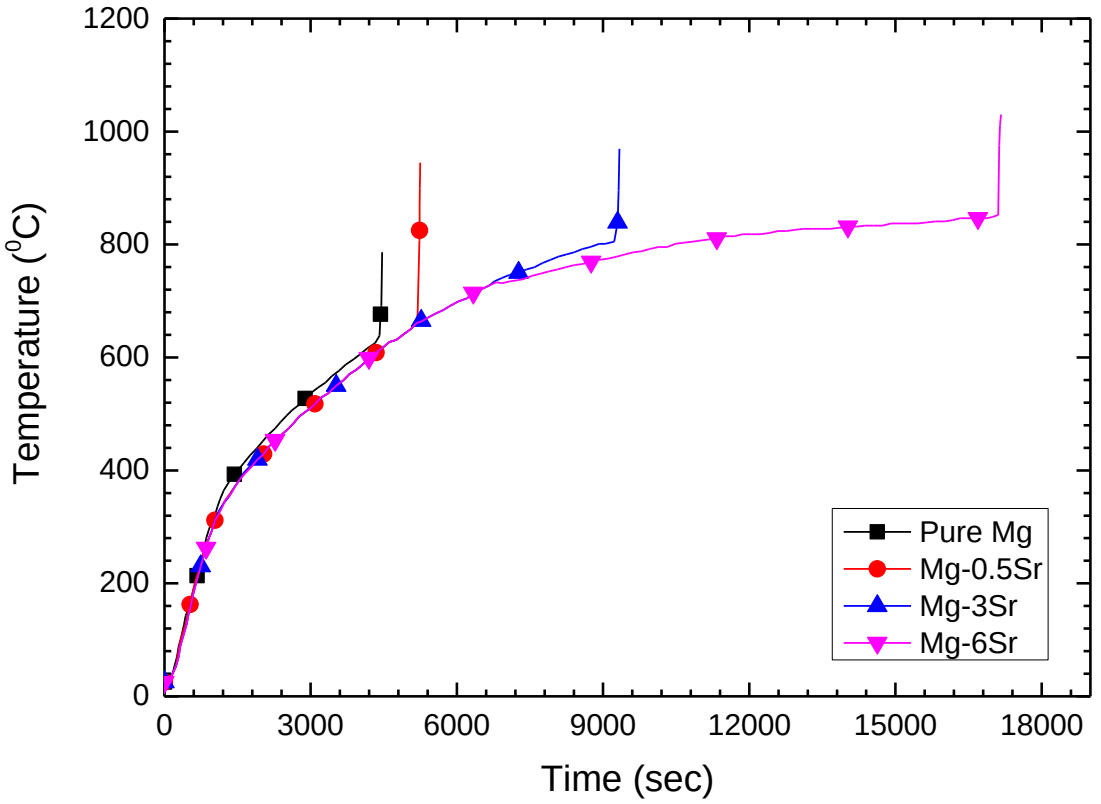

Figure 23: Ignition temperatures of pure Mg and Mg-Sr alloys. The ignition temperature of Mg increases with increasing Sr content. Redrawn from Aydin [180] and used with permission of Springer.

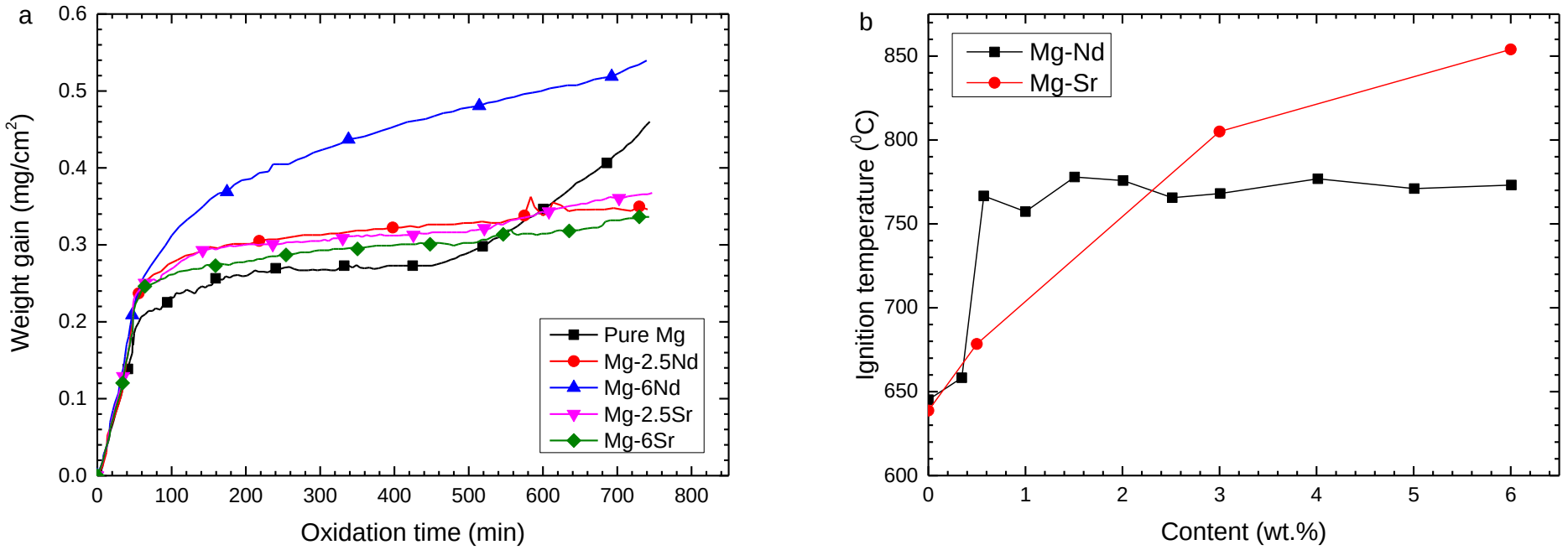

Figure 24: (a) Oxidation kinetics of pure Mg, Mg-2.5Nd, Mg-6Nd, Mg-2.5Sr and Mg-6Sr at 500 °C in air for 700 minutes; (b) ignition temperatures of Mg-Nd and Mg-Sr alloys. Nd and Sr had similar role on the oxidation resistance. However, the effect of Sr was more remarkable on the ignition temperature. The ignition temperature of Mg increased with increasing Sr content. Redrawn from Aydin [46, 147, 178, 180] and used with permission of Springer.

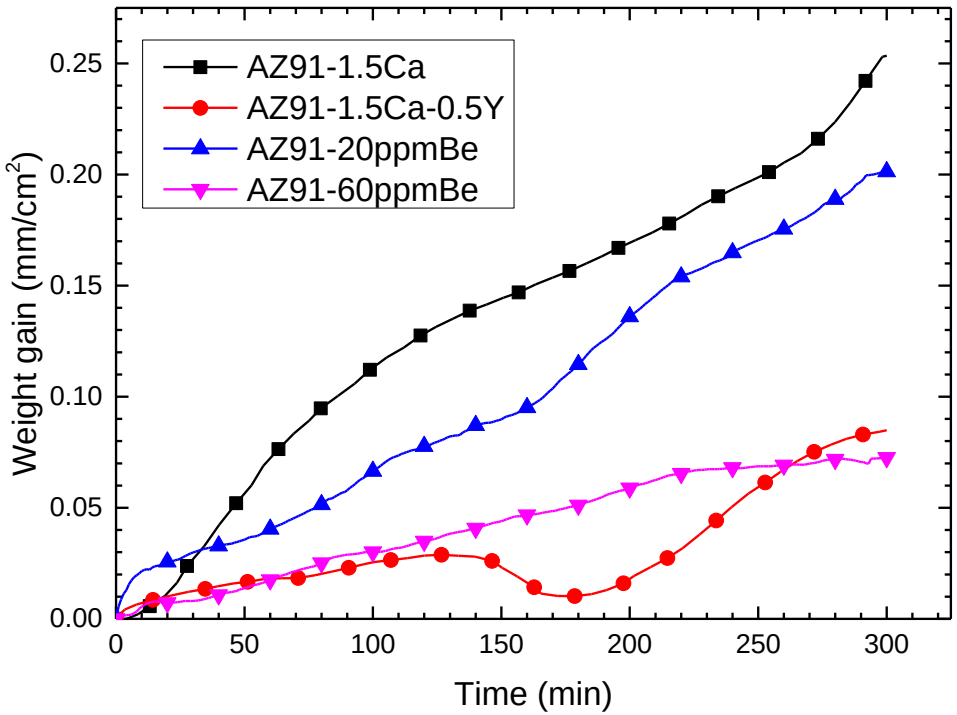

Figure 25: Oxidation kinetics of AZ91-1.5Ca, AZ91-1.5Ca-0.5Y, AZ91-20 ppm (wt) Be and AZ91-60 ppm (wt) Be at 400 °C in air for 300 min. The AZ91 containing 20 ppm (wt) Be shows a lower oxidation rate than that of AZ91-1.5Ca. Addition of 60 ppm (wt) Be has a better effect on the oxidation resistance than that of addition of 1.5 Ca and 0.5 Y. Redrawn from Cheng and Tan [111, 169] and used with permissions of Springer and Elsevier.

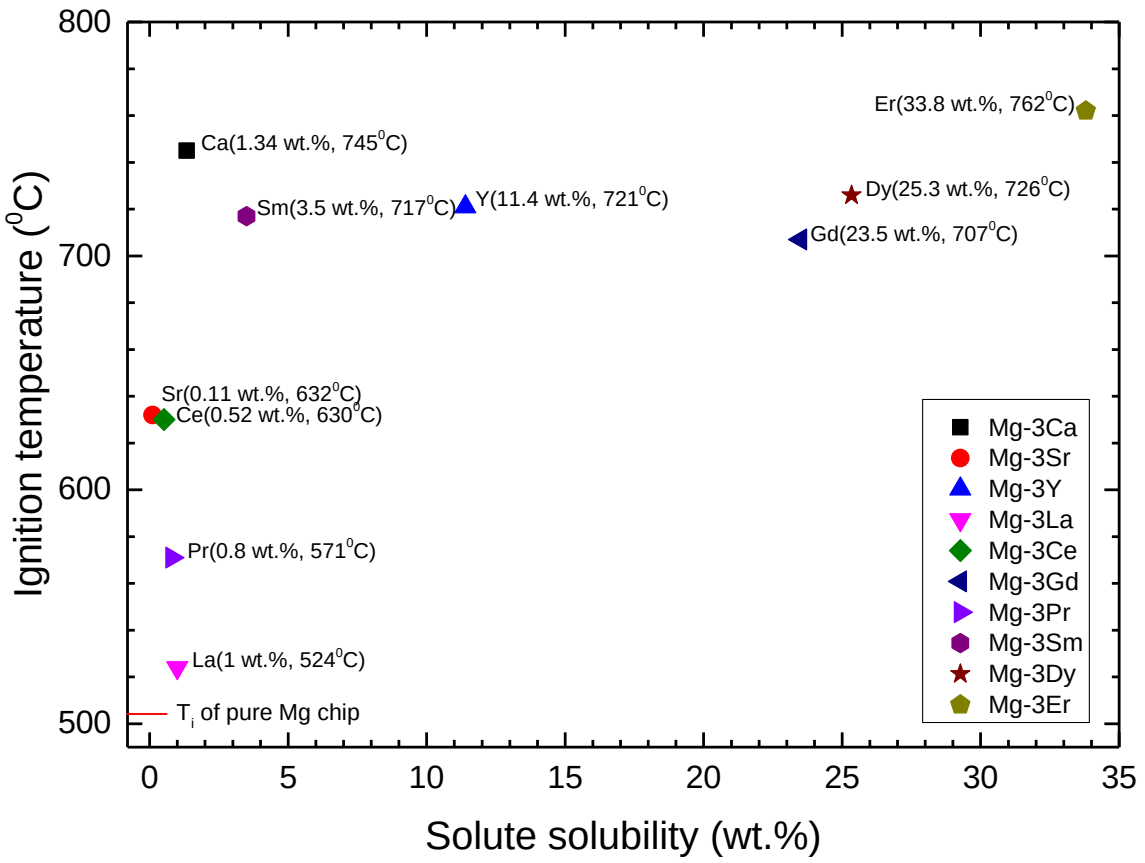

Figure 26: Ignition temperatures (T_i) of various binary Mg alloys chips and the solute solubility of the alloying elements in Mg. Mg-3La provides the lowest ignition temperature of 524 °C and La has a low solubility in Mg (1 wt.%). Mg-3Er has the highest ignition temperature of 762 °C and Er has the highest solubility in Mg (33.8 wt.%). Alloying element with a higher solubility trends to perform better in improving the ignition resistance of Mg. Data retrieved from Kim [105] and used with permission from Elsevier.

Table 1: Incubation period (min) of various Mg alloys at various temperatures (°C). (Chemical compositions are represented by mass fraction).

Alloys	**Incubation period (min) at various temperatures (°C)**							**Ref.**
	400	**430**	**450**	**500**	**550**	**600**	**700**	
Pure Mg				440				[46]
AM50	Over 700		95	85				[38]
			41					[196]
AM60	Over 700		80	75				[38]
AE42	Over 700		130	95				[38]
ZE41	Over 330		Over 330	90				[41]
Mg-0.3Nd				480				[46]
Mg-0.5Nd				670				[46]
Mg-2.5Nd				Over 700				[147]
Mg-6Nd				Over 700				[147]
Mg-2.5Sr				Over 700				[178]
Mg-6Sr				Over 700				[178]
Mg-10Gd-3Y	Over 90		Over 90	Over 90	Over 90	Over 90		[151]
Y surface implanted Mg				Over 90				[126]
Mg-1.5Ca				Over 300				[110]
Mg-3.08Y-0.68Ce	Over 140			Over 140		16		[129]
Mg-5.13Y-0.25Zn-0.32Zr	Over 16200							[132]
AZ91	150							[169]
	180		20					[38]
AZ91-1.5Ca	270							[111]
AZ91-1.5Ca-0.5Y	Over 300							[111]
AZ91-2Ca							55	[197]
AZ91-5Ca							Over 60	[197]
AZ91-60ppm (wt) Be	Over 300							[169]
ZC63-10SiC		90	55					[40]
AZ91-5SiC		120	60					[194]
AZ91-10SiC		Over 300	90					[194]
AZ91-20SiC		Over 300	Over 300					[194]
AM50-0.28Y			Over 60					[196]
AM50-1Y			57					[196]
AZ31-0.75La			36					[155]
AZ31-0.3Ca			Over 1200	Over 1200				[113]

Table 2: Ignition temperature of various magnesium alloys and P-B ratios [62] of the corresponding oxides. (Chemical compositions are represented by mass fraction).

Alloy elements	**Oxide**	**P-B Ratio**	**Alloy**	**Shape**	T_i	**Ref.**
Mg	MgO	0.81	Pure Mg	Ingot	620-650 °C	[45-47]
				Chip	504 °C	[105]
				Powder	437 °C	[82]
Al	Al_2O_3	1.29	Mg-3Al	Chip	474 °C	[105]
			AM50	Powder	485 °C	[143]
Al, Zn	Al_2O_3 ZnO	1.29 1.59	Mg-9Al-1Zn	Ingot	520-600 °C	[48, 49, 118]
				Powder	484 °C	[143]
			Mg-3Al-1Zn	Ingot	628 °C	[48]
Ca	CaO	0.65	Mg-3Ca	Chip	745 °C	[105]
			Mg-5Ca	Ingot	727 °C	[112]
			AZ91-1.5Ca	Ingot	750 °C	[111]
			AZ91-2Ca	Ingot	900 °C	[117]
			AZ91-6Ca	Ingot	869.4 °C	[118]
Y	Y_2O_3	1.13	Mg-3Y	Chip	721 °C	[105]
			Mg-5.8Y	Ingot	665 °C	[115]
			Mg-10Y	Ingot	900 °C	[130]
			WE43	Ingot	750 °C 644 °C	[55] [48]
Ca, Y	CaO Y_2O_3	0.65 1.13	Mg-3.5Y-0.5Ca	Ingot	847 °C	[115]
			AZ91-1.5Ca-0.5Y	Ingot	775 °C	[111]
Ce	Ce_2O_3 CeO_2	1.14 1.15	Mg-3Ce	Chip	630 °C	[105]
			AM50-0.25Ce	Powder	535 °C	[143]
			AZ91-0.25Ce	Powder	525 °C	[143]
Nd	Nd_2O_3	1.13	Mg-0.5Nd	Ingot	770 °C	[46]
			AZ91-5Nd	Ingot	520 °C	[148]
Gd	Gd_2O_3	1.23	Mg-3Gd	Chip	707 °C	[105]
			Mg-15.3Gd-1.9Ag-0.3Zr	Ingot	930 °C	[152]
La	La_2O_3	1.11	Mg-3La	Chip	524 °C	[105]
			AZ31-0.7La	Ingot	570 °C	[155]
Be	BeO	1.70	Mg-0.15Be	Ingot	750 °C	[198]
Be, Ca	BeO CaO	1.70 0.65	Mg-2Ca-0.03Be	Ingot	1050 °C	[165]
Sr	SrO	0.66	Mg-3Sr	Chip	632 °C	[105]
			Mg-6Sr	Ingot	854 °C	[180]
SiC	-	-	AM60-10SiC	Ingot	603 °C	[193]